Kroll, E., Bayon, C., Rudd, J. J., Armer, V., Magaji-Umashankar, A., Ames, R., Urban, M., Brown, N. A. and Hammond-Kosack, K. E. 2025. A conserved fungal Knr4/Smi1 protein is vital for maintaining cell wall integrity and host plant pathogenesis . *PLOS Pathogens.* 21 (1), p. e1012769. https://doi.org/10.1371/journal.ppat.1012769

A conserved fungal Knr4/Smi1 protein is vital for maintaining cell wall integrity and host plant pathogenesis

Erika Kroll[1,2], Carlos Bayon[1], Jason Rudd[1], Victoria Armer[1], Anjana Magaji-Umashankar[1], Ryan Ames[3], Martin Urban[1], Neil A. Brown[2], and Kim Hammond-Kosack[1,*]

Author addresses: [1]Strategic Area: Protecting Crops and the Environment, Rothamsted Research, Harpenden, AL5 2JQ, UK

[2]Department of Life Sciences, University of Bath, Bath, BA2 7AY, UK

[3]Biosciences and Living Systems Institute, University of Exeter, EX4 4PY, Exeter, UK

Corresponding authors:

***To whom correspondence should be addressed. Tel: +44 1582 938240. Email:

kim.hammond-kosack@rothamsted.ac.uk

Abstract

Filamentous plant pathogenic fungi pose significant threats to global food security, particularly through diseases like Fusarium Head Blight (FHB) and Septoria Tritici Blotch (STB) which affects cereals. With mounting challenges in fungal control and increasing restrictions on fungicide use due to environmental concerns, there is an urgent need for innovative control strategies. Here, we present a comprehensive analysis of the stage-specific infection process of *Fusarium graminearum* in wheat spikes by generating a dual weighted gene co-expression network (WGCN). Notably, the network contained a mycotoxin-enriched fungal module that exhibited a significant correlation with a detoxification gene-enriched wheat module. This correlation in gene expression was validated through quantitative PCR.

By examining a fungal module with genes highly expressed during early symptomless infection, we identified a gene encoding FgKnr4, a protein containing a Knr4/Smi1 disordered domain. Through comprehensive analysis, we confirmed the pivotal role of FgKnr4 in various biological processes, including morphogenesis, growth, cell wall stress tolerance, and pathogenicity. Further studies confirmed the observed phenotypes are partially due to the involvement of FgKnr4 in regulating the fungal cell wall integrity pathway by modulating the phosphorylation of the MAP-kinase MGV1. Orthologues of *FgKnr4* are widespread across the fungal kingdom but are absent in other Eukaryotes, suggesting the protein has potential as a promising intervention target. Encouragingly, the restricted growth and highly reduced virulence phenotypes observed for *ΔFgknr4* were replicated upon deletion of the orthologous gene in the wheat fungal pathogen *Zymoseptoria tritici*. Overall, this study demonstrates the utility of an integrated network-level analytical approach to pinpoint genes of high interest to pathogenesis and disease control.

Keywords*: Fusarium graminearum*, *Zymoseptoria tritici*, Weighted Gene Co-expression Network (WGCNA), dual host-pathogen transcriptomics, cell wall stress, MAP-kinase signalling, fungal specific gene family, fungal virulence.

Introduction

The wheat crop (*Triticum* species) plays a crucial role in global food security, contributing about 20% of dietary calories and protein worldwide (Saldivar, 2016), while also supplying essential nutrients and bioactive food components (Shewry and Hey, 2015). Pathogen and pest burden substantially contribute to wheat losses globally, accounting for ~21.5% of wheat losses annually (Savary et al., 2019). Of these, the five highest global contributors to wheat yield and quality losses are all fungal diseases and include Fusarium Head Blight disease (FHB) and Septoria tritici blotch disease (STB), which account for 2.85% and 2.44% of wheat losses, respectively (Savary et al., 2019).

FHB is a mycotoxigenic pre-harvest fungal disease of most cereals, caused by different *Fusaria* within the *Fusarium sambucinum* species complex that is increasingly prevalent in most cereal growing regions globally (O'Donnell et al., 2000; Kanja et al., 2021; Johns et al., 2022; Armer et al., 2024). Floral Infections lead to contamination of grain with mycotoxins that are subject to strict legal limits in different global regions (European Commission, 2006; EFSA, 2017; AHDB, 2023). Despite ongoing endeavours to manage FHB, mycotoxin contamination continues to significantly impact the economies of cereal and livestock producers, as well as the food, drink, and feed industries (Latham et al., 2023). The B-type sesquiterpenoid deoxynivalenol (DON) is the most common FHB mycotoxin in European food and feed wheat (Johns et al., 2022). The globally predominant DON producing species is *Fusarium graminearum* (O'Donnell et al., 2000). During wheat spike colonisation, *F. graminearum* undergoes a biphasic mode of infection. Initially, the fungus evades the host immune response by growing between cells, causing no visible symptoms for ~3 days. This

is followed by an extended symptomatic stage marked by wheat tissue bleaching and reduced grain development behind the advancing hyphal front (Brown et al., 2010, 2011). STB disease on wheat leaves is caused by the fungus *Zymoseptoria tritici.* This fungus has an extended symptomless stage of infection ~9 days, followed by a switch to symptomatic disease (Goodwin et al., 2011; Steinberg, 2015). However, unlike *F. graminearum*, *Z. tritici* colonisation is strictly confined to the sub-stomatal cavities and apoplastic spaces, without ever invading host cells (Kema et al., 1996). Both pathogens are currently managed using semi effective sources of host resistance mediated by major genes or QTLs (Brown et al., 2015; Bai et al., 2018; Buerstmayr et al., 2020) as well as fungicide applications (Fones and Gurr, 2015; Torriani et al., 2015; Buerstmayr et al., 2020; Kanja et al., 2021). But effective control faces escalating issues caused by fungicide resistance (Estep et al., 2015; Lucas et al., 2015; McDonald et al., 2019; de Chaves et al., 2022). There is a critical need to develop new methods to combat these and other wheat fungal pathogens.

Understanding the genetic and molecular mechanisms driving host infection in numerous interaction types continues to be a major goal of the international molecular plant pathology community (Nelson, 2020; Jeger et al., 2021). Gene expression data can be organised into co-expression networks, which group genes based on shared co-expression patterns. Network representations are advantageous because these present biological data on a systems-wide level, clustering genes in modules representative of specific stages or functions. This modelling can be achieved using the weighted gene co-expression network analysis (WGCNA) framework (Langfelder and Horvath, 2008). WGCNA has been repeatedly applied to analyse fungal gene expression data. For instance, this approach has been employed to identify effectors in *Magnaporthe oryzae* (Yan et al., 2023), shared genes during *Fusarium oxysporum* infection across multiple hosts (Cai et al., 2022), and virulence genes of *Colletotrichum siamense* (Liu et al., 2023). Although WGCNA has been used to study wheat host responses to *F. graminearum* infection (Kugler et al., 2013; Pan et al., 2018) and responses of *F. graminearum* under *in vitro* stress (L. Zhang et al., 2022; Park et

al., 2023), there has been no study of wheat-*F. graminearum* co-expression profiles during infection.

To gain deeper insight on the expression patterns of genes during the different stages of the *F. graminearum* infection the WGCNA framework was used to generate a fungal pathogen/wheat dual co-expression network. Significantly, this framework can facilitate the correlation of both fungal and host plant expression (Mateus et al., 2019). Within this approach, genes are grouped into modules based on shared co-expression patterns separately for the pathogen and the host. Modules are then correlated between the pathogen and host networks to predict shared expression dynamics. In this study, correlated expression between a mycotoxin gene-enriched fungal module and a detoxification gene-enriched wheat module, validated the host-pathogen network. The study then focused on the unique fungal module F16, characterised by high expression levels during the earliest symptomless infection stage, and led to the discovery of *FgKnr4*. A subsequent comprehensive experimental analysis revealed the pivotal role of *FgKnr4* in various biological processes, including morphogenesis, growth, cell wall stress tolerance, and virulence in *F. graminearum*. The *Knr4* gene is not restricted to *F. graminearum* but is distributed widely across the fungal kingdom and is absent in other Eukaryotes. The various mutant phenotypes observed in the *F. graminearum ΔFgknr4* strain were replicated upon deletion of the orthologous gene in the wheat pathogen *Z. tritici*. Overall, this study highlights the value of using network analyses to model spatio-temporal pathogen-host interactions and to identify novel conserved genes associated with virulence.

Results

Generation of a dual *F. graminearum*-wheat co-expression network

F. graminearum floral infections can be divided into symptomatic or symptomless stages of infection. Disease spread through the rachis internodes (RI) can be further broken down to four different key stages of infection. Namely early symptomless (RI7-8), late symptomless (RI5-6), early symptomatic (RI3-4), and late symptomatic (RI1-2) infection **(Figure 1A)**. A spatio-temporal transcriptomics dataset of *F. graminearum* floral infection of the susceptible wheat cultivar Bobwhite, which distinguishes between these key distinct stages, was previously generated (Dilks et al., 2019). This dataset also included spikelet tissue (SP) sampled at 3 (early symptomatic) and 7 days post-infection (dpi) (late symptomatic). The WGCNA framework (Zhang and Horvath, 2005; Langfelder and Horvath, 2008) was used to construct a dual co-expression network to model fungal pathogen/crop interaction in wheat using this dataset.

Normalised counts were used to generate two distinct networks: one for *F. graminearum* and another for *T. aestivum*. The *F. graminearum* network consisted of 10,189 genes organised into 18 modules (with 2629 – 60 genes per module), while the *T. aestivum* network consisted of 47,458 genes distributed among 25 modules (with 23063 – 83 genes per module) **(Figure 2 – figure supplement 1, Supplementary File 1)**. Both networks met scale free model criteria at their selected soft thresholding power **(Figure 2 – figure supplement 2 A-B)**. The examination of module quality statistics found that each module within both networks were of a high quality (Z-Summary > 10), with the exception of F16 (Z-Summary = 9.67), which still markedly surpasses the minimum Z-Summary score of > 2 (Langfelder et al., 2011) **(Figure 2 – figure supplement 2C**). This indicates a substantial preservation of modules compared to a random selection of all network genes. Additionally, preservation statistic calculations confirmed that all modules maintain preservation (Z-summary > 2) across both networks with all modules of the wheat network and the majority of the fungal modules (11/18) having strong preservation (Z-summary > 10) **(Figure 2 – figure supplement 2D**). These findings suggest a consistent preservation of within-network topology across modules (Langfelder et al., 2011). For each module, a single summarised expression pattern, the eigengene value,

was calculated. The fungal and wheat modules were correlated by their eigengene expression values, and modules displaying significant correlation ($p \geq 0.001$) formed the dual co-expression network **(Figure 2A)**.

To gain insight into the function of individual modules, a Gene Ontology (GO) enrichment analysis was performed for both network sets (**Figure 2D-E, Figure 2 – figure supplement 1)**. To confirm these enrichment patterns were not due to chance, a random network was generated for both the fungal and wheat datasets. No significant enrichment was found for the random wheat network and fungal network.

Among the eight wheat modules within the dual co-expression network, five of them were significantly enriched for disease resistance genes (TO:0000112, $p \geq 0.05$) and one was specifically enriched for wheat stripe rust resistance genes (TO:0020055) **(Figure 2E),** suggesting the wheat modules in the network are needed for plant defence. One of these wheat modules, W12, was significantly enriched in the GO terms detoxification (GO:0098754; $p = 7.13 \times 10^{-7}$) and response to toxic substances (GO:0009636; $p = 2.11 \times 10^{-6}$). This module was correlated to the fungal module F12, which was enriched in genes belonging to the trichothecene biosynthesis (*TRI)* gene cluster ($p = 1.92 \times 10^{-4}$) and for the GO term terpenoid biosynthesis (GO:0016114 ; $p = 0.00085$) **(Figure 2D, Table 1)**. Notably, the module F12 was most highly expressed in the late symptomless stage of infection. Expression of this module then rapidly decreases during the symptomatic stages of infection. Module F12 therefore appears to be positioned specifically at the transition between the late symptomless stage and the early symptomatic stage. The production of the DON mycotoxin is essential for the transition to the extensive symptomatic stage (Cuzick et al., 2008; Jansen et al., 2005). DON inhibits protein translation, which then eventually leads to cell death and the bleached phenotype distinctive of symptomatic *F. graminearum* infection (Desmond et al., 2008; Arunachalam and Doohan, 2013). High expression of module F12 in the symptomless stage is also supported by previous data which found that genes involved in mycotoxin biosynthesis are highly expressed in symptomless wheat tissue (Brown et al.,

2017). The correlation with the wheat module W12 therefore implies that detoxification genes in the module are being expressed in response to production of fungal mycotoxins.

Interestingly, the fungal module F10 contains genes that are highly expressed in the earliest and latest stages of *F. graminearum* infection, but not intermediate stages **(Figure 4).** The fungal module F10 includes the Killer toxin 4 genes (*KP4L*) -1, -2, and -3. These genes also have some of the highest module membership scores (>0.90) within the module. The *KP4L* genes are necessary for virulence and expressed during both self and non-self interactions **(Table 1)**. It is suggested that KPL4 proteins provide *F. graminearum* with a competitive advantage when occupying new niches (Vicente et al., 2022), which would explain their expression during the earliest stage of infection. High expression during late infection may be necessary for intraspecific interactions, when the fungus is coordinating growth at a high fungal density.

The stress-responsive mitogen-activated protein kinase *FgOS-2* is a key regulator *in F. graminearum* and acts upstream of the ATF/CREB-activating transcription factor *FgAtf-1* **(Table 1)**. Both *FgOS-2* and *FgAtf-1* cluster in module F10. These proteins are involved in broad functions, including secondary metabolite production, sexual reproduction, and stress tolerance (Nguyen et al., 2013). Module F10 also contains two hydrophobin genes, *FgHyd3* and *FgHyd5*. *FgHyd3* is necessary for attachment to hydrophobic surfaces, while both genes are necessary for the production of aerial mycelia **(Table 1)**. These genes are likely to play a crucial role during early infection for surface attachment and are possibly expressed again during the late stage of infection to facilitate the production of aerial mycelia.

The fungal module F10 is correlated with the wheat module W06 ($R = 0.85$, $p = 6 \times 10^{-6}$), which is enriched in protein catabolism (GO:0010498; $p = 1.60 \times 10^{-19}$) and autophagy (GO:0006914; $p = 2.31 \times 10^{-4}$) **(Table 1)**. Autophagy plays a dual role in plant immunity where it is involved in immune signalling and programmed cell death to restrict pathogen spread, but also in response to pathogen induced necrotic cell death (Sertsuvalkul et al., 2022). Therefore, it is likely these genes are expressed during early infection as an

198 immediate immune response and then expressed again in highly colonised tissue for late-
199 stage necrotrophic damage control.

200

201 Wheat genes in module W12 are expressed in response to
202 DON production

203 To validate the correlation between modules F12 and W12 **(Figure 3A)**, expression of wheat
204 genes in the detoxification module W12 in response to *F. graminearum* infection without
205 DON was examined. This was achieved by inoculating wheat plants with either the wild-type
206 *F. graminearum* reference strain PH-1, or the DON deficient *ΔFgtri5* mutant strain generated
207 in the PH-1 background. Expression of three wheat genes was studied, including two
208 phenylalanine ammonia-lyases (*PAL1* and *2*; TraesCS4A02G401300 and
209 TraesCS2D02G377200) which were annotated with the term disease resistance
210 (TO:0000112), and a predicted transmembrane exporter, detoxification gene 16 (*DTX16*;
211 TraesCS5B02G371100).

212 The first two rachis internodes below the point of inoculation (POI) were sampled at 3 days
213 post inoculation (dpi). Levels of *FgActin* cDNA were not significantly different between
214 treatments **(Figure 3B)**. Expression of the three wheat genes from module W12 was
215 significantly lower in the *ΔFgtri5* infected samples relative to wild-type infection **(Figure 3C)**.
216 This indicates that expression of genes in module W12 is correlated with DON production,
217 thereby supporting the correlated co-expression patterns observed between modules of the
218 two networks.

219 Dual co-expression networks as a tool to identify key
220 genes necessary for virulence

To pinpoint *F. graminearum* genes that are necessary for virulence, the stage specific expression patterns of each module was examined **(Figure 4, Figure 4 – figure supplement 1)**. The module F16 is uniquely highly expressed during the earliest stages of infection, with markedly decreased expression at all the other stages of infection. This module is highly correlated to two wheat modules. These are W01 (R = 0.91; $p = 5 \times 10^{-7}$) and W05 (R = 0.85, $p = 2 \times 10^{-5}$). W01 is the largest wheat module and is enriched for defence response genes (GO:0006952; $p = 3.60 \times 10^{-08}$), but also maintenance genes which include photosynthesis (GO:0015979; $p = 4.59 \times 10^{-29}$) and RNA modification (GO:0009451; $p = 1.42 \times 10^{-47}$) GO terms. The wheat module W05 is enriched for disease resistance (TO:0000112, $p = 2.55 \times 10^{-178}$), suggesting that despite the continued symptomless infection the host is already expressing genes for defence. Four genes in module F16 result in reduced virulence when individually deleted. These are *FgNPC1* (sterol trafficking) (Breakspear et al., 2011), *FgSrp2* (mRNA splicing) (Zhang et al., 2020), and the transcription factors *Gzcon7* and *Gzc2h045* (Son et al., 2011) **(Table 1, Supplementary File 2)**. However, no gene deletion mutants exhibiting a loss of pathogenicity or highly reduced virulence phenotype have yet been identified within this module, even though the eigengene expression pattern clearly indicates an association with the early establishment of the fungus in this key host tissue.

To identify genes in F16 that are likely involved in virulence, the 74 genes within this module were examined. Key genes were defined as those exhibiting elevated module membership (MM) within the module, which were also strongly correlated (R > |0.70|) with corresponding wheat modules. Genes with a high MM value have expression patterns closely aligned with the module's overall eigengene expression and are the most representative of the module. The initial candidate gene list was selected by starting with the 15 key genes with the highest MM within the module. Genes were then excluded that were likely to have functional redundancy (i.e. belonged to a gene family or had ancient paralogues within PH-1) to avoid compensatory effects when performing single gene deletion **(Supplementary Table S1)**.

Ultimately, only two genes met these criteria: FGRAMPH1_0T23707 and FGRAMPH1_01T27545. FGRAMPH1_01T27545 has been previously characterised as the Niemann–Pick type C gene (*FgNPC1*). *FgNPC1* is necessary for sterol trafficking, with its deletion resulting in ergosterol accumulation within the vacuole and a reduced virulence upon wheat infection (Breakspear et al., 2011). Orthologue analysis identified that the FGRAMPH1_0T23707 gene was a 1:1 orthologue of Killer-nine resistant 4 (KNR4) in *Saccharomyces cerevisiae* (Martin et al., 1999), therefore the orthologue in *F. graminearum* is henceforth referred to as *FgKnr4.*

FgKnr4, a key gene of module F16, is necessary for establishment of fungal infection

FgKnr4 was deleted using a split hygromycin replacement cassette **(Figure 6 – figure supplement 1 A-B)**. *T. aestivum* cv. Bobwhite was inoculated at anthesis with three independent *ΔFgknr4* transformants. No symptomatic disease progression past the inoculated spikelets was observed with each *ΔFgknr4* transformant **(Figure 5 A-B)**. While the inoculated spikelets developed symptoms, these did not exhibit full bleaching of the spikelet characteristic of FHB infection. Instead, eye-shaped lesions formed akin to those evident following *ΔFgtri5* mutant infection **(Figure 5C)** (Cuzick et al., 2008). Plating of surface sterilised wheat dissected into its constituent parts revealed the absence of fungal growth in un-inoculated spikelets **(Figure 5 – figure supplement 1)**. Nevertheless, browning was noted in the rachis tissue immediately adjacent to the point inoculated spikelet, accompanied by fungal growth. However, this colonisation did not occur past the rachis internode of the 3rd spikelet. These data suggest that, despite entering the rachis, the *ΔFgknr4* mutant is unable to grow through the rachis node tissue and re-enter other spikelets. Microscopic examination revealed a more pronounced plant defence response to *ΔFgknr4* infection. This was characterised by a visibly reduced fungal burden **(Figure 5D)**. Despite highly reduced virulence, DON mycotoxin was detected in the inoculated spikelet

and attached rachis internodes ($\geq$ 0.2 ppm). However, DON was undetectable in the neighbouring uninoculated spikelet (< 0.2 ppm). Complementation of the mutant with wild-type *FgKnr4* restored virulence to wild-type levels **(Figure 5 E-F)**.

FgKnr4 influences cell wall structure, stress resistance, and growth

In vitro growth of *ΔFgknr4* was examined by culturing the fungus on both high or low nutrient agar. In both conditions a decreased growth rate relative to the wild-type was apparent **(Figure 6A, Figure 6 – figure supplement 1 and 2)**. In addition to this, conidia of *ΔFgknr4* appear smaller than wild-type **(Figure 6 – figure supplement 3 A,C)**. Despite these morphological differences *ΔFgknr4* retains the ability to produce perithecia and ascospores, albeit 8 days later than the wild-type **(Figure 6 – figure supplement 3 D-E)**.

Stresses encountered by the fungus during *in planta* infection were mimicked *in vitro* using chemical stressors. *ΔFgknr4* had increased susceptibility to osmotic stress (1.5M NaCl), oxidative stress (H_2O_2), and calcofluor white induced cell wall damage compared to the wild-type and complemented strains **(Figure 6A, Figure 6 – figure supplement 1C & 2C)**. These susceptibilities may be due to changes in the cell wall structure of the *ΔFgknr4* strain. Corroborating this hypothesis, staining for chitin found an irregular deposition of chitin on the *ΔFgknr4* conidial cell wall, specifically along the tips and septa of the conidia **(Figure 6B, Figure 6 – figure supplement 4)**. Furthermore, an irregular cell wall structure was observed upon transmission electron microscopy (TEM) analysis of the *ΔFgknr4* conidia, indicative of an abnormal cell wall composition **(Figure 6C, Figure 6 – figure supplement 5)**.

The *FgKnr4* (F16) module was correlated with the wheat module W05, which exhibits a significant enrichment in the term oxidative stress (TO: 0002657; $p = 3.88 \times 10^{-34}$) that encompasses a total of 1143 genes. Among these genes are two respiratory burst oxidase

299 homologues (RBOH), specifically a predicted homolog of RBOF (TraesCS1A02G347700)
300 and RBOHE (TraesCS5D02G222100), along with predicted catalase homologues, CAT3
301 (TraesCS7B02G473400) (Ghorbel et al., 2023; Yan Zhang et al., 2022), and two CAT4
302 genes (TraesCS5B02G023300, TraesCS5D03G0079400) (Andleeb et al., 2022). W05 is
303 also enriched for sodium content (TO: 0000608; $p = 0.00014$) and salt tolerance (TO:
304 0006001; $p = 3.00 \times 10^{-18}$). The necessity of a functional *FgKnr4* gene in oxidative and
305 osmotic stress tolerance **(Figure 6A, Figure 6 – figure supplement 1C & 2C)** suggests that
306 *FgKnr4* is critical during this early infection stage, where the fungus confronts hydrogen
307 peroxide and osmotic stress induced by the plant.

308 The involvement of *FgKnr4* in cell wall metabolism was further studied by examining its
309 effect on the cell wall integrity pathway (CWI). The fungal CWI pathway is triggered in
310 response to various stresses (e.g. oxidative stress, osmotic pressure, cell wall damage)
311 (Dichtl et al., 2016) and in *F. graminearum* is activated through the phosphorylation of the
312 MAP-kinase (MAPK) *FgMGV1* (Hou et al., 2002; Yun et al., 2014). A Western blot was run
313 on mycelium samples grown with and without a cell wall stress (calcofluor white).
314 Constitutive activation of MGV1 in the absence of stress and increased phosphorylation
315 under stress was observed in *ΔFgknr4* when compared to the wild-type (**Figure 6D-E**). This
316 finding is consistent with previous observations in *S. cerevisiae* (Martin-Yken et al., 2003).
317 This reinforces the biological function of *FgKnr4*, suggesting an involvement in fungal stress
318 responses and cell wall morphology in *F. graminearum*.

319 The orthologous gene in wheat pathogen *Zymoseptoria*
320 *tritici* is also important for cell wall integrity and virulence
321 on wheat

322 Analysis of the Knr4 protein conservation found that orthologues were highly distributed
323 across the Dikarya, occurring in both Ascomycota and Basidiomycota **(Figure 7).** Notably,

no orthologues of the gene were found in other Eukaryotes, highlighting its specificity to the fungal lifestyle. This high level of conservation across fungi suggests that phenotypes observed in *F. graminearum* may also be conserved in other economically significant pathogenic fungi.

The orthologous *KNR4* gene in another wheat fungal pathogen *Z. tritici* (*ZtKnr4*, Mycgr3G105330) was disrupted to test for conserved gene function. Despite the phylogenetic distance between the two fungi, the *FgKnr4* and *ZtKnr4* proteins share 43.5% pairwise identity. Mirroring the phenotype observed in *F. graminearum,* reduced virulence (chlorosis but limited to no necrosis) was observed when wheat leaves were inoculated with *ΔZtknr4* **(Figure 8A)**. In addition to this the *ΔZtknr4* mutant was susceptible to calcofluor white induced cell wall stress and exhibited reduced hyphal branching **(Figure 8B-C)**. These results highlight the potential of employing the *Fusarium*-wheat dual co-expression approach to gain insights into fungal-plant interactions, both within *Fusarium* species and across the fungal kingdom.

Discussion

The generated dual *F. graminearum*-wheat co-expression network was successfully used to identify a gene necessary for virulence. By analysing stage-specific modules of infection, module F16 was identified, which exhibited high gene expression levels during the symptomless stage of FHB infection. Within this module, the gene *FgKnr4* was found to have a high module membership score, indicating its central role in the module. Experimental validation showed that *FgKnr4* is essential for responding to chemical compounds that induce cell wall stress, early establishment of *in planta* infection, and subsequent disease progression in wheat spikes. Similarly, the deletion of *Knr4* in another pathogenic species, namely *Z. tritici* resulted in a reduced virulence phenotype in leaves and displayed a comparable cell wall stress phenotype. This highlights the utility of pathogen-

host co-expression network analysis in identifying conserved virulence genes across wheat fungal pathogens.

The predictions from the WGCNA were validated for the F12-W12 correlation through the experimental confirmation of the co-regulation of the Fusarium trichothecene mycotoxin and wheat detoxification genes during infection. For Fusarium, module F12 was of exceptionally high interest because of its positioning specifically at the transition between the late symptomless stage and the early symptomatic stage. For wheat genes in the correlated module W12, the studied genes included two phenylalanine ammonia-lyases (*PAL1* and *2)* along with a predicted detoxifying efflux transporter (*TaDTX16*). Although *TaPAL1* and *2* have not been previously studied for their direct involvement in disease resistance in the wheat - Fusarium interaction, the *PAL* gene family is known to be associated with disease resistance and other phenotypes (Duba et al., 2019). In multiple plant species (including *Arabidopsis,* pepper (*Capsicum annuum)*, and rice (*Oryzae sativa)*), *PAL* is induced in response to biotic and abiotic stresses, which includes pathogen induced stress, (Hahlbrock and Scheel, 1989; Kim and Hwang, 2014; Tonnessen et al., 2015; Chen et al., 2017) and in numerous genetically incompatible host-pathogen interactions mediated by cognate R-Avr proteins including responses to fungi (Maher et al., 1994; Ramaroson et al., 2022). *TaDTX16* is part of the multidrug and toxic compound extrusion (MATE) gene family and was named after its orthologue in *Arabidopsis thaliana* (Li et al., 2002). DTX/MATE take part in heavy metal and lethal compound detoxification in plants and could be involved in mycotoxin detoxification (Perincherry et al., 2019). Previously, a wheat DTX gene was reported to be highly expressed in resistant cultivars of wheat compared to a susceptible wheat cultivar when infected with *F. graminearum* (Pan et al., 2018). *TaDTX16* is located on chromosome 5BL within an interval harbouring a resistance QTL for defence against the necrotrophic fungal disease Septoria nodorum blotch (Li et al., 2021).

The characterisation of *FgKnr4*, underscores the importance of identifying genes necessary for full virulence through gene expression studies. This approach is essential because

predicting the pathogenic potential of Fusarium species based solely on comparative genomics is challenging due to the absence of significant differences in secreted effector proteins, carbohydrate-active enzymes, or gene repertoires between pathogenic and endophytic strains of Fusarium and Fusarioid species (Hill et al., 2022). *FgKnr4* was investigated further for its multifaceted roles in growth, stress response, and cell wall integrity. Supporting previous findings in *Fusarium asiaticum* (Yu Zhang et al., 2022), this study demonstrates that *FgKnr4* is involved in regulating growth rate, conidial spore morphology, and sensitivity to osmotic and oxidative stresses, as well as virulence and cell wall stress tolerance in *F. graminearum*. Moreover, this study establishes that KNR4 influences the well-studied cytoplasmically located Mgv1 cell wall integrity (CWI) MAPK pathway (Xu et al., 2022), resulting in visible abnormalities of the conidial cell wall **(Figure 6C, Figure 6 – figure supplement 5)**. The cell wall integrity pathway in *F. graminearum* is well-characterised, with each MAP-kinase in the cascade having been identified, studied, and shown to have roles in virulence and/or asexual and sexual spore formation (Hou et al., 2002; Jenczmionka et al., 2003; Urban et al., 2003; Zheng et al., 2012). Through experimental validation, our findings reveal an additional layer of control within the *F. graminearum* cell wall integrity pathway mediated by *FgKnr4*. This discovery contributes to and further improves our understanding of the regulatory mechanisms governing cell wall integrity in *F. graminearum*. This new finding also, offers the first insights into the regulatory effects of KNR4 in a filamentous fungus. This additional knowledge aid the development of novel strategies to mitigate losses caused by FHB disease and DON contamination.

Z. tritici possesses one of the most expansive publicly available eukaryotic pangenomes, with approximately 42% of its genes categorised as accessory (Plissonneau et al., 2018). *ZtKnr4* is part of the core *Z. tritici* genome of the European pangenome (Chen et al., 2023) and designated within the core orthogroup OG0008320 within the global (Europe, Asia, North and South America, Australia and Africa) pangenome (Badet et al., 2020). Given the highly variable nature of accessory chromosomes in *Z. tritici*, the assignment of *ZtKnr4* to the

core genome in two separate pangenomic analyses underscores its importance in fungal physiology. *ZtKnr4* is also expressed throughout the wheat infection process (Rudd et al., 2015). Disruption of the gene resulting in a reduced virulence phenotype reinforces the potential of *ZtKnr4* as a candidate target for fungicide development, emphasising its significance in combating *Z. tritici* infections and mitigating agricultural losses. Despite the ever present global importance of STB disease for many decades (Dean et al., 2012; Savary et al., 2019) *Z. tritici* has far fewer functionally characterised genes, with only 99 genes with a characterised phenotype within the Pathogen Host-Interactions database and only 50 of these genes associated with a loss in pathogenicity or reduced virulence (Urban et al., 2022; Cuzick et al., 2023). The reduced virulence phenotype observed in the *ZtKnr4* mutant therefore marks a valuable contribution to the characterisation of one of the >9000 core genes across the known *Z. tritici* pangenomes (Badet et al., 2020; Chen et al., 2023).

The high conservation and exclusivity of KNR4 within the fungal kingdom, combined with its absence in other eukaryotes and its conserved function across related species, suggest that KNR4 could be an ideal target for intervention. This could be achieved through the development of chemical fungicides that disrupt the protein's function (Aamir et al., 2018) or through the application of RNA interference techniques (Cools and Hammond-Kosack, 2013; Machado et al., 2018; Mann et al., 2023). Stricter EU regulation of chemicals suitable for fungicide use in agricultural, medical and/or veterinary settings (European Commission, 2022), combined with significant losses in fungicide efficacy due to the evolution of pathogen populations means there is a pressing need to identify new target sites for control. Therefore, this research not only advances our understanding of fungal virulence mechanisms but also offers promising directions for the development of effective strategies for disease control in agriculture.

Materials and Methods

Gene co-expression network analysis

RNAseq reads from Dilks et al. (2019) were provided by Dr Neil Brown (European Nucleotide Archive: PRJEB75530). Read quality was assessed with FastQC v. 0.11.9 (Andrews, 2010). Reads were mapped to a combined Fusarium – wheat genome, consisting of v. 5 of the *Fusarium graminearum* PH-1 genome (King et al., 2017) and the high confidence (HC) transcripts of the v. 2.1 of the International Wheat Genome Sequencing Consortium (IWGSC) *Triticum aestivum* genome (Zhu et al., 2021). Genome indexing and read alignment were performed using STAR aligner 2.7.8a. Soft clipping was turned off to prevent reads incorrectly mapping to similar regions of the highly duplicated hexaploid wheat genome. Reads were filtered using the filterByExpr function part of the R package Edge R v.3.32.1 (Robinson et al., 2010). Counts were normalised separately for fungal and wheat reads by performing a variance stabilising transformation (VST) using the DESeq2 v 1.30.1 R package (Love et al., 2014) in R (v4.0. 2, https://www.r-project.org/).

The VST normalised counts were filtered to remove any excessive missing values using the function goodSamplesGenesMS in the WGCNA R package (Langfelder and Horvath, 2008). Standard methods were implemented to generate the network using the WGCNA R package, with the following parameters. A signed-hybrid network was constructed using the filtered counts. The soft thresholding power (β) was uniquely selected per network according to scale free model criteria (Zhang and Horvath, 2005), where β = 9 for the fungal network and β = 18 for the wheat network **(Figure 2 – figure supplement 2)**. A deepSplit of 3 was paired with a standard cutheight of 0.25. A minimum module size of 50 was selected to minimise potential transcriptional noise when assigning modules using smaller datasets (Oldham, 2014; Walsh et al., 2016). The function multiSetMEs from the WGCNA package was used to calculate module eigengene expression. Module eigengenes with similar expression profiles were then merged.

Module quality and preservation was calculated using the function modulePreservation present in the WGCNA R package (Langfelder and Horvath, 2008; Langfelder et al., 2011). When calculating module preservation, the original wheat or fungal network was considered

457 the reference network. Then 50 different test networks were created, each built upon
458 randomly resampling (with replacement) a proportion of samples from the original dataset.
459 The average preservation metrics (i.e. Z-score) between the original network and the 50 test
460 networks was calculated for both the fungal and wheat networks.

461 Module Enrichment an Annotation

462 Gene ontology (GO) annotations of the v. 5 PH-1 genome (GCA_900044135.1) were
463 generated using Blast2GO v .5 (Götz et al., 2008). Enrichment was calculated using a
464 background set of all genes present in the fungal network. GO annotations for the IWGSC
465 v.2.1 genome were provided by Dr Keywan Hassani-Pak of the KnetMiner team (Hassani-
466 Pak et al., 2021). This was generated by performing a BLASTx search on the NCBI nb
467 database using DIAMOND v 2.0.13-GCC-11.2.0 (Buchfink et al., 2015), then Blast2GO v.5
468 was used to annotate the BLAST hits with GO terms. GO term enrichment was calculated for
469 each high level GO ontology (Biological Process, Molecular Function and Cellular
470 Component) using the R package topGO v 2.46.0 (Alexa and Rahnenfuhrer, 2009).

471 Plant Trait Ontology (TO) (Cooper et al., 2024) enrichment analysis was performed using
472 annotations derived from the KnetMiner knowledge graph (release 51) for wheat (Hassani-
473 Pak et al., 2021) and KnetMiner datasets and enrichment analysis notebooks are available
474 at https://github.com/Rothamsted/knetgraphs-gene-traits/. Predicted effectors were
475 determined using EffectorP v.3.0 (Sperschneider and Dodds, 2022). Alongside this,
476 predictions to identify extracellularly localised genes were done using SignalP v6.0 (Teufel et
477 al., 2022). Custom *F. graminearum* gene set enrichment of the network modules was
478 calculated by performing a Fisher's exact test using all the genes in the fungal network as
479 the background gene set. A BH correction was calculated for both GO and custom
480 enrichments (Benjamini and Hochberg, 1995). Modules were deemed significantly enriched
481 if P-corr < 0.05.

Gene lists included in GSEA consisted of predicted secreted effector proteins, alongside known gene families associated with virulence, such as biological metabolite clusters (BMCs) (Sieber et al., 2014), polyketide synthases (Gaffoor et al., 2005), protein kinases (Wang et al., 2011) and transcription factors (Son et al., 2011). Due to their well-established importance in *F. graminearum* pathology, a separate enrichment for genes of the *TRI* gene cluster was also performed.

Annotation from PHI-base was obtained by mapping genes to version PHI-base (v4.16) annotation using UniProt gene IDs and any through Decypher Tera-Blast™ P (TimeLogic, Inc. Carlsbad, California, USA) (E-value = 0) against the PHI-base (v4.16) BLAST database (Cuzick et al., 2023).

Fungal material and growth conditions

F. graminearum strains were cultured and conidia prepared as previously described (Brown et al., 2010). Fungal strains were grown for 4 days on nutrient-rich potato dextrose agar (PDA), nutrient-poor synthetic nutrient agar (SNA; 0.1% KH2PO4, 0.1% KNO3, 0.1% MgSO4·7H2O, 0.05% KCL, 0.02% glucose, 0.02% sucrose and 2% agar) and PDA with different cell wall stresses. Plates were point inoculated with 20 µl of 4-fold dilution series starting with 1 x 10^6 conidia/ml. For the growth rate assay, fungi were grown on PDA and images were taken at 7 days. Surface sterilisation of wheat spikes was performed by submerging single wheat spikelets in 1/8 diluted thin bleach for 3 min, followed by three washes with distilled H2O. Dissection was done using a razor blade to separate the point inoculated spikelets and adjacent spikelets **(Figure 5 – supplement 1)**. Wheat tissue was placed on SNA and images taken after 3-day incubation at room temperature in the dark. Perithecia induction was achieved as described in Cavinder et al. (2019). All plate images were taken using an Olympus OM-D camera using a 60mm ED M.Zuiko macro lens. Conidia and ascospore images were taken using the Axiomager 2 (Zeiss, Oberkochen, Germany)

under brightfield illumination. Conidia lengths (N=50) and perithecia heights (N= 50) were measured using ImageJ (Schneider et al., 2012).

Fusarium graminearum genetic manipulations

The *FgKnr4* gene was deleted through split marker-mediated transformation targeted fungal replacement with the hygromycin by homologous recombination (Yu et al., 2004). *F. graminearum* gene deletion construct assembly and fungal transformation was preformed following methods outlined in King et al., 2017. Primers were designed for the fusion of the 5' and 3' constructs using the NEBbuilder® Assembly Tool v.1 (https://nebuilderv1.neb.com/). Using the Gibson Master Mix (New England Biolabs, UK) the paired split marker fragments were ligated into the pGEM® - T Easy Vector (Promega, UK) then transformed into DH5α competent *Escherichia coli* (C2987H, New England Biolabs, UK) following standard manufacturer protocol. Diagnostic PCRs done using DreamTaq polymerase (ThermoFisher, UK) and standard cycling conditions. For the single gene deletion, three separate transformants two diagnostic PCRs detect the presence of the replacement cassette flanks (P3-4,P5-6) and the absence of the wild-type gene (P1-2) **(Figure 6 – figure supplement 1 A-B)**. Complementation was performed following the protocol developed by Darino et al. (2024). Diagnostic PCRs for the complemented strains involved amplification of insertion cassette flanks (P7-8; P9-10), absence of short 868 bp empty intragenic locus amplicon (P11-P12), and test for heterozygosity of geneticin gene (P13-P14) **(Figure 6 – figure supplement 2 A-B**. Full primer list available in Supplementary File 3.

Wheat host inoculation

The susceptible spring wheat (*T. aestivum*) cultivar, Bobwhite, was grown to anthesis. The 5th and 6th spikelets from the top of the wheat spike were inoculated on both sides using 5 µl of 5 x 10^5 conidia/ml. Each treatment included 10 separate wheat plants (N=10). After inoculation, plants were kept in a high humidity chamber for 48 h in the dark. Disease

progression was documented every two days by scoring the number of bleached spikelets. At 15 dpi wheat spikelet tissue and adjacent rachis internode was separated, frozen in liquid nitrogen, and ground to form a fine powder. The presence of DON mycotoxin was assessed using the Deoxynivalenol (DON) Plate Kit (Cat. 20-0016, Beacon Analytical Systems Inc., USA) following standard protocol. Experiment was replicated with three biological replicates per treatment (N=3). All plate images were taken using an Olympus OM-D camera using a 60mm ED M.Zuiko macro lens.

For resin dissection microscopy wheat cv. Bobwhite was inoculated 7th and 8th true spikelets from base inoculated each side w/ 5x10^{5} spores /ml in dH2O. After inoculation, plants were kept in a high humidity chamber for 48 h in the dark. Lemma tissues were excised from infected spikelets at 7 dpi, fixed in a 4% paraformaldehyde, 2.5% glutaraldehyde solution with 0.05M Sorensen's phosphate buffer (NaH2PO4:Na2HPO4, pH 7.0). Samples then underwent 3 further buffer washes, a subsequent ethanol dehydration protocol (0-100% EtOH) over 48hrs and LR White resin (TAAB) infiltration diluted with dry ethanol at increasing ratios (1:4, 2:3, 3:2, 4:1, 100%). Samples were inserted into capsules (TAAB) and resin polymerised at 60°C for 16 hours in a nitrogen oven (TAAB). Ultra-thin 1µm sections of samples were cut on an ultramicrotome (Reichert-Jung, Ultracut) with glass knives, placed onto glass polysine slides (Sigma Aldrich, UK), dried at 70°C, stained with 0.1% (w/v) Toluidine Blue O and mounted in DPX mounting medium (Fisher Scientific). Stained sections were imaged on a Zeiss Axioimager (Axiocam 512 color, Zeiss, Jena, Germany) light microscope with brightfield illumination.

Gene expression of module W12 genes

Bobwhite wheat plants were point inoculated at anthesis with either wild-type PH-1, *ΔFgtri5* or water only (Mock) following the protocol outlined in Dilks et al., (2019). Each experimental condition was replicated in triplicate, with each replicate deriving from three pooled

independent wheat spikes. Tissues from rachis internodes 1 and 2 were sampled and frozen in liquid nitrogen at 3 dpi. Frozen samples were ground and RNA was extracted using the Monarch® Total RNA Miniprep Kit (NEB, UK). Equal amounts of RNA was used to synthesise cDNA with Revertaid cDNA synthesis kit (ThermoScientific, UK). PowerTrack™ SYBR Green Master Mix (ThermoScientific, UK) was used for qPCR. Each biological replicate included three technical replicates.

Western blot

A 200 ul aliquot of a *F. graminearum* spore solution (1 x 10^6 spores/ml) was added to 10 ml potato dextrose broth (PDB) at 27 °C. Calcofluor white was added to a concentration of 200 µg/ml after 24 h of incubation at 180 rpm. Twenty-four hours after the addition of the stress, mycelium was harvested, flash frozen and freeze dried To lyse the samples Y-PER Yeast Protein Extraction Reagent (ThermoScientific, UK) was added to the freeze-dried samples at 1.5 ml per 150 mg tissue, alongside Protease Inhibitor Cocktail (100x) (ThermoScientific, UK). Samples were lysed using the FastPrep-24™machine for 20s (MP Biomedical, USA). The supernatant was mixed with 5xSDS loading buffer (National Diagnostics, USA).

Equal amounts of protein (60 µg) were resolved on 8% SDS-PAGE gels (Mini-PROTEAN, Bio-Rad, UK) and transferred on to a nitrocellulose membrane. Immunoblots were performed by standard procedures using the Phospho-p44/42 MAPK (Erk1/2) (cat. #4370) and p44/42 MAPK (Erk1/2) (cat. #9102S) (Cell Signalling Technologies, USA) antibodies at their specified dilutions. The blots were developed using ECL Plus Western Blotting Detection Kit and images were acquired using Odyssey Imaging System (LI-COR Biosciences Ltd, Cambridge, UK).

Microscopic examination of cell wall

Spores were induced by plating 200 µl of frozen spores (1 x 10^6) PDA and incubating plates in for 3 days. For conventional transmission electron microscopy (TEM), fresh spores were

harvested the same day from the PDA plates and pellets were fixed in a mixture of 2.5% glutaraldehyde and 4% Paraformaldehyde in Sorenson's buffer (SB) at pH 7.2 overnight at 4°C. The samples were rinsed in SB and post fixed in 1% osmium tetroxide for 60 min at room temperature. The samples were dehydrated for 10 min per step into increasing concentrations of alcohol (30%, 50%, 70%, 90% and final 100%×3). Subsequently, the pure alcohol was replaced with propylene oxide, and the specimens were infiltrated with increasing concentrations (25%, 50%, 75%, and 100%) of Spurr resin mixed with propylene oxide for a minimum of 2 hr per step. The samples were embedded in pure, fresh Spurr resin and polymerised at 60 °C for 24 hr. Ultrathin sections (70 nm) were cut using an ultramicrotome (Leica UC7, Germany) and post-stained, first with uranyless for 1 min and then with Reynolds lead citrate for 2 min at room temperature, prior to observation using a Transmission Electron Microscope (Jeol 2100plus, UK) operated at 200 kV.

F. graminearum spore solution (1 x 10^6 spores/ml) was stained with Wheat Germ Agglutinin, Alexa Fluor™ 488 Conjugate (WGA) (10 µg/ml) for 10 minutes each. Samples were washed three times in sterile distilled water after staining. A ZEISS 780 Confocal Laser Scanning Microscope (ZEISS, Germany) was used to image spores.

Phylogenetic tree construction

Eggnogmapper-v5 (Huerta-Cepas et al., 2019) was used to map *FgKnr4* to the eggnog Orthologue Group (OG) ENOG502QTAZ and generate the phylogenetic tree. The tree was visualised and annotated using the interactive Tree of Life (iTOL) software (Letunic and Bork, 2024).

Functional characterisation of the *Knr4* orthologue in *Z. tritici*

Separate analyses using Orthologous Matrix (OMA) (Altenhoff et al., 2021) and Eggnogmapper (Huerta-Cepas et al., 2019) identified a single orthologous sequence in the

genome of *Z. tritici* isolate IPO323 (https://fungi.ensembl.org/Zymoseptoria_tritici/Info/Index) (Goodwin et al., 2011). The gene has a Rothamsted gene model Id of ZtritIPO323_04g12347 (King et al., 2017; Chen et al., 2023) and is present on Chromosome 8 at start position 230142 bp. This maps to Mycgr3P105330 in the current genome call on Joint Genome Institute (JGI) Mycocosm (Goodwin et al., 2011).

Agrobacterium-mediated fungal transformation (Motteram et al., 2011) was performed to generate a series of independent gene disruption mutants of *ZtKnr4*. Flanking sequences and the hygromycin resistance gene were amplified from either genomic DNA or from plasmid pCHYG and using Phusion polymerase (NEB, UK). Fragments were gel purified using QIAquick Gel Extraction Kit (QIAGEN, UK) and assembled into the backbone (Kpn1 and BamH1 digested) of pCHYG by Gibson Assembly (NEB, UK). The resulting plasmids were transformed into Agrobacterium strain AgL1 and fungal transformation of isolate IPO323 was performed as per standard protocols (Motteram et al., 2011). Positive transformants containing a disrupted *ZtKnr4* gene were identified by diagnostic PCR **(Figure 8 – figure supplement 1)**. Complementation of validated *ZtKnr4* mutants was performed through Agrobacterium-mediated transformation with plasmid pCGEN (digested EcoR1 and Kpn1) containing the native gene plus 1 kb upstream (5') and 300 bp (3') downstream genomic DNA, amplified by Phusion PCR (NEB, UK).

Attached leaf virulence assays were performed as per standard protocols (Keon et al., 2007) on wheat cultivar Riband. Leaf blades (N = 3) were inoculated with spore suspensions of 1 x 10^6 spores / ml in sterile water + 0.05% v:v Tween 20. Final disease assessments were made 21 days after inoculation. *In vitro* hyphal growth assays were performed following droplet inoculation of spore suspensions onto 1% Tap Water Agar (TWA) plates. Hyphal growth morphologies were determined by light microscopy and / or photography 10 days after inoculation. Calcofluor white sensitivity assays were performed to ascertain changes in cell wall strength. For this, spore suspensions were inoculated onto YPD agar (Formedium, UK) plates (control) and onto YPD agar plates containing 200 µg / ml calcofluor white. Plates

were incubated at RT for 8 days and then growth was monitored and recorded by photography. Images of *ZtKnr4 in planta* and *in vitro* experiments were taken with a Nikon D3200 camera.

Data availability

Full lists of all genes clustered into modules is available on https://github.com/erikakroll/Fusarium-wheat_WGCNA. This includes comma separated value (CSV) files for all genes in each module for both fungal and wheat modules, which are annotated with Module Membership (MM) values, mean FPKM values, InterPro annotation, Gene Ontology annotation, and Trait Ontology annotation. Text documents containing module eigengene values and gene module assignments are also available on the repository.

References

Aamir M, Singh VK, Dubey MK, Meena M, Kashyap SP, Katari SK, Upadhyay RS, Umamaheswari A, Singh S. 2018. In silico Prediction, Characterization, Molecular Docking, and Dynamic Studies on Fungal SDRs as Novel Targets for Searching Potential Fungicides Against Fusarium Wilt in Tomato. *Front Pharmacol* **9**:1038. doi:10.3389/fphar.2018.01038

AHDB. 2023. Risk assessment for fusarium mycotoxins in wheat | AHDB. https://ahdb.org.uk/mycotoxins

Alexa A, Rahnenfuhrer J. 2009. Gene set enrichment analysis with topGO. *Bioconductor Improv* **27**:1–26.

Altenhoff AM, Train C-M, Gilbert KJ, Mediratta I, Mendes de Farias T, Moi D, Nevers Y, Radoykova H-S, Rossier V, Warwick Vesztrocy A, Glover NM, Dessimoz C. 2021. OMA orthology in 2021: website overhaul, conserved isoforms, ancestral gene order and more. *Nucleic Acids Res* **49**:D373–D379. doi:10.1093/nar/gkaa1007

Andleeb T, Knight E, Borrill P. 2022. Wheat NAM genes regulate the majority of early monocarpic senescence transcriptional changes including nitrogen remobilization genes. *G3 GenesGenomesGenetics* **13**. doi:10.1093/g3journal/jkac275

Andrews S. 2010. FastQC: a quality control tool for high throughput sequence data.

667 Armer V, Kroll, Erika, Darino, Martin, Urban, Martin, Smith, Dan, Hammond-Kosack
668 K. 2024. Navigating the Fusarium species complex: Host-Range Plasticity and
669 Genome Variations. Re-submitted post peer review for special issue in Fungal
670 Biology.
671 Arunachalam C, Doohan FM. 2013. Trichothecene toxicity in eukaryotes: Cellular
672 and molecular mechanisms in plants and animals. *Toxicol Lett* **217**:149–158.
673 doi:10.1016/j.toxlet.2012.12.003
674 Badet T, Oggenfuss U, Abraham L, McDonald BA, Croll D. 2020. A 19-isolate
675 reference-quality global pangenome for the fungal wheat pathogen
676 *Zymoseptoria tritici*. *BMC Biol* **18**:12. doi:10.1186/s12915-020-0744-3
677 Bai G, Su Z, Cai J. 2018. Wheat resistance to Fusarium head blight. *Can J Plant*
678 *Pathol*.
679 Benjamini Y, Hochberg Y. 1995. Controlling the False Discovery Rate: A Practical
680 and Powerful Approach to Multiple Testing. *J R Stat Soc Ser B Methodol*
681 **57**:289–300. doi:10.1111/j.2517-6161.1995.tb02031.x
682 Breakspear A, Pasquali M, Broz K, Dong Y, Kistler HC. 2011. Npc1 is involved in
683 sterol trafficking in the filamentous fungus *Fusarium graminearum*. *Fungal*
684 *Genet Biol FG B* **48**:725–730. doi:10.1016/j.fgb.2011.03.001
685 Brown JKM, Chartrain L, Lasserre-Zuber P, Saintenac C. 2015. Genetics of
686 resistance to *Zymoseptoria tritici* and applications to wheat breeding. *Fungal*
687 *Genet Biol* **79**:33–41. doi:10.1016/j.fgb.2015.04.017
688 Brown NA, Bass C, Baldwin TK, Chen H, Massot F, Carion PWC, Urban M, van de
689 Meene AML, Hammond-Kosack KE. 2011. Characterisation of the *Fusarium*
690 *graminearum*-Wheat Floral Interaction. *J Pathog* **2011**:e626345.
691 doi:10.4061/2011/626345
692 Brown NA, Evans J, Mead A, Hammond-Kosack KE. 2017. A spatial temporal
693 analysis of the *Fusarium graminearum* transcriptome during symptomless and
694 symptomatic wheat infection. *Mol Plant Pathol* **18**:1295–1312.
695 doi:10.1111/mpp.12564
696 Brown NA, Urban M, van de Meene AML, Hammond-Kosack KE. 2010. The infection
697 biology of *Fusarium graminearum*: defining the pathways of spikelet to
698 spikelet colonisation in wheat ears. *Fungal Biol* **114**:555–571.
699 doi:10.1016/j.funbio.2010.04.006
700 Buchfink B, Xie C, Huson DH. 2015. Fast and sensitive protein alignment using
701 DIAMOND. *Nat Methods* **12**:59–60. doi:10.1038/nmeth.3176
702 Buerstmayr M, Steiner B, Buerstmayr H. 2020. Breeding for Fusarium head blight
703 resistance in wheat—Progress and challenges. *Plant Breed* **139**:429–454.
704 doi:10.1111/pbr.12797
705 Cai H, Yu N, Liu Y, Wei X, Guo C. 2022. Meta-analysis of fungal plant pathogen
706 *Fusarium oxysporum* infection-related gene profiles using transcriptome
707 datasets. *Front Microbiol* **13**:970477. doi:10.3389/fmicb.2022.970477
708 Cavinder B, Sikhakolli U, Fellows KM, Trail F. 2012. Sexual Development and
709 Ascospore Discharge in *Fusarium graminearum*. *J Vis Exp JoVE* 3895.
710 doi:10.3791/3895
711 Chen H, King R, Smith D, Bayon C, Ashfield T, Torriani S, Kanyuka K, Hammond-
712 Kosack K, Bieri S, Rudd J. 2023. Combined pangenomics and transcriptomics
713 reveals core and redundant virulence processes in a rapidly evolving fungal
714 plant pathogen. *BMC Biol* **21**:24. doi:10.1186/s12915-023-01520-6
715 Chen Y, Li F, Tian L, Huang M, Deng R, Li X, Chen W, Wu P, Li M, Jiang H, Wu G.
716 2017. The Phenylalanine Ammonia Lyase Gene LjPAL1 Is Involved in Plant

717 Defense Responses to Pathogens and Plays Diverse Roles in *Lotus*
718 *japonicus*-Rhizobium Symbioses. *Mol Plant Microbe Interact* **30**:739–753.
719 doi:10.1094/MPMI-04-17-0080-R
720 Cools HJ, Hammond-Kosack KE. 2013. Exploitation of genomics in fungicide
721 research: current status and future perspectives. *Mol Plant Pathol* **14**:197–
722 210. doi:10.1111/mpp.12001
723 Cooper L, Elser J, Laporte M-A, Arnaud E, Jaiswal P. 2024. Planteome 2024
724 Update: Reference Ontologies and Knowledgebase for Plant Biology. *Nucleic*
725 *Acids Res* **52**:D1548–D1555. doi:10.1093/nar/gkad1028
726 Cuzick A, Seager J, Wood V, Urban M, Rutherford K, Hammond-Kosack KE. 2023.
727 A framework for community curation of interspecies interactions literature.
728 *eLife* **12**:e84658. doi:10.7554/eLife.84658
729 Cuzick A, Urban M, Hammond-Kosack K. 2008. *Fusarium graminearum* gene
730 deletion mutants map1 and tri5 reveal similarities and differences in the
731 pathogenicity requirements to cause disease on Arabidopsis and wheat floral
732 tissue. *New Phytol* **177**:990–1000. doi:10.1111/j.1469-8137.2007.02333.x
733 Darino M, Urban M, Kaur N, Machado Wood A, Grimwade-Mann M, Smith D,
734 Beacham A, Hammond-Kosack K. 2024. Identification and functional
735 characterisation of a locus for target site integration in *Fusarium*
736 *graminearum*. *Fungal Biol Biotechnol* **11**:2. doi:10.1186/s40694-024-00171-8
737 de Chaves MA, Reginatto P, da Costa BS, de Paschoal RI, Teixeira ML, Fuentefria
738 AM. 2022. Fungicide Resistance in *Fusarium graminearum* Species Complex.
739 *Curr Microbiol* **79**:62. doi:10.1007/s00284-021-02759-4
740 Dean R, Van Kan JAL, Pretorius ZA, Hammond-Kosack KE, Di Pietro A, Spanu PD,
741 Rudd JJ, Dickman M, Kahmann R, Ellis J, Foster GD. 2012. The Top 10
742 fungal pathogens in molecular plant pathology. *Mol Plant Pathol* **13**:414–430.
743 doi:10.1111/j.1364-3703.2011.00783.x
744 Desmond OJ, Manners JM, Stephens AE, Maclean DJ, Schenk PM, Gardiner DM,
745 Munn AL, Kazan K. 2008. The Fusarium mycotoxin deoxynivalenol elicits
746 hydrogen peroxide production, programmed cell death and defence
747 responses in wheat. *Mol Plant Pathol* **9**:435–445. doi:10.1111/j.1364-
748 3703.2008.00475.x
749 Dichtl K, Samantaray S, Wagener J. 2016. Cell wall integrity signalling in human
750 pathogenic fungi. *Cell Microbiol* **18**:1228–1238. doi:10.1111/cmi.12612
751 Dilks T, Halsey K, De Vos RP, Hammond-Kosack KE, Brown NA. 2019. Non-
752 canonical fungal G-protein coupled receptors promote Fusarium head blight
753 on wheat. *PLoS Pathog* **15**:e1007666. doi:10.1371/journal.ppat.1007666
754 Duba A, Goriewa-Duba K, Wachowska U, Głowacka K, Wiwart M. 2019. The
755 Associations between Leaf Morphology, Phenylalanine Ammonia Lyase
756 Activity, Reactive Oxygen Species, and Fusarium Resistance in Selected
757 Species of Wheat with Different Ploidy Levels. *Plants* **8**:360.
758 doi:10.3390/plants8100360
759 Dyer RB, Plattner RD, Kendra DF, Brown DW. 2005. *Fusarium graminearum* TRI14
760 is required for high virulence and DON production on wheat but not for DON
761 synthesis in vitro. *J Agric Food Chem* **53**:9281–9287. doi:10.1021/jf051441a
762 EFSA. 2017. Risks to human and animal health related to the presence of
763 deoxynivalenol and its acetylated and modified forms in food and feed |
764 EFSA. https://www.efsa.europa.eu/en/efsajournal/pub/4718
765 Estep LK, Torriani SFF, Zala M, Anderson NP, Flowers MD, McDonald BA, Mundt
766 CC, Brunner PC. 2015. Emergence and early evolution of fungicide resistance

767 in North American populations of *Zymoseptoria tritici*. *Plant Pathol* **64**:961–
768 971. doi:10.1111/ppa.12314
769 European Commission. 2022. Farm to Fork.
770 https://ec.europa.eu/commission/presscorner/detail/en/qanda_22_3694
771 European Commission. 2006. On the presence of deoxynivalenol, zearalenone,
772 ochratoxin A, T-2 and HT-2 and fumonisins in products intended for animal
773 feeding. *Off J Eur Union*, L 229/7.
774 Fones H, Gurr S. 2015. The impact of Septoria tritici Blotch disease on wheat: An EU
775 perspective. *Fungal Genet Biol* **79**:3–7. doi:10.1016/j.fgb.2015.04.004
776 Gaffoor I, Brown DW, Plattner R, Proctor RH, Qi W, Trail F. 2005. Functional
777 analysis of the polyketide synthase genes in the filamentous fungus
778 *Gibberella zeae* (anamorph *Fusarium graminearum*). *Eukaryot Cell* **4**:1926–
779 1933. doi:10.1128/EC.4.11.1926-1933.2005
780 Ghorbel M, Zribi I, Besbes M, Bouali N, Brini F. 2023. Catalase Gene Family in
781 Durum Wheat: Genome-Wide Analysis and Expression Profiling in Response
782 to Multiple Abiotic Stress Conditions. *Plants* **12**:2720.
783 doi:10.3390/plants12142720
784 Goodwin SB, M'barek SB, Dhillon B, Wittenberg AHJ, Crane CF, Hane JK, Foster
785 AJ, Van der Lee TAJ, Grimwood J, Aerts A, Antoniw J, Bailey A, Bluhm B,
786 Bowler J, Bristow J, van der Burgt A, Canto-Canché B, Churchill ACL, Conde-
787 Ferràez L, Cools HJ, Coutinho PM, Csukai M, Dehal P, De Wit P, Donzelli B,
788 van de Geest HC, van Ham RCHJ, Hammond-Kosack KE, Henrissat B, Kilian
789 A, Kobayashi AK, Koopmann E, Kourmpetis Y, Kuzniar A, Lindquist E,
790 Lombard V, Maliepaard C, Martins N, Mehrabi R, Nap JPH, Ponomarenko A,
791 Rudd JJ, Salamov A, Schmutz J, Schouten HJ, Shapiro H, Stergiopoulos I,
792 Torriani SFF, Tu H, de Vries RP, Waalwijk C, Ware SB, Wiebenga A, Zwiers
793 L-H, Oliver RP, Grigoriev IV, Kema GHJ. 2011. Finished genome of the fungal
794 wheat pathogen *Mycosphaerella graminicola* reveals dispensome structure,
795 chromosome plasticity, and stealth pathogenesis. *PLoS Genet* **7**:e1002070.
796 doi:10.1371/journal.pgen.1002070
797 Götz S, García-Gómez JM, Terol J, Williams TD, Nagaraj SH, Nueda MJ, Robles M,
798 Talón M, Dopazo J, Conesa A. 2008. High-throughput functional annotation
799 and data mining with the Blast2GO suite. *Nucleic Acids Res* **36**:3420–3435.
800 doi:10.1093/nar/gkn176
801 Hahlbrock K, Scheel D. 1989. Physiology and Molecular Biology of Phenylpropanoid
802 Metabolism. *Annu Rev Plant Physiol Plant Mol Biol* **40**:347–369.
803 doi:10.1146/annurev.pp.40.060189.002023
804 Hassani-Pak K, Singh A, Brandizi M, Hearnshaw J, Parsons JD, Amberkar S,
805 Phillips AL, Doonan JH, Rawlings C. 2021. KnetMiner: a comprehensive
806 approach for supporting evidence-based gene discovery and complex trait
807 analysis across species. *Plant Biotechnol J* **19**:1670–1678.
808 doi:10.1111/pbi.13583
809 Hill R, Buggs RJA, Vu DT, Gaya E. 2022. Lifestyle Transitions in Fusarioid Fungi are
810 Frequent and Lack Clear Genomic Signatures. *Mol Biol Evol* **39**.
811 doi:10.1093/molbev/msac085
812 Hou Z, Xue C, Peng Y, Katan T, Kistler HC, Xu J-R. 2002. A mitogen-activated
813 protein kinase gene (MGV1) in *Fusarium graminearum* is required for female
814 fertility, heterokaryon formation, and plant infection. *Mol Plant-Microbe*
815 *Interact MPMI* **15**:1119–1127. doi:10.1094/MPMI.2002.15.11.1119

Huerta-Cepas J, Szklarczyk D, Heller D, Hernández-Plaza A, Forslund SK, Cook H, Mende DR, Letunic I, Rattei T, Jensen LJ, von Mering C, Bork P. 2019. eggNOG 5.0: a hierarchical, functionally and phylogenetically annotated orthology resource based on 5090 organisms and 2502 viruses. *Nucleic Acids Res* **47**:D309–D314. doi:10.1093/nar/gky1085

Jansen C, von Wettstein D, Schäfer W, Kogel K-H, Felk A, Maier FJ. 2005. Infection patterns in barley and wheat spikes inoculated with wild-type and trichodiene synthase gene disrupted Fusarium graminearum. *Proc Natl Acad Sci* **102**:16892–16897. doi:10.1073/pnas.0508467102

Jeger M, Beresford R, Bock C, Brown N, Fox A, Newton A, Vicent A, Xu X, Yuen J. 2021. Global challenges facing plant pathology: multidisciplinary approaches to meet the food security and environmental challenges in the mid-twenty-first century. *CABI Agric Biosci* **2**:20. doi:10.1186/s43170-021-00042-x

Jenczmionka NJ, Maier FJ, Lösch AP, Schäfer W. 2003. Mating, conidiation and pathogenicity of *Fusarium graminearum*, the main causal agent of the head-blight disease of wheat, are regulated by the MAP kinase gpmk1. *Curr Genet* **43**:87–95. doi:10.1007/s00294-003-0379-2

John E, Singh KB, Oliver RP, Tan K-C. 2021. Transcription factor control of virulence in phytopathogenic fungi. *Mol Plant Pathol* **22**:858–881. doi:10.1111/mpp.13056

Johns LE, Bebber DP, Gurr SJ, Brown NA. 2022. Emerging health threat and cost of Fusarium mycotoxins in European wheat. *Nat Food* **3**:1014–1019. doi:10.1038/s43016-022-00655-z

Kanja C, Wood AKM, Baggaley L, Walker C, Hammond-Kosack KE. 2021. Cereal-Fusarium interactions: Improved fundamental insights into Fusarium pathogenomics and cereal host resistance reveals new ways to achieve durable disease control. Achieving Durable Disease Resistance in Cereals. Burleigh Dodds Science Publishing.

Kema GHJ, Yu D, Frits H. J R, Michael W. S, Robert P. B. 1996. Histology of the Pathogenesis of *Mycosphaerella graminicola* in Wheat. *Phytopathology* **86**:777–786.

Keon J, Antoniw J, Carzaniga R, Deller S, Ward JL, Baker JM, Beale MH, Hammond-Kosack K, Rudd JJ. 2007. Transcriptional adaptation of *Mycosphaerella graminicola* to programmed cell death (PCD) of its susceptible wheat host. *Mol Plant-Microbe Interact MPMI* **20**:178–193. doi:10.1094/MPMI-20-2-0178

Kim DS, Hwang BK. 2014. An important role of the pepper phenylalanine ammonia-lyase gene (PAL1) in salicylic acid-dependent signalling of the defence response to microbial pathogens. *J Exp Bot* **65**:2295–2306. doi:10.1093/jxb/eru109

Kimura M, Tokai T, Takahashi-Ando N, Ohsato S, Fujimura M. 2007. Molecular and genetic studies of fusarium trichothecene biosynthesis: pathways, genes, and evolution. *Biosci Biotechnol Biochem* **71**:2105–2123. doi:10.1271/bbb.70183

King R, Urban M, Hammond-Kosack KE. 2017. Annotation of *Fusarium graminearum* (PH-1) Version 5.0. *Genome Announc* **5**:e01479-16. doi:10.1128/genomeA.01479-16

Kugler KG, Siegwart G, Nussbaumer T, Ametz C, Spannagl M, Steiner B, Lemmens M, Mayer KF, Buerstmayr H, Schweiger W. 2013. Quantitative trait loci-dependent analysis of a gene co-expression network associated with

Fusarium head blight resistance in bread wheat (*Triticum aestivum L.*). *BMC Genomics* **14**:728. doi:10.1186/1471-2164-14-728

Langfelder P, Horvath S. 2008. WGCNA: an R package for weighted correlation network analysis. *BMC Bioinformatics* **9**:559. doi:10.1186/1471-2105-9-559

Langfelder P, Luo R, Oldham MC, Horvath S. 2011. Is My Network Module Preserved and Reproducible? *PLOS Comput Biol* **7**:e1001057. doi:10.1371/journal.pcbi.1001057

Latham RL, Boyle JT, Barbano A, Loveman WG, Brown NA. 2023. Diverse mycotoxin threats to safe food and feed cereals. *Essays Biochem* **67**:797–809. doi:10.1042/EBC20220221

Letunic I, Bork P. 2024. Interactive Tree of Life (iTOL) v6: recent updates to the phylogenetic tree display and annotation tool. *Nucleic Acids Res*. doi:10.1093/nar/gkae268

Li D, Walker E, Francki M. 2021. Genes Associated with Foliar Resistance to Septoria Nodorum Blotch of Hexaploid Wheat (*Triticum aestivum L.*). *Int J Mol Sci* **22**:5580. doi:10.3390/ijms22115580

Li L, He Z, Pandey GK, Tsuchiya T, Luan S. 2002. Functional Cloning and Characterization of a Plant Efflux Carrier for Multidrug and Heavy Metal Detoxification. *J Biol Chem* **277**:5360–5368. doi:10.1074/jbc.M108777200

Liu Z, Zhu Z, Huang Y, Nong S, Jiang M, Yi S, Xie D, Hu H. 2023. Identification of gene modules and hub genes associated with *Colletotrichum siamense* infection in mango using weighted gene co-expression network analysis. *BMC Genomics* **24**:710. doi:10.1186/s12864-023-09811-6

Love MI, Huber W, Anders S. 2014. Moderated estimation of fold change and dispersion for RNA-seq data with DESeq2. *Genome Biol* **15**:550. doi:10.1186/s13059-014-0550-8

Lu S, Faris JD. 2019. *Fusarium graminearum* KP4-like proteins possess root growth-inhibiting activity against wheat and potentially contribute to fungal virulence in seedling rot. *Fungal Genet Biol* **123**:1–13. doi:10.1016/j.fgb.2018.11.002

Lucas JA, Hawkins NJ, Fraaije BA. 2015. The evolution of fungicide resistance. *Adv Appl Microbiol* **90**:29–92. doi:10.1016/bs.aambs.2014.09.001

Machado AK, Brown NA, Urban M, Kanyuka K, Hammond-Kosack KE. 2018. RNAi as an emerging approach to control Fusarium head blight disease and mycotoxin contamination in cereals. *Pest Manag Sci* **74**:790–799. doi:10.1002/ps.4748

Maher EA, Bate NJ, Ni W, Elkind Y, Dixon RA, Lamb CJ. 1994. Increased disease susceptibility of transgenic tobacco plants with suppressed levels of preformed phenylpropanoid products. *Proc Natl Acad Sci* **91**:7802–7806. doi:10.1073/pnas.91.16.7802

Mann CWG, Sawyer A, Gardiner DM, Mitter N, Carroll BJ, Eamens AL. 2023. RNA-Based Control of Fungal Pathogens in Plants. *Int J Mol Sci* **24**:12391. doi:10.3390/ijms241512391

Martin H, Dagkessamanskaia A, Satchanska G, Dallies N, François J. 1999. KNR4, a suppressor of *Saccharomyces cerevisiae* cwh mutants, is involved in the transcriptional control of chitin synthase genes. *Microbiol Read Engl* **145 (Pt 1)**:249–258. doi:10.1099/13500872-145-1-249

Martin-Yken H, Dagkessamanskaia A, Basmaji F, Lagorce A, Francois J. 2003. The interaction of Slt2 MAP kinase with Knr4 is necessary for signalling through the cell wall integrity pathway in *Saccharomyces cerevisiae*. *Mol Microbiol* **49**:23–35. doi:10.1046/j.1365-2958.2003.03541.x

Mateus ID, Masclaux FG, Aletti C, Rojas EC, Savary R, Dupuis C, Sanders IR. 2019. Dual RNA-seq reveals large-scale non-conserved genotype × genotype-specific genetic reprograming and molecular crosstalk in the mycorrhizal symbiosis. *ISME J* **13**:1226–1238. doi:10.1038/s41396-018-0342-3

McDonald MC, Renkin M, Spackman M, Orchard B, Croll D, Solomon PS, Milgate A. 2019. Rapid Parallel Evolution of Azole Fungicide Resistance in Australian Populations of the Wheat Pathogen *Zymoseptoria tritici*. *Appl Environ Microbiol* **85**:e01908-18. doi:10.1128/AEM.01908-18

Motteram J, Lovegrove A, Pirie E, Marsh J, Devonshire J, van de Meene A, Hammond-Kosack K, Rudd JJ. 2011. Aberrant protein N-glycosylation impacts upon infection-related growth transitions of the haploid plant-pathogenic fungus *Mycosphaerella graminicola*. *Mol Microbiol* **81**:415–433. doi:10.1111/j.1365-2958.2011.07701.x

Nelson R. 2020. International Plant Pathology: Past and Future Contributions to Global Food Security. *Phytopathology* **110**:245–253. doi:10.1094/PHYTO-08-19-0300-IA

Nguyen T, Kröger C, Bönnighausen J, Schäfer W, Bormann J. 2013. The ATF/CREB Transcription Factor Atf1 Is Essential for Full Virulence, Deoxynivalenol Production, and Stress Tolerance in the Cereal Pathogen *Fusarium graminearum*. *Mol Plant-Microbe Interact MPMI* **26**. doi:10.1094/MPMI-04-13-0125-R

O'Donnell K, Kistler HC, Tacke BK, Casper HH. 2000. Gene genealogies reveal global phylogeographic structure and reproductive isolation among lineages of *Fusarium graminearum*, the fungus causing wheat scab. *Proc Natl Acad Sci* **97**:7905–7910. doi:10.1073/pnas.130193297

Oldham M. 2014. M. Transcriptomics: from differential expression to coexpression. The OMICs: Applications in Neuroscience. Oxford University Press, UK.

Pan Y, Liu Z, Rocheleau H, Fauteux F, Wang Y, McCartney C, Ouellet T. 2018. Transcriptome dynamics associated with resistance and susceptibility against fusarium head blight in four wheat genotypes. *BMC Genomics* **19**:642. doi:10.1186/s12864-018-5012-3

Park J, Lee H-H, Moon H, Lee N, Kim S, Kim J-E, Lee Y, Min K, Kim H, Choi GJ, Lee Y-W, Seo Y-S, Son H. 2023. A combined transcriptomic and physiological approach to understanding the adaptive mechanisms to cope with oxidative stress in *Fusarium graminearum*. *Microbiol Spectr* **11**:e01485-23. doi:10.1128/spectrum.01485-23

Perincherry L, Lalak-Kańczugowska J, Stępień Ł. 2019. Fusarium-Produced Mycotoxins in Plant-Pathogen Interactions. *Toxins* **11**:664. doi:10.3390/toxins11110664

Plissonneau C, Hartmann FE, Croll D. 2018. Pangenome analyses of the wheat pathogen *Zymoseptoria tritici* reveal the structural basis of a highly plastic eukaryotic genome. *BMC Biol* **16**:5. doi:10.1186/s12915-017-0457-4

Ramaroson M-L, Koutouan C, Helesbeux J-J, Le Clerc V, Hamama L, Geoffriau E, Briard M. 2022. Role of Phenylpropanoids and Flavonoids in Plant Resistance to Pests and Diseases. *Molecules* **27**:8371. doi:10.3390/molecules27238371

Robinson MD, McCarthy DJ, Smyth GK. 2010. edgeR: a Bioconductor package for differential expression analysis of digital gene expression data. *Bioinforma Oxf Engl* **26**:139–140. doi:10.1093/bioinformatics/btp616

Rudd JJ, Kanyuka K, Hassani-Pak K, Derbyshire M, Andongabo A, Devonshire J, Lysenko A, Saqi M, Desai NM, Powers SJ, Hooper J, Ambroso L, Bharti A,

Farmer A, Hammond-Kosack KE, Dietrich RA, Courbot M. 2015. Transcriptome and Metabolite Profiling of the Infection Cycle of *Zymoseptoria tritici* on Wheat Reveals a Biphasic Interaction with Plant Immunity Involving Differential Pathogen Chromosomal Contributions and a Variation on the Hemibiotrophic Lifestyle Definition. *Plant Physiol* **167**:1158–1185. doi:10.1104/pp.114.255927

Saldivar SOS. 2016. Cereals: Dietary Importance In: Caballero B, Finglas PM, Toldrá F, editors. Encyclopedia of Food and Health. Oxford: Academic Press. pp. 703–711. doi:10.1016/B978-0-12-384947-2.00130-6

Savary S, Willocquet L, Pethybridge SJ, Esker P, McRoberts N, Nelson A. 2019. The global burden of pathogens and pests on major food crops. *Nat Ecol Evol* **3**:430–439. doi:10.1038/s41559-018-0793-y

Schneider CA, Rasband WS, Eliceiri KW. 2012. NIH Image to ImageJ: 25 years of image analysis. *Nat Methods* **9**:671–675. doi:10.1038/nmeth.2089

Sertsuvalkul N, DeMell A, Dinesh-Kumar SP. 2022. The complex roles of autophagy in plant immunity. *FEBS Lett* **596**:2163–2171. doi:10.1002/1873-3468.14356

Shewry PR, Hey SJ. 2015. The contribution of wheat to human diet and health. *Food Energy Secur* **4**:178–202. doi:10.1002/fes3.64

Shin Y-K, Kim D-W, Lee S-W, Lee M-J, Gi Baek S, Lee T, Yun S-H. 2022. Functional roles of all five putative hydrophobin genes in growth, development, and secondary metabolism in *Fusarium graminearum*. *Fungal Genet Biol* **160**:103683. doi:10.1016/j.fgb.2022.103683

Sieber CMK, Lee W, Wong P, Münsterkötter M, Mewes H-W, Schmeitzl C, Varga E, Berthiller F, Adam G, Güldener U. 2014. The *Fusarium graminearum* Genome Reveals More Secondary Metabolite Gene Clusters and Hints of Horizontal Gene Transfer. *PLOS ONE* **9**:e110311. doi:10.1371/journal.pone.0110311

Son H, Seo Y-S, Min K, Park AR, Lee J, Jin J-M, Lin Y, Cao P, Hong S-Y, Kim E-K, Lee S-H, Cho A, Lee S, Kim M-G, Kim Y, Kim J-E, Kim J-C, Choi GJ, Yun S-H, Lim JY, Kim M, Lee Y-H, Choi Y-D, Lee Y-W. 2011. A Phenome-Based Functional Analysis of Transcription Factors in the Cereal Head Blight Fungus, *Fusarium graminearum*. *PLoS Pathog* **7**:e1002310. doi:10.1371/journal.ppat.1002310

Sperschneider J, Dodds PN. 2022. EffectorP 3.0: Prediction of Apoplastic and Cytoplasmic Effectors in Fungi and Oomycetes. *Mol Plant-Microbe Interact MPMI* **35**:146–156. doi:10.1094/MPMI-08-21-0201-R

Steinberg G. 2015. Cell biology of *Zymoseptoria tritici*: Pathogen cell organization and wheat infection. *Fungal Genet Biol* **79**:17–23. doi:10.1016/j.fgb.2015.04.002

Teufel F, Almagro Armenteros JJ, Johansen AR, Gíslason MH, Pihl SI, Tsirigos KD, Winther O, Brunak S, von Heijne G, Nielsen H. 2022. SignalP 6.0 predicts all five types of signal peptides using protein language models. *Nat Biotechnol* **40**:1023–1025. doi:10.1038/s41587-021-01156-3

Tonnessen BW, Manosalva P, Lang JM, Baraoidan M, Bordeos A, Mauleon R, Oard J, Hulbert S, Leung H, Leach JE. 2015. Rice phenylalanine ammonia-lyase gene OsPAL4 is associated with broad spectrum disease resistance. *Plant Mol Biol* **87**:273–286. doi:10.1007/s11103-014-0275-9

Torriani SFF, Melichar JPE, Mills C, Pain N, Sierotzki H, Courbot M. 2015. *Zymoseptoria tritici:* A major threat to wheat production, integrated approaches to control. *Fungal Genet Biol* **79**:8–12. doi:10.1016/j.fgb.2015.04.010

Urban M, Cuzick A, Seager J, Wood V, Rutherford K, Venkatesh SY, Sahu J, Iyer SV, Khamari L, De Silva N, Martinez MC, Pedro H, Yates AD, Hammond-Kosack KE. 2022. PHI-base in 2022: a multi-species phenotype database for Pathogen–Host Interactions. *Nucleic Acids Res* **50**:D837–D847. doi:10.1093/nar/gkab1037

Urban M, Mott E, Farley T, Hammond-Kosack K. 2003. The *Fusarium graminearum* MAP1 gene is essential for pathogenicity and development of perithecia. *Mol Plant Pathol* **4**:347–359. doi:10.1046/j.1364-3703.2003.00183.x

Vicente I, Quaratiello G, Baroncelli R, Vannacci G, Sarrocco S. 2022. Insights on KP4 Killer Toxin-like Proteins of Fusarium Species in Interspecific Interactions. *J Fungi* **8**:968. doi:10.3390/jof8090968

Walsh CJ, Batt J, Herridge MS, Mathur S, Bader GD, Hu P, dos Santos CC. 2016. Transcriptomic analysis reveals abnormal muscle repair and remodeling in survivors of critical illness with sustained weakness. *Sci Rep* **6**:29334. doi:10.1038/srep29334

Wang C, Zhang S, Hou R, Zhao Z, Zheng Q, Xu Q, Zheng D, Wang G, Liu H, Gao X, Ma J-W, Kistler HC, Kang Z, Xu J-R. 2011. Functional analysis of the kinome of the wheat scab fungus *Fusarium graminearum*. *PLoS Pathog* **7**:e1002460. doi:10.1371/journal.ppat.1002460

Xu M, Wang Q, Wang G, Zhang X, Liu H, Jiang C. 2022. Combatting Fusarium head blight: advances in molecular interactions between *Fusarium graminearum* and wheat. *Phytopathol Res* **4**:37. doi:10.1186/s42483-022-00142-0

Yan X, Tang B, Ryder LS, MacLean D, Were VM, Eseola AB, Cruz-Mireles N, Ma W, Foster AJ, Osés-Ruiz M, Talbot NJ. 2023. The transcriptional landscape of plant infection by the rice blast fungus *Magnaporthe oryzae* reveals distinct families of temporally co-regulated and structurally conserved effectors. *Plant Cell* **35**:1360–1385. doi:10.1093/plcell/koad036

Yu J-H, Hamari Z, Han K-H, Seo J-A, Reyes-Domínguez Y, Scazzocchio C. 2004. Double-joint PCR: a PCR-based molecular tool for gene manipulations in filamentous fungi. *Fungal Genet Biol FG B* **41**:973–981. doi:10.1016/j.fgb.2004.08.001

Yun Y, Liu Z, Zhang J, Shim W-B, Chen Y, Ma Z. 2014. The MAPKK FgMkk1 of *Fusarium graminearum* regulates vegetative differentiation, multiple stress response, and virulence via the cell wall integrity and high-osmolarity glycerol signaling pathways. *Environ Microbiol* **16**:2023–2037. doi:10.1111/1462-2920.12334

Zhang B, Horvath S. 2005. A general framework for weighted gene co-expression network analysis. *Stat Appl Genet Mol Biol* **4**:Article17. doi:10.2202/1544-6115.1128

Zhang L, Zhou X, Li P, Wang Y, Hu Q, Shang Y, Chen Y, Zhu X, Feng H, Zhang C. 2022. Transcriptome Profile of *Fusarium graminearum* Treated by Putrescine. *J Fungi* **9**:60. doi:10.3390/jof9010060

Zhang Yu, Chen W, Shao W, Tan S, Shi D, Ma H, Chen C. 2022. FaSmi1 Is Essential for the Vegetative Development, Asexual Reproduction, DON Production and Virulence of *Fusarium asiaticum*. *J Fungi* **8**:1189. doi:10.3390/jof8111189

Zhang Y, Dai Y, Huang Y, Wang K, Lu P, Xu H, Xu J-R, Liu H. 2020. The SR-protein FgSrp2 regulates vegetative growth, sexual reproduction and pre-mRNA processing by interacting with FgSrp1 in *Fusarium graminearum*. *Curr Genet* **66**:607–619. doi:10.1007/s00294-020-01054-2

Zhang Yan, Zheng L, Yun L, Ji L, Li G, Ji M, Shi Y, Zheng X. 2022. Catalase (CAT) Gene Family in Wheat (*Triticum aestivum L.*): Evolution, Expression Pattern and Function Analysis. *Int J Mol Sci* **23**:542. doi:10.3390/ijms23010542

Zheng D, Zhang S, Zhou X, Wang C, Xiang P, Zheng Q, Xu J-R. 2012. The FgHOG1 Pathway Regulates Hyphal Growth, Stress Responses, and Plant Infection in *Fusarium graminearum*. *PLOS ONE* **7**:e49495. doi:10.1371/journal.pone.0049495

Zhu T, Wang L, Rimbert H, Rodriguez JC, Deal KR, De Oliveira R, Choulet F, Keeble-Gagnère G, Tibbits J, Rogers J, Eversole K, Appels R, Gu YQ, Mascher M, Dvorak J, Luo M-C. 2021. Optical maps refine the bread wheat *Triticum aestivum* cv. Chinese Spring genome assembly. *Plant J* **107**:303–314. doi:10.1111/tpj.15289

Funding

E.K and V.A are supported by the BBSRC-funded South West Biosciences Doctoral Training Partnership (BB/T008741/1). K.H.K and M.U are supported by the Biotechnology and Biological Sciences Research Council (BBSRC) Institute Strategic Programme (ISP) Grants, Designing Future Wheat (BBS/E/C/000I0250) and Delivering Sustainable Wheat (BB/X011003/1 and BBS/E/RH/230001B) and the BBSRC grants (BB/X012131/1 and BB/W007134/1). N.A.B was supported by the BBSRC Future Leader Fellowship BB/N011686/1. J.R and C.B are funded by the BBSRC ISPs Designing Future Wheat (BBS/E/C/000I0250), Delivering Sustainable Wheat (BB/X011003/1 and BBS/E/RH/230001B), and Growing Health (BB/X010953). R.A was supported by a BBSRC/EPSRC Interface Innovation Fellowship (EP/S001352/1).

Author's contributions

E.K conducted the experiments and wrote the manuscript. N.A.B, M.U, and K.H.K provided project oversight, experimental design and manuscript planning, development, and revisions. R.A helped with experimental design and data analysis. C.B and J.R generated ZtKnr4 mutant and completed associated characterisation

experiments. A.M.U embedded, sectioned, and imaged samples for TEM analysis. V.A undertook the resin embedding, sectioning, and imaging.

Competing interests

No competing interests declared.

Tables and Figures

Table 1. Function of correlated expression between wheat and fungal modules. This table illustrates the relationship between wheat and fungal gene expression at different stages of infection, detailing the associated functions and key fungal genes involved.

Expression Stages	Wheat Module	Predicted function	Correlated Fungal Module	Key Fungal Genes	Fungal Gene Functions	References
Early symptomless stage of infection	W01	Maintenance genes (photosynthesis, RNA modification) and early defence response.	F16	*FgNPC1*	Regulation of membrane trafficking and sterol metabolism, which are essential for maintaining cellular integrity and function during the infection stages.	Breakspear et al. 2011
				Gzc2h045	Msn2 C2H2 transcription factor, associated with virulence and coordination of adaptation to environmental stressors including heat, osmotic, and oxidative stress.	Son et al., 2011; John et al., 2021
	W05	Disease resistance genes, including reactive oxygen species genes associated with programmed cell death response to restrict pathogen spread.		*GzCon7*	Msn2 C2H2 transcription factor, associated with virulence and regulation of cell wall biosynthesis.	Son et al., 2011; John et al., 2021
				FgSrp2	Pre-mRNA processing, alternative splicing, and virulence	Zhang et al., 2020

Early symptomless and late symptomatic stages of infection	W06	Enriched in protein catabolism and autophagy, involved in immune signalling, programmed cell death, and necrotrophic damage control.	F10	*KP4L-1, KP4L-2, KP4L-3*	Necessary for virulence, provide competitive advantage during new niche occupation, essential for intraspecific interactions at high fungal density	Lu and Faris, 2019; Vicente et al., 2022
				FgOS-2, FgAtf-1	Regulation of secondary metabolite production, sexual reproduction, and stress tolerance	Nguyen et al., 2013
				FgHyd3, FgHyd5	Attachment to hydrophobic surfaces, production of aerial mycelia	Shin et al., 2022
Late symptomless to early symptomatic	W12	Detoxification, response to toxic substances, and defence response.	F12	*TRI* genes (*TRI3, TRI4, TRI11, TRI12, TRI14)*	Production of DON mycotoxin needed for virulence.	Dyer et al., 2005; Kimura et al., 2007

1103

1104

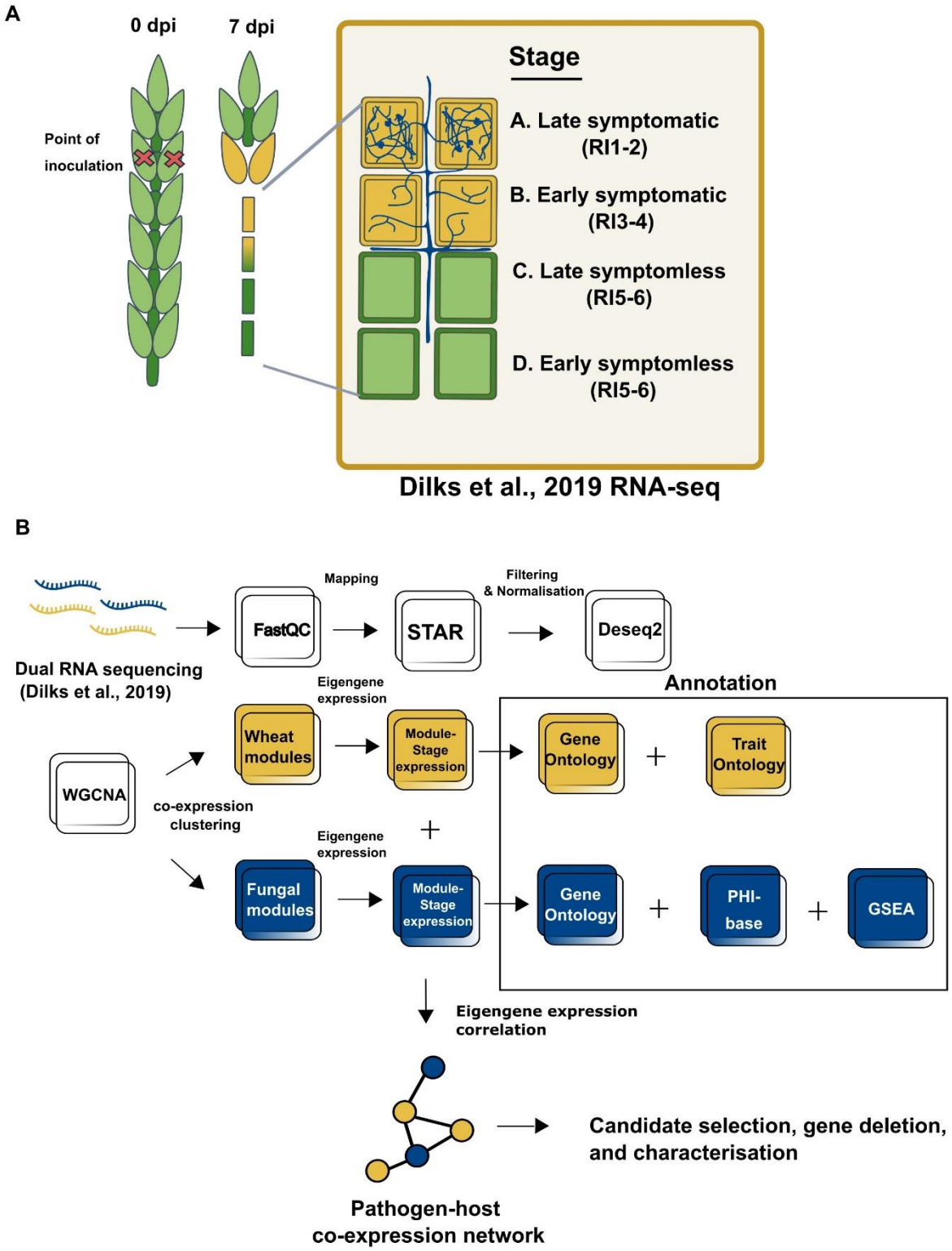

1105

1106 **Figure 1. Dual RNA-seq dataset and bioinformatics pipeline used for constructing the**

1107 **dual co-expression network. A.** Schematic illustration depicting the symptomatic (yellow)

and symptomless (green) stages of *Fusarium graminearum* infection of wheat spikes denoted as stages A through D, corresponding to tissue samples collected for generating the RNA-seq data published in Dilks et al. 2019. *F. graminearum* hyphae growing in either the apoplast or inside the wheat cells are depicted in blue. **B.** Summary outlining the bioinformatics pipeline used for processing raw reads and constructing the dual RNA-seq network. The dual RNA-seq reads were initially processed together (processes depicted as white squares) before being separated to generate two distinct weighted gene co-expression networks. The bioinformatic pipelines are annotated accordingly, with yellow indicating the wheat reads-only pipeline and blue indicating the fungal reads-only pipeline. Annotation includes Gene Ontology terms (GO), Trait Ontology terms (TO), unique Gene Set Enrichment Analysis (GSEA), and PHI-base phenotypes. The modules from the two separate networks are then correlated to each other by their Eigengene values to form the dual co-expression network.

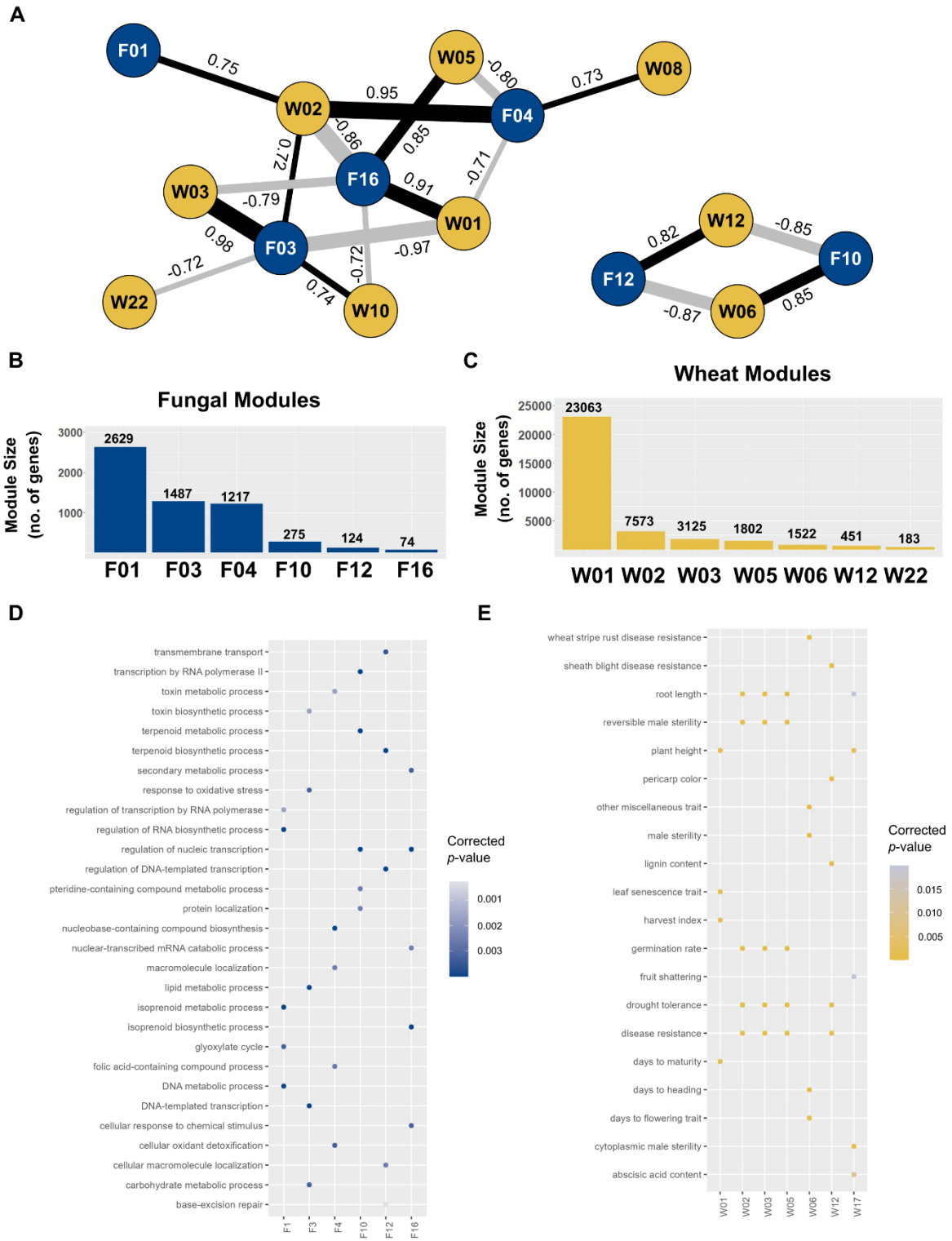

Figure 2. Dual Fungal-Wheat co-expression network. A. Network summarising significant co-expression patterns ($p \geq 0.001$) between fungal modules (blue nodes) and wheat modules (yellow nodes). Positive correlations are depicted as black edges, while negative

correlations are shown as grey edges. R-squared values are indicated next to edges, with edge width corresponding to the value. **B.** Fungal modules sizes. **C.** Wheat module sizes (**Supplementary File 1**). **D. Fungal module enrichment.** Significant ($p \leq 0.05$) Biological Processes (BP) Gene Ontology (GO) enrichment results for all fungal modules in the network. Higher significance is indicated by darker blues. **E. Wheat module enrichment.** Significant Plant Trait Ontology (TO) enrichment results ($p \leq 0.05$) for all wheat modules in the network. Higher significance is indicated by brighter yellows.

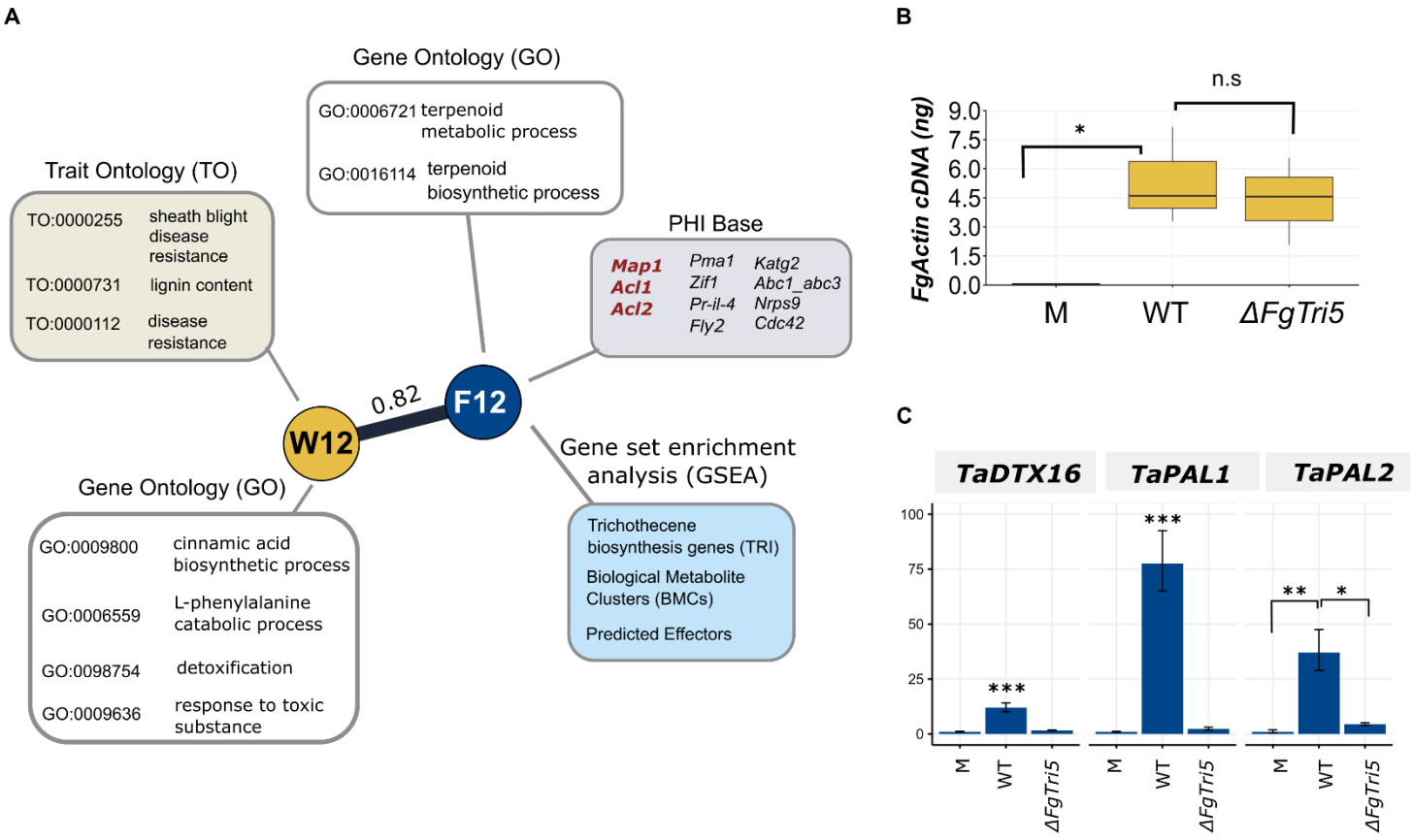

1135 **Figure 3. Validation of correlation between the trichothecene mycotoxin biosynthesis**
1136 **gene enriched module (F12) and the detoxification gene enriched module (W12).** A.
1137 Modules F12 (N = 124) and W12 (N = 451) depicted with significant enrichment annotations
1138 and genes with known phenotypes from PHI-base. Three genes listed in red in the PHI-base
1139 annotation (grey box) exhibit a loss of pathogenicity phenotype, while the remaining genes
1140 display a reduced virulence phenotype when individually deleted in *F. graminearum*. B.
1141 Equal levels of fungal burden were observed in tissue samples ($p > 0.05$). Absolute quantity
1142 of actin cDNA in Mock, *ΔFgtri5*, and wild-type (WT)-recovered RI1-2 tissue sampled at 3 dpi.
1143 Significance was determined by a one-way ANOVA followed by Tukey HSD correction. C.
1144 Normalised fold change expression of selected W12 wheat genes in Mock, *ΔFgtri5*, and WT-
1145 recovered RI1-2 tissue sampled at 3 dpi (N = 3). Significance is denoted as * = $p \leq 0.05$, ** =
1146 $p \leq 0.01$, and *** = $p \leq 0.001$. Significance was determined by a one-way ANOVA followed
1147 by Tukey HSD correction.

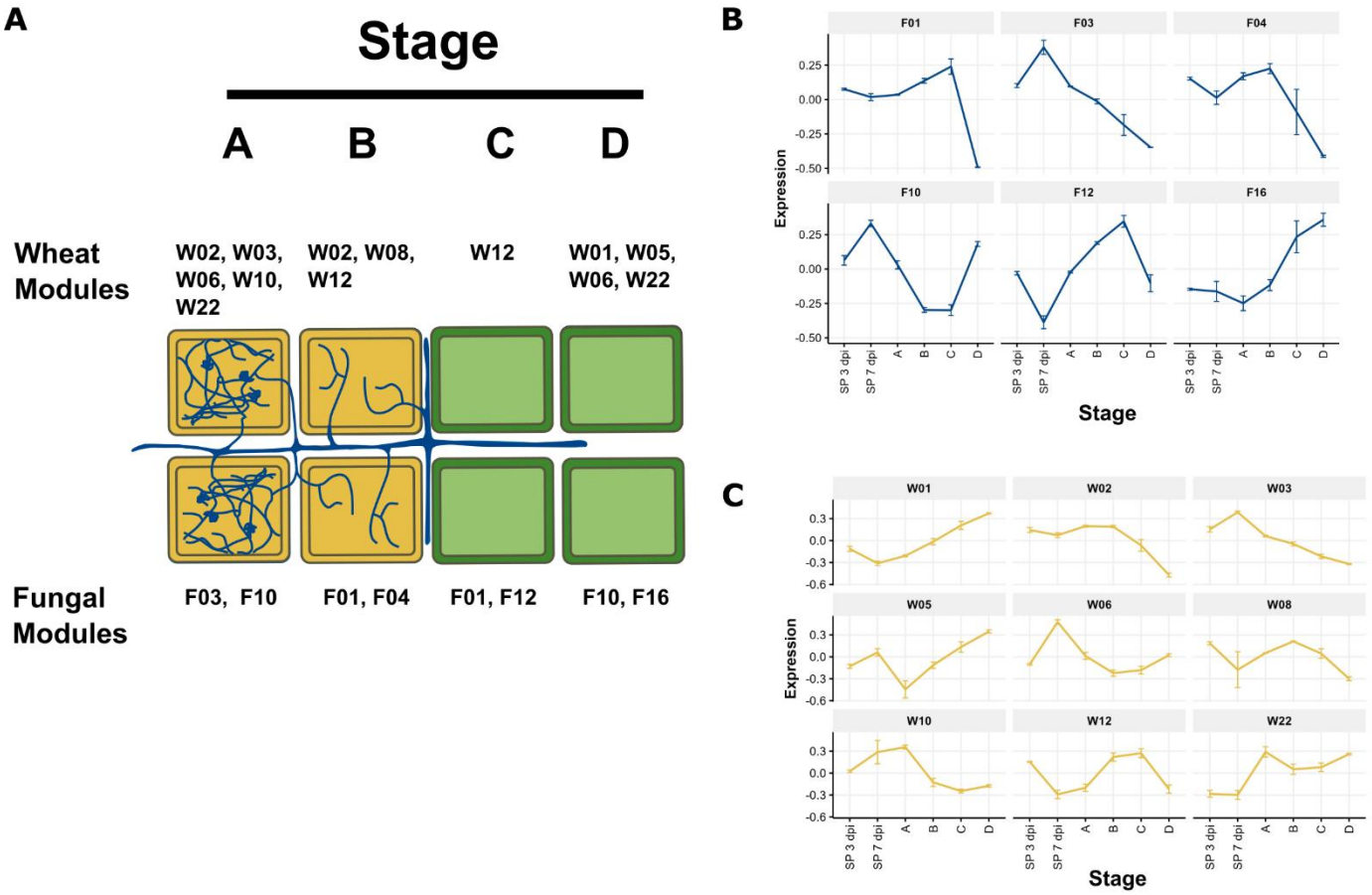

1148

1149 **Figure 4. Stage-specific expression of modules in the dual co-expression network. A.**

1150 Expression of modules across stages of *F. graminearum* infection. Illustration depicting

1151 symptomatic (yellow) and symptomless (green) stages of infection (A through D) annotated

1152 with specific modules (W or F) from the dual co-expression network that were highly

1153 expressed at specific stages **B. Eigengene summarised expression of fungal modules**

1154 and **C. wheat modules**. Eigengene summarised expression plots illustrating the expression

1155 patterns of genes in wheat modules across different stages of infection as illustrated in panel

1156 A, along with spikelet tissue (SP) at 3 and 7 dpi.

1157

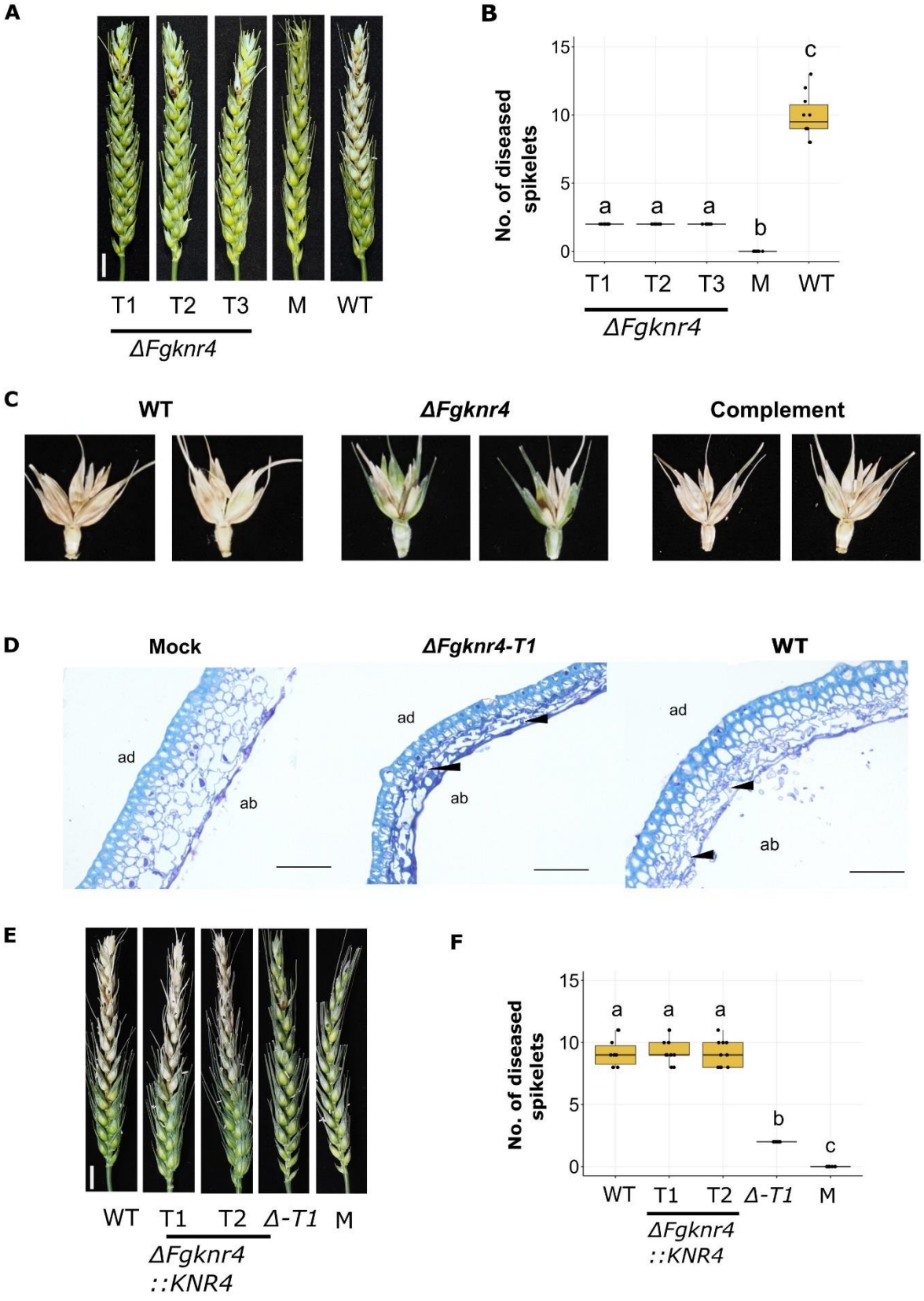

Figure 5. Decreased virulence observed during *in planta* infection with *ΔFgknr4*. A. Wheat spike infection assay done on the susceptible cultivar Bobwhite point inoculated with sterile water only (Mock), wild-type *F. graminearum* conidia, or conidia from three independent single gene deletion *F. graminearum* mutants lacking *Knr4* (*ΔFgknr4,* T1-3). Images were captured at 15 dpi. Scale bar = 1 cm. **B.** Number of diseased spikelets per wheat spike at 15 dpi. Letters indicate significant differences (ANOVA, TukeyHSD $p < 0.05$). C. Symptom development on the inoculated spikelets and adjacent rachis tissues at 15 dpi D**.** Ultra-thin 1µm LR White resin sections stained with 0.1% Toluidine Blue for visualisation of wheat cell walls (light blue) and fungal hyphae (purple). Black arrows indicate fungal hyphae. Fungal hyphae typically proliferate in the abaxial cell layer. Ab = abaxial and ad = adaxial. Scale bar = 50 µm. Tissue harvested at 7 dpi. **E.** Wheat spike infection complementation assay done on the susceptible cultivar Bobwhite treated with conidia either from wild-type *F. graminearum*, different complemented transformants (*ΔFgknr4::KNR4-T1* and *T2*), the single gene deletion mutant (*ΔFgknr4-T1*), or sterile water (mock). Images were taken at 15 days post inoculation. **F.** Number of diseased spikelets per wheat spike at 15 dpi. Letters indicate significant differences (ANOVA, TukeyHSD $p < 0.05$).

1177

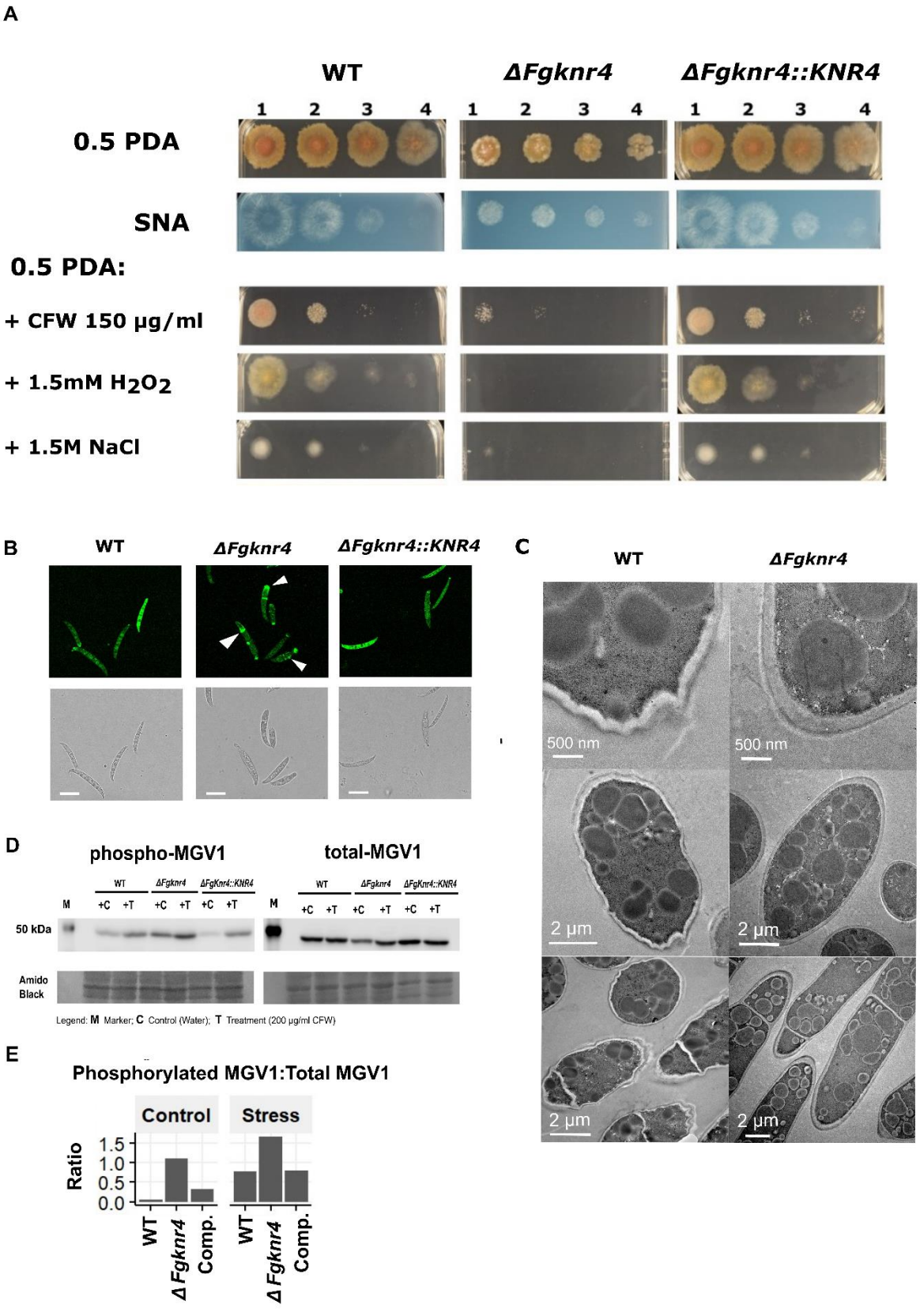

1178

Figure 6. Cell wall stress sensitivity and abnormal cell wall morphology of *ΔFgknr4*. **A**. Dilution series of wild-type (WT), *ΔFgknr4*, and *ΔFgknr4::KNR4* strains on Synthetic Nutrient Agar (SNA) and half-strength Potato Dextrose Agar (0.5 PDA) with and without the addition of calcofluor white (CFW), hydrogen peroxide (H_2O_2), and sodium chloride (NaCL). The dilution series begins at 1: 1 x 10^6 and continues with 10-fold dilutions (2: 1/10, 3: 1/100, and 4: 1/100). Images taken after 3 days of growth at room temperature. **B**. Abnormal chitin deposition patterns in *ΔFgknr4* conidia. Chitin-stained in conidia visualised using Wheat Germ Agglutinin Alexa Fluor™ 488 Conjugate (WGA). Scale bar = 50 µm. **C**. TEM imaging of wild-type and *ΔFgknr4* conidia, showing differences in cell wall structure **D.** Western blot of proteins extracted from, *ΔFgknr4* and *ΔFgknr4::KNR4* mycelium incubated with (T) or without (C) the addition of 200 µg/ml Calcofluor White (CFW) for 24 h. Phospho-p44/42 MAPK (Erk1/2) and p44/42 MAPK (Erk1/2) antibodies were used to detect phosphorylated and total MGV1, respectively. Amido black total protein staining was performed to compare protein loading. E. Ratio of phosphorylated MAPK/total MAPK based on quantification of band intensity.

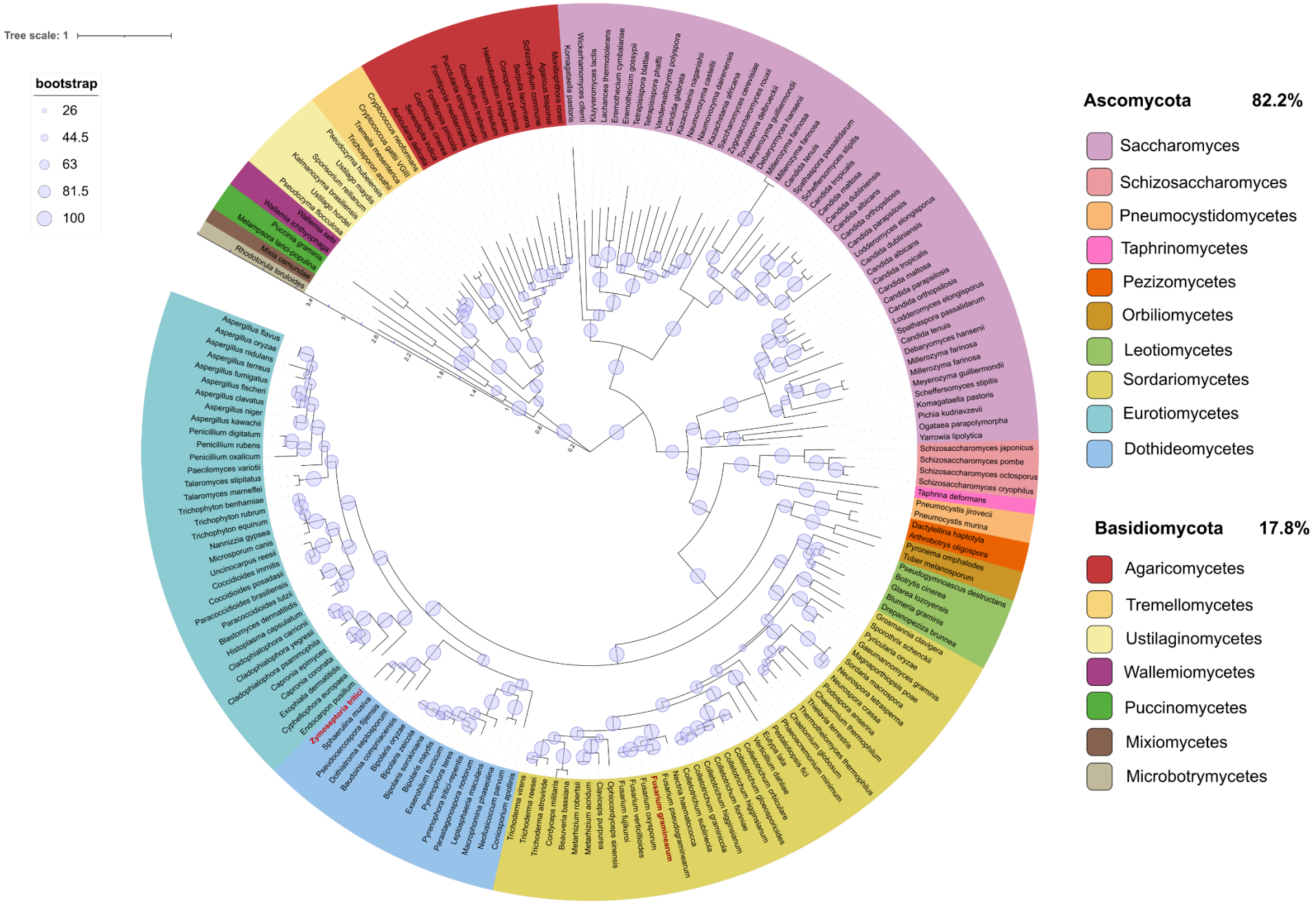
Tree scale: 1
bootstrap
26
44.5
63
81.5
100
Ascomycota 82.2%
Saccharomyces
Schizosaccharomyces
Pneumocystidomycetes
Taphrinomycetes
Pezizomycetes
Orbiliomycetes
Leotiomycetes
Sordariomycetes
Eurotiomycetes
Dothideomycetes
Basidiomycota 17.8%
Agaricomycetes
Tremellomycetes
Ustilaginomycetes
Wallemiomycetes
Puccinomycetes
Mixiomycetes
Microbotrymycetes
Monilophthora roreri
Komagataella pastoris
Agaricus bisporus
Schizophyllum commune
Serpula lacrymans
Coniophora puteana
Heterobasidion irregulare
Stereum hirsutum
Gloeophyllum trabeum
Punctularia strigosozonata
Fomitopsis pinicola
Coprinopsis cinerea
Serendipita indica
Auricularia delicata
Cryptococcus neoformans
Cryptococcus gattii VGIII
Tremella mesenterica
Trichosporon asahii
Pseudozyma hubeiensis
Ustilago maydis
Sporisorium reilianum
Kalmanozyma brasiliensis
Ustilago hordei
Pseudozyma flocculosa
Wallemia ichthyophaga
Wallemia sebi
Melampsora larici-populina
Puccinia graminis
Mixia osmundae
Rhodotorula toruloides
Yarrowia lipolytica
Ogataea parapolymorpha
Pichia kudriavzevii
Komagataella pastoris
Scheffersomyces stipitis
Meyerozyma guilliermondii
Millerozyma farinosa
Debaryomyces hansenii
Candida tenuis
Spathaspora passalidarum
Lodderomyces elongisporus
Candida orthopsilosis
Candida parapsilosis
Candida tropicalis
Candida albicans
Candida dubliniensis
Candida maltosa
Schizosaccharomyces japonicus
Schizosaccharomyces pombe
Schizosaccharomyces octosporus
Schizosaccharomyces cryophilus
Taphrina deformans
Pneumocystis jirovecii
Pneumocystis murina
Dactylellina haptotyla
Arthrobotrys oligospora
Pyronema omphalodes
Tuber melanosporum
Pseudogymnoascus destructans
Botrytis cinerea
Glarea lozoyensis
Blumeria graminis
Drepanopeziza brunnea
Grosmannia clavigera
Sporothrix schenckii
Pyricularia oryzae
Gaeumannomyces graminis
Magnaporthiopsis poae
Sordaria macrospora
Neurospora crassa
Neurospora tetrasperma
Podospora anserina
Chaetomium thermophilum
Thielavia terrestris
Thermothelomyces thermophilus
Chaetomium globosum
Phaeoacremonium minimum
Phialophora hoffmannii
Pestalotiopsis fici
Eutypa lata
Verticillium dahliae
Colletotrichum orbiculare
Colletotrichum gloeosporioides
Colletotrichum higginsianum
Colletotrichum fioriniae
Colletotrichum graminicola
Colletotrichum subrenicola
Nectria haematococca
Fusarium pseudograminearum
Fusarium graminearum
Fusarium oxysporum
Fusarium verticillioides
Fusarium fujikuroi
Ophiocordyceps sinensis
Claviceps purpurea
Metarhizium acridum
Metarhizium robertsii
Beauveria bassiana
Cordyceps militaris
Trichoderma atroviride
Trichoderma reesei
Trichoderma virens
Coniosporium apollinis
Neofusicoccum parvum
Macrophomina phaseolina
Leptosphaeria maculans
Parastagonospora nodorum
Pyrenophora tritici-repentis
Pyrenophora teres
Pyrenophora turicum
Exserohilum turcicum
Bipolaris maydis
Bipolaris sorokiniana
Bipolaris zeicola
Bipolaris oryzae
Baudoinia compniacensis
Dothistroma septosporum
Pseudocercospora fijiensis
Sphaerulina musiva
Zymoseptoria tritici
Cyphellophora europaea
Exophiala dermatitidis
Endocarpon pusillum
Capronia coronata
Capronia epimyces
Cladophialophora psammophila
Cladophialophora yegresii
Cladophialophora carrionii
Histoplasma capsulatum
Blastomyces dermatitidis
Paracoccidioides lutzii
Paracoccidioides brasiliensis
Coccidioides posadasii
Coccidioides immitis
Uncinocarpus reesii
Microsporum canis
Nannizzia gypsea
Trichophyton equinum
Trichophyton rubrum
Trichophyton benhamiae
Talaromyces marneffei
Talaromyces stipitatus
Paecilomyces variotii
Penicillium oxalicum
Penicillium rubens
Penicillium digitatum
Aspergillus kawachii
Aspergillus niger
Aspergillus clavatus
Aspergillus fischeri
Aspergillus fumigatus
Aspergillus terreus
Aspergillus nidulans
Aspergillus oryzae
Aspergillus flavus

Figure 7. Distribution of KNR4 orthologues across eukaryotes reveals exclusive presence in fungi. A phylogenetic tree depicting the distribution of *KNR4* orthologues across Eukaryota, with the positions of *F. graminearum* and *Z. tritici* highlighted in red. Different taxonomic levels are indicated in various colours as specified in the legend, alongside the percent distribution of orthologues between Ascomycota and Basidiomycota. Evolutionary distances between species or taxa are denoted by an internal scale (range 0 - 3.5) Bootstrapping confidence values are depicted as pale blue circles, with increasing size corresponding to higher confidence levels.

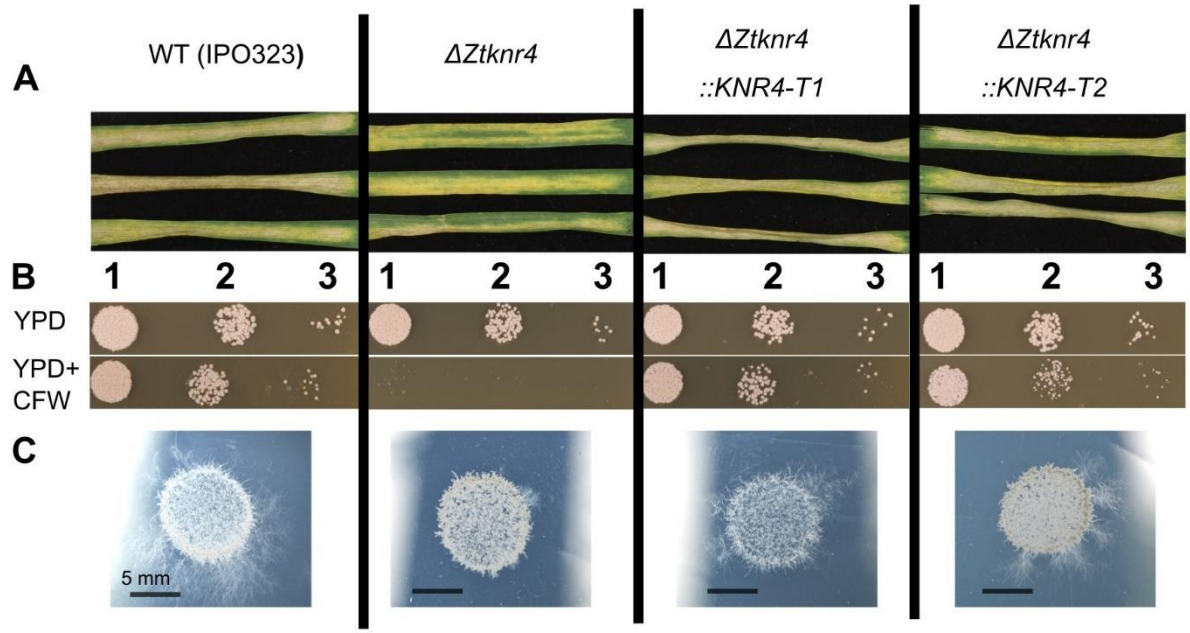

Figure 8. Functional characterisation of the *Zymoseptoria tritici ΔZtknr4* gene deletion mutant. A. Detached wheat leaves inoculated with wild-type (WT) *Z. tritici* (IPO323), *ΔZtknr4* mutant strain, and two complemented strains (*ΔZtknr4::KNR4-T1 and T2*). Image taken at 20 dpi. **B** WT *Z. tritici*, the *ΔZtknr4* mutant and two complemented strains (*ΔZtknr4::KNR4-T1 and T2*) spot inoculated onto YPD agar with (bottom) and without (top) calcofluor white (CFW). Dilution series begins at 1: 1 x 10^5 and continues with 10-fold dilutions (2: 1/10 and 3: 1/100). Images taken after 3 days of growth at room temperature (RT). **C** WT *Z. tritici*, the *ΔZtknr4* mutant and two complemented strains (*ΔZtknr4::KNR4-T1 and T2*) spot inoculated onto 1% Tap Water Agar (TWA). Images taken after 10 days of growth at room temperature (RT).

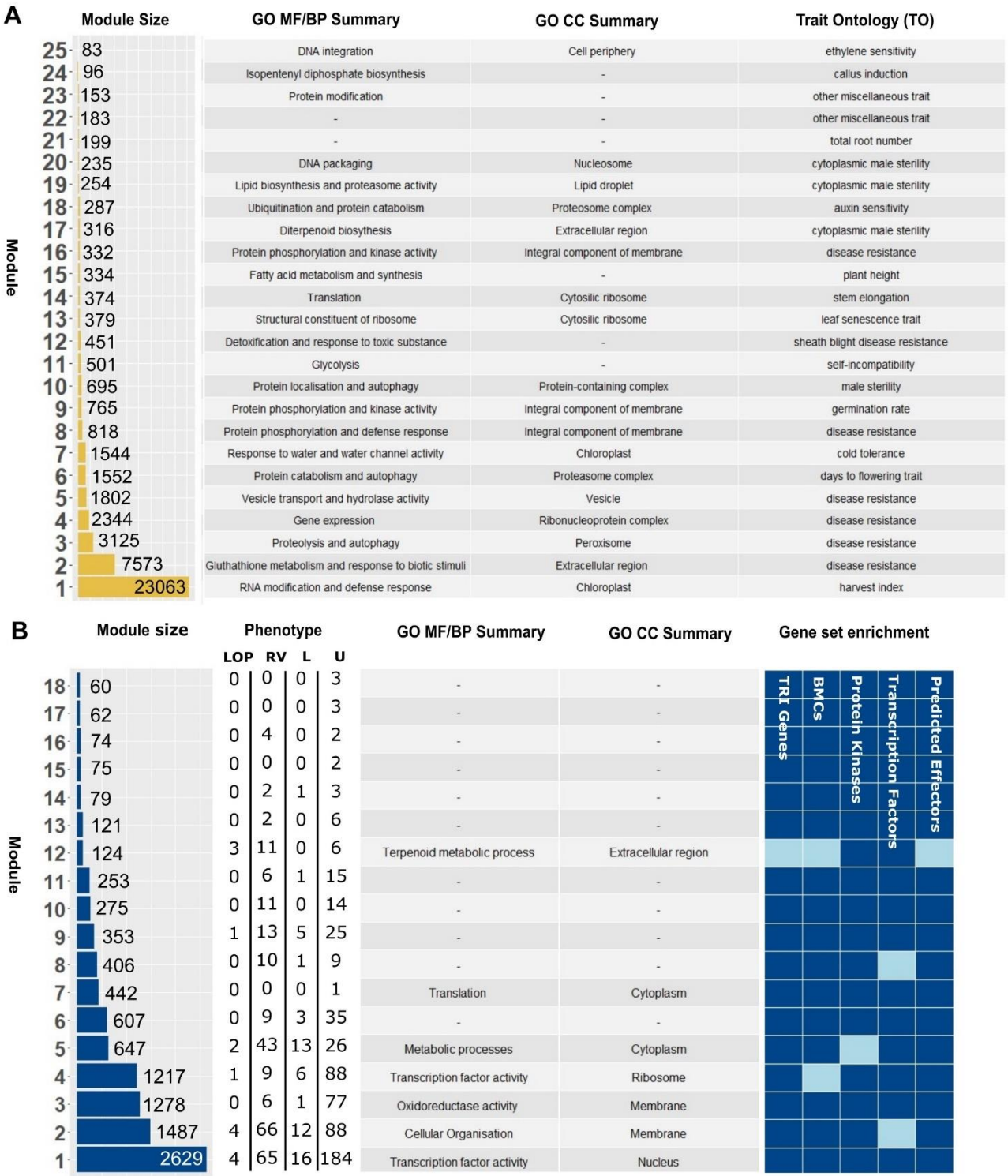

Figure 2 – figure supplement 1. Network Summary. A. Summary of all modules in the wheat network, including module size (number of genes), Gene Ontology (GO) and Trait Ontology (TO) enrichment summaries. B. Summary of all modules in the fungal network, including modules size, Gene Ontology (GO) enrichment summaries and Gene Set

Enrichment Analysis (GSEA). The number of genes with different phenotypes in PHI-base are depicted, with LOP, RV, L and U denoting different PHI-base phenotypes (LOP = Loss of pathogenicity; RV = Reduced virulence; L = Lethal; U = Unaffected pathogenicity) **(Urban et al., 2022**).

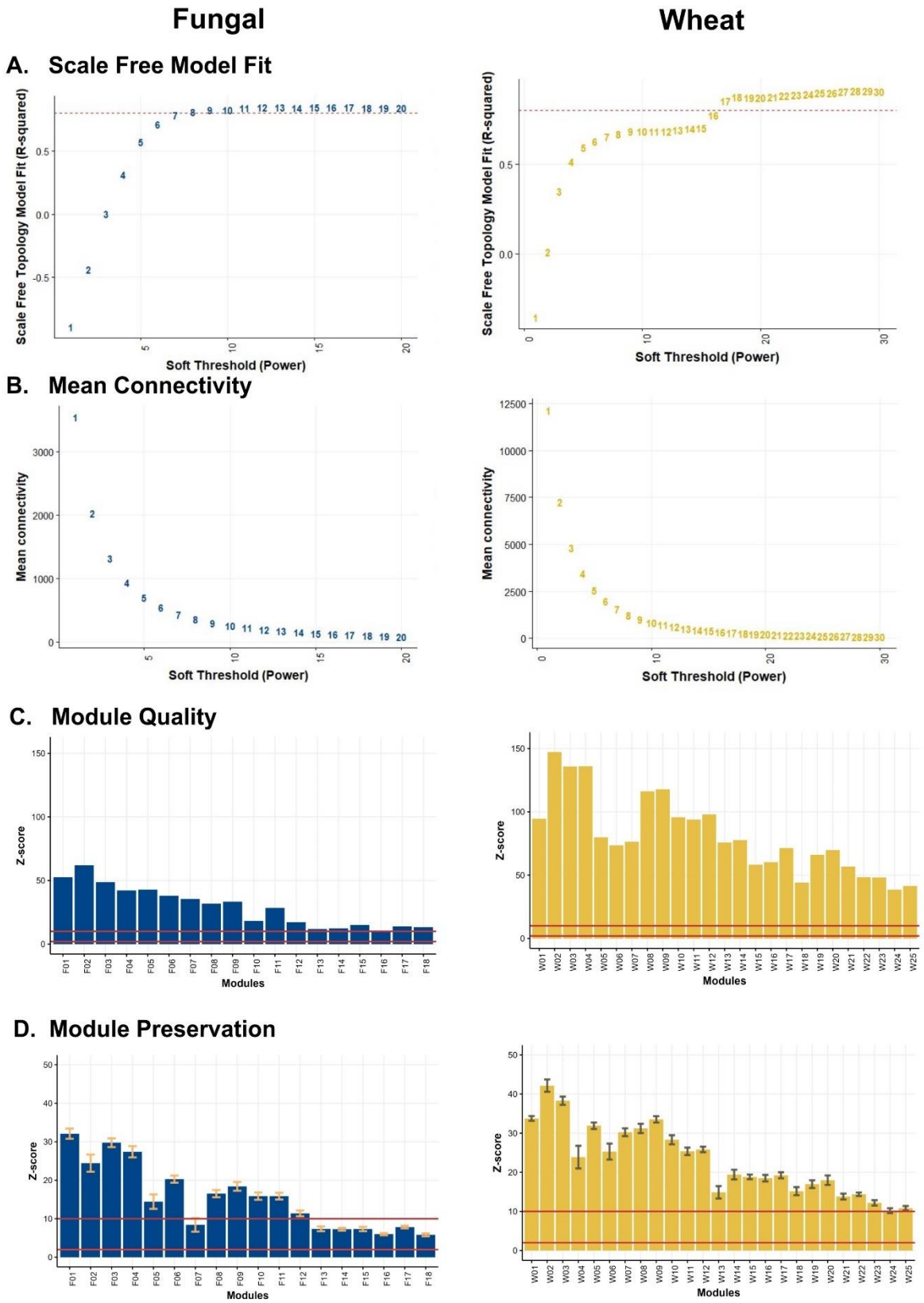

Figure 2 – figure supplement 2. Network statistics. A. Strength of correlation of network model (R-squared value) to scale free model at different soft thresholding powers. Dotted

red line is at an R-squared value of 0.80, the threshold needed for generating a WGCNA network. **B.** Mean connectivity of genes in each network at different soft thresholding powers. A low mean connectivity is desired to meet the scale free network criteria. **C.** Module quality across all modules as determined by a Z-score calculation. Solid red lines at minimum quality (Z = 2) and high quality scores (Z = 10). **D.** Module preservation as determined by Z-score calculation against 50 random test networks. Solid red lines at minimum preservation (Z = 2) and high preservation scores (Z = 10).

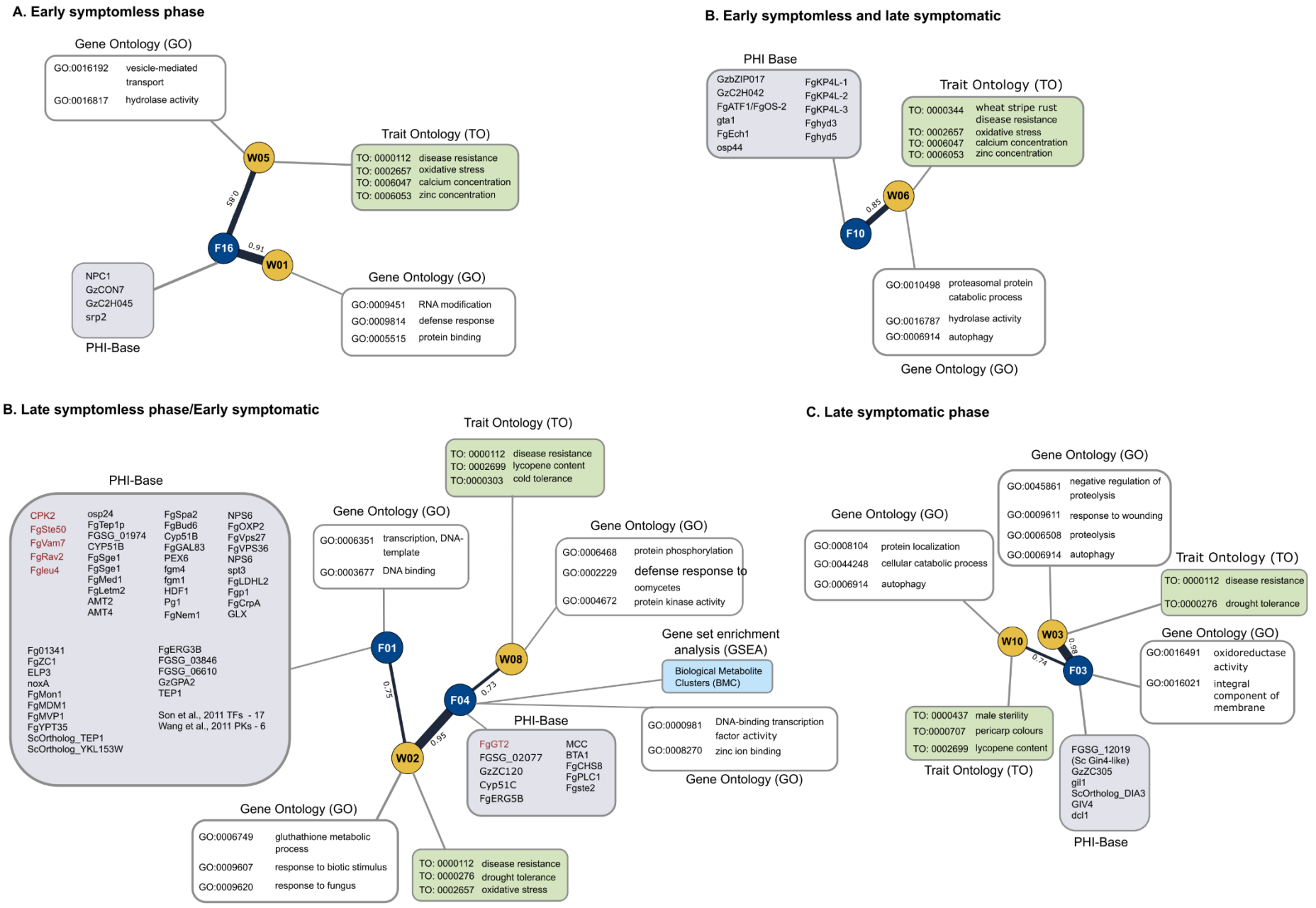
A. Early symptomless phase
Gene Ontology (GO)
GO:0016192 vesicle-mediated transport
GO:0016817 hydrolase activity
Trait Ontology (TO)
TO: 0000112 disease resistance
TO: 0002657 oxidative stress
TO: 0006047 calcium concentration
TO: 0006053 zinc concentration
W05
0.85
F16
0.91
W01
NPC1
GzCON7
GzC2H045
srp2
PHI-Base
Gene Ontology (GO)
GO:0009451 RNA modification
GO:0009814 defense response
GO:0005515 protein binding
B. Early symptomless and late symptomatic
PHI Base
GzbZIP017
GzC2H042
FgATF1/FgOS-2
gta1
FgEch1
osp44
FgKP4L-1
FgKP4L-2
FgKP4L-3
Fghyd3
Fghyd5
Trait Ontology (TO)
TO: 0000344 wheat stripe rust disease resistance
TO: 0002657 oxidative stress
TO: 0006047 calcium concentration
TO: 0006053 zinc concentration
W06
0.85
F10
GO:0010498 proteasomal protein catabolic process
GO:0016787 hydrolase activity
GO:0006914 autophagy
Gene Ontology (GO)
B. Late symptomless phase/Early symptomatic
PHI-Base
CPK2
FgSte50
FgVam7
FgRav2
Fgleu4
osp24
FgTep1p
FGSG_01974
CYP51B
FgSge1
FgSge1
FgMed1
FgLetm2
AMT2
AMT4
FgSpa2
FgBud6
Cyp51B
FgGAL83
PEX6
fgm4
fgm1
HDF1
Pg1
FgNem1
NPS6
FgOXP2
FgVps27
FgVPS36
NPS6
spt3
FgLDHL2
Fgp1
FgCrpA
GLX
Fg01341
FgZC1
ELP3
noxA
FgMon1
FgMDM1
FgMVP1
FgYPT35
ScOrtholog_TEP1
ScOrtholog_YKL153W
FgERG3B
FGSG_03846
FGSG_06610
GzGPA2
TEP1
Son et al., 2011 TFs - 17
Wang et al., 2011 PKs - 6
Trait Ontology (TO)
TO: 0000112 disease resistance
TO: 0002699 lycopene content
TO:0000303 cold tolerance
Gene Ontology (GO)
GO:0006351 transcription, DNA-template
GO:0003677 DNA binding
Gene Ontology (GO)
GO:0006468 protein phosphorylation
GO:0002229 defense response to oomycetes
GO:0004672 protein kinase activity
Gene set enrichment analysis (GSEA)
Biological Metabolite Clusters (BMC)
F01
0.75
W02
0.95
W08
0.73
F04
PHI-Base
FgGT2
FGSG_02077
GzZC120
Cyp51C
FgERG5B
MCC
BTA1
FgCHS8
FgPLC1
Fgste2
GO:0000981 DNA-binding transcription factor activity
GO:0008270 zinc ion binding
Gene Ontology (GO)
Gene Ontology (GO)
GO:0006749 gluthathione metabolic process
GO:0009607 response to biotic stimulus
GO:0009620 response to fungus
TO: 0000112 disease resistance
TO: 0000276 drought tolerance
TO: 0002657 oxidative stress
C. Late symptomatic phase
Gene Ontology (GO)
GO:0045861 negative regulation of proteolysis
GO:0009611 response to wounding
GO:0006508 proteolysis
GO:0006914 autophagy
Gene Ontology (GO)
GO:0008104 protein localization
GO:0044248 cellular catabolic process
GO:0006914 autophagy
Trait Ontology (TO)
TO: 0000112 disease resistance
TO:0000276 drought tolerance
W10
0.74
W03
0.58
F03
Gene Ontology (GO)
GO:0016491 oxidoreductase activity
GO:0016021 integral component of membrane
TO: 0000437 male sterility
TO:0000707 pericarp colours
TO: 0002699 lycopene content
Trait Ontology (TO)
FGSG_12019
(Sc Gin4-like)
GzZC305
gil1
ScOrtholog_DIA3
GIV4
dcl1
PHI-Base

Figure 4 – figure supplement 1. Annotation of stage-specific modules. Fungal modules (F) and wheat modules (W) depicted with significant enrichment annotations. Fungal modules are additionally annotated with known phenotypes from PHI-base. Genes listed in red in the PHI-base annotation (grey box) exhibit a loss of pathogenicity phenotype when deleted, while the remaining genes display a reduced virulence phenotype when deleted. Plots are separated by modules with highest expression in a given stage of infection, namely **A. Early symptomless, B. Early symptomless and late symptomatic, C. Late symptomless/Early symptomatic, and D. Late symptomatic.**

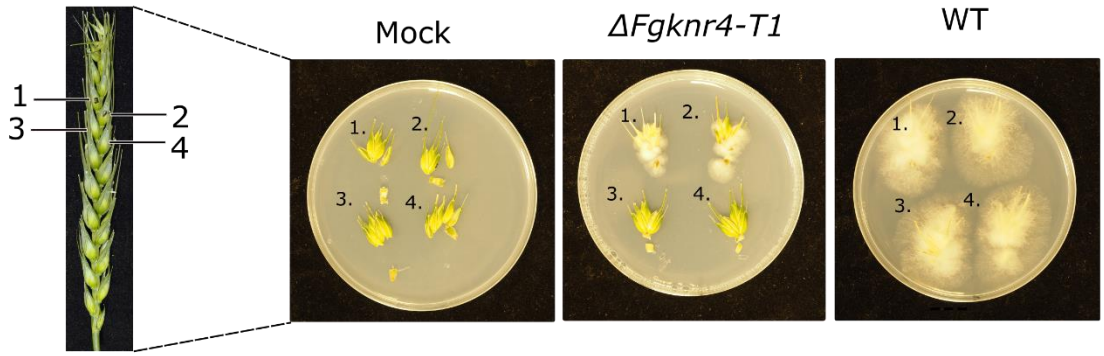

Figure 5 – supplement 1. Surface sterilisation of dissected wheat floral tissue. .

Dissection at 15 dpi of wheat spikes followed by separation of infected wheat spikelet and rachis tissues and subsequent plating onto synthetic nutrient agar (SNA) separated at 15 dpi. Plate images taken 3 days later.

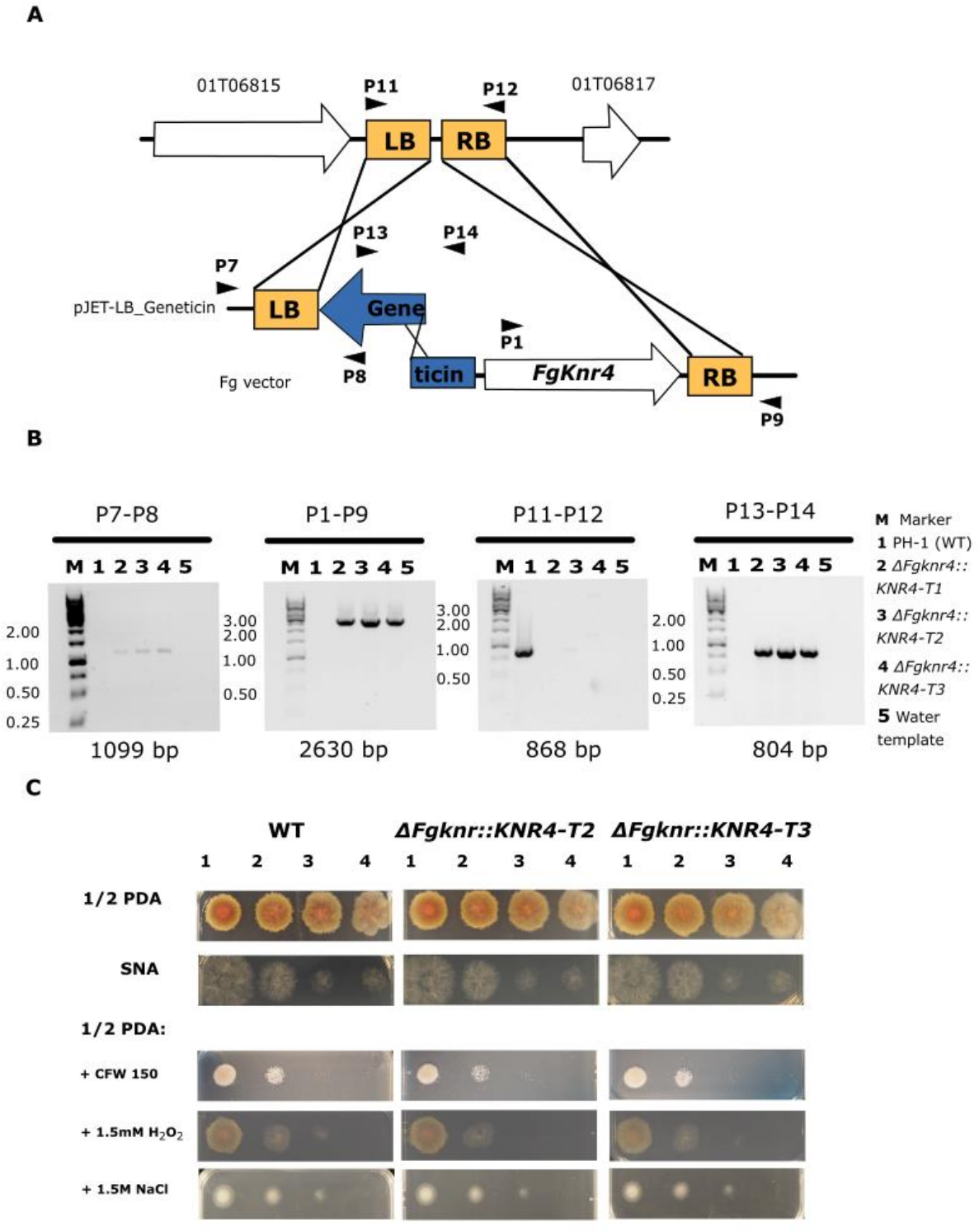

1245

1246 **Figure 6 – figure supplement 1. *FgKnr4* single gene deletion strategy and**

1247 **characterisation of additional transformants. A.** Schematic for the hygromycin split

1248 marker deletion strategy including diagnostic primer locations (P1-6). **B.** Diagnostic PCR

1249 with primer sets depicted in panel A. PCR samples were separated on 7.5 % agarose gel
1250 with a 1 kb DNA ladder. The expected amplicon size is written below the corresponding gel
1251 image. **C.** Dilution series of wild-type (WT) and additional *ΔFgknr4* transformants (*T2* and
1252 *T3*) on Synthetic Nutrient Agar (SNA) and half-strength Potato Dextrose Agar (0.5 PDA) with
1253 and without the addition of single stresses. The dilution series begins at 1: 1 x 10^6 and
1254 continues with 10-fold dilutions (2: 1/10, 3: 1/100, and 4: 1/100). Images taken after 3 days.

1255
1256

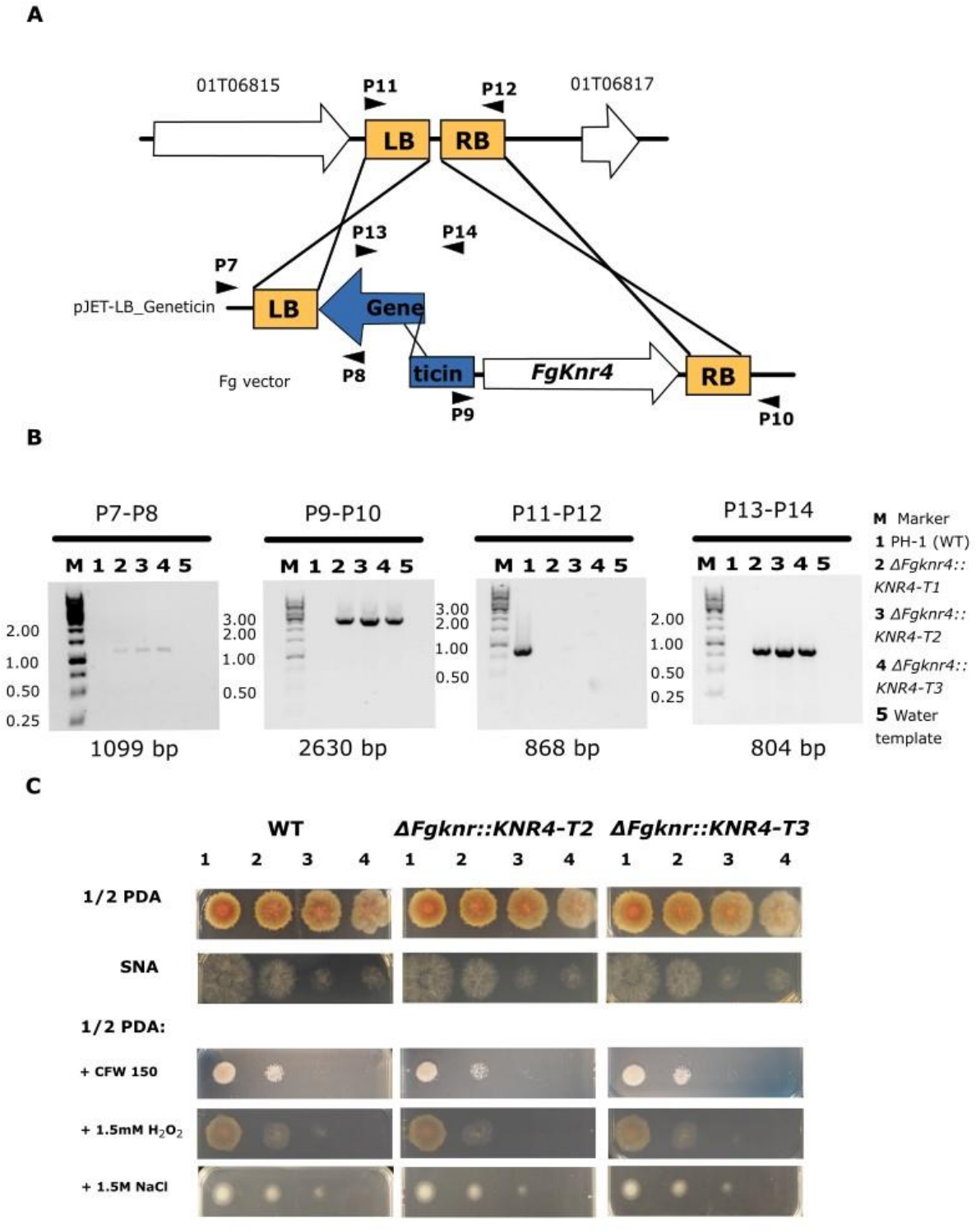

Figure 6 – figure supplement 2. *ΔFgknr4-T1* complementation strategy and characterisation of additional transformants. A. Schematic of gene complementation into the *Fg* transformation locus (Darino et al. (2024), including diagnostic primer locations (P7-

P14). **B.** Diagnostic PCR with primer sets depicted in panel A. PCR samples were separated on 7.5 % agarose gel with a 1 kb DNA ladder. Expected amplicon size is written below the corresponding gel image. **C.** Dilution series of wild-type (WT) and additional *ΔFgknr4::KNR4* transformants (*T2* and *T3*) on Synthetic Nutrient Agar (SNA) and half-strength Potato Dextrose Agar (0.5 PDA) with and without the addition of single stresses. The dilution series begins at 1: 1 x 10^6 and continues with 10-fold dilutions (2: 1/10, 3: 1/100, and 4: 1/100). Image taken after 3 days.

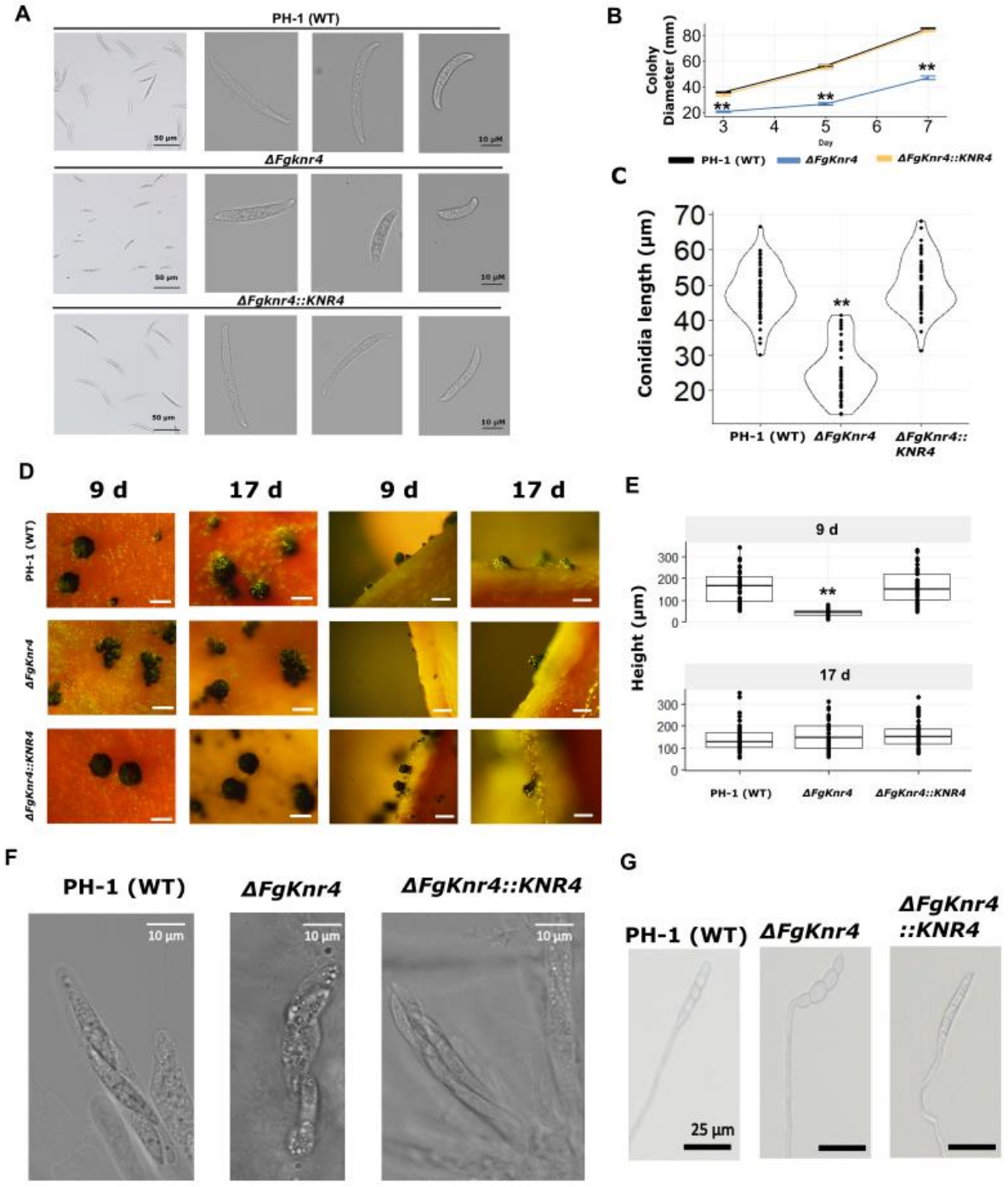

Figure 6 – figure supplement 3. Characterisation of growth rate, conidial size and ascospore production in *ΔFgknr4* and complemented strains. A. Decreased condial size observed in *ΔFgknr4.* Single conidial images to represent long, middle length, and short conidia across strains. B. Mean colony diameter of wild-type (WT), *ΔFgknr4*, and *ΔFgknr4::KNR4* grown on Potato Dextrose Agar (PDA) (N=5). C. Distribution of conidial

length from N = 50 spores for wild-type (WT), *ΔFgknr4*, and *ΔFgknr4::KNR4* strains. D. Representative perithecia images taken after perithecia induction in carrot agar medium using wild-type (WT), *ΔFgknr4*, and *ΔFgknr4::KNR4* strains. Images taken from above (left panels) and from agar sections placed on slides (right panels) on day 9 and day 17. Scale bar = 500 µm. F. Ascospores in intact ascus produced by wild-type (WT), *ΔFgknr4* or *ΔFgknr4::KNR4* strains. Scale bar = 10 µM. G. Ascospores obtained from squashed perithecia of wild-type (WT), *ΔFgknr4* or *ΔFgknr4::KNR4* strains are viable and form germ tubes. Scale bar = 25 µm. Significance is denoted as **= $p \leq 0.01$. Significance was determined by a one-way ANOVA followed by Tukey HSD correction.

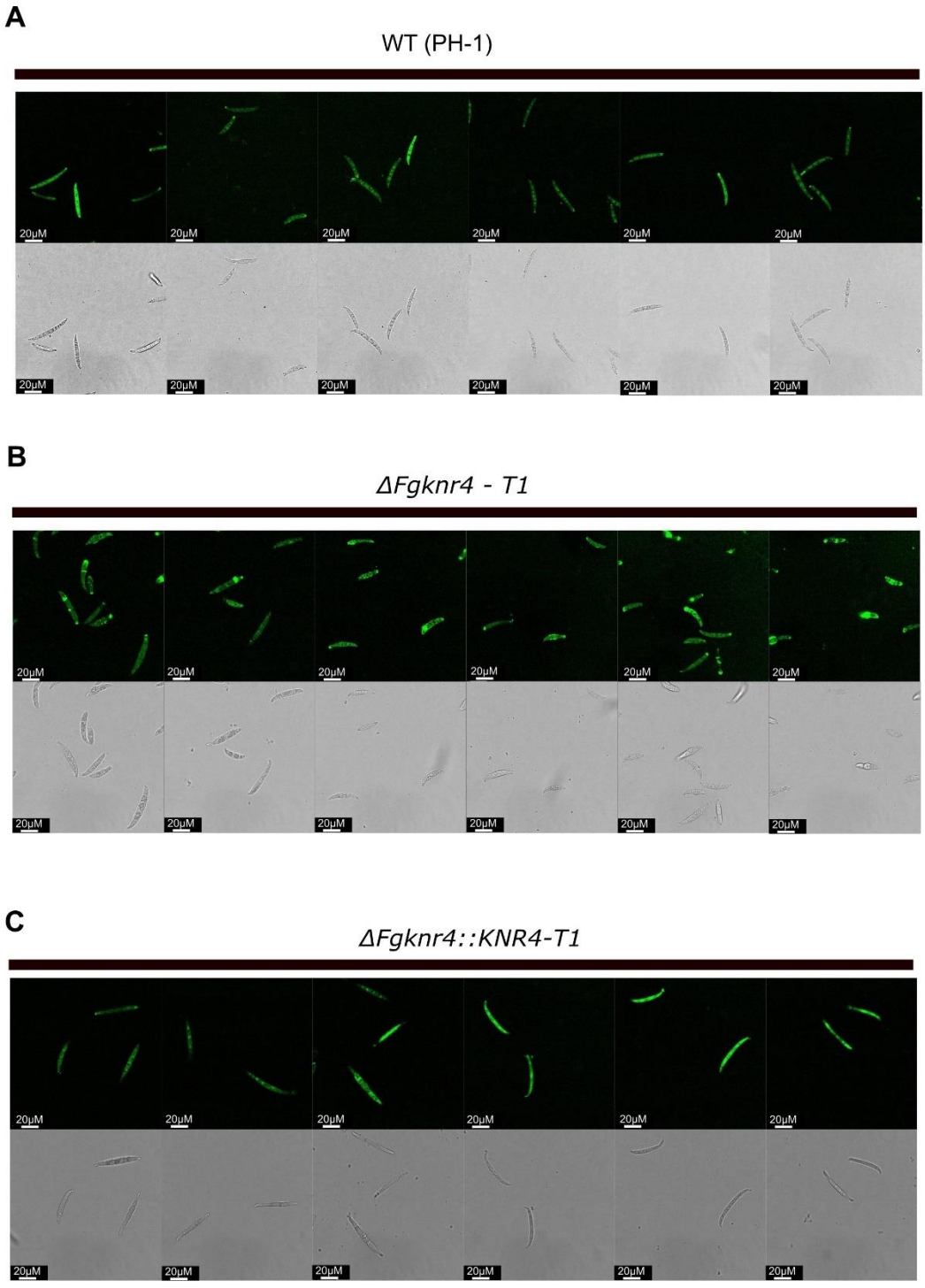

Supplementary Figure 6 – figure supplement 4. Additional fluorescent microscopy images of irregular chitin distribution in *ΔFgknr4* conidia . Visualisation of chitin-stained conidia with Wheat Germ Agglutinin Alexa Fluor™ 488 Conjugate (WGA) in wild-type (WT) (A), *ΔFgknr4* (B) and *ΔFgknr4::KNR4* (C).

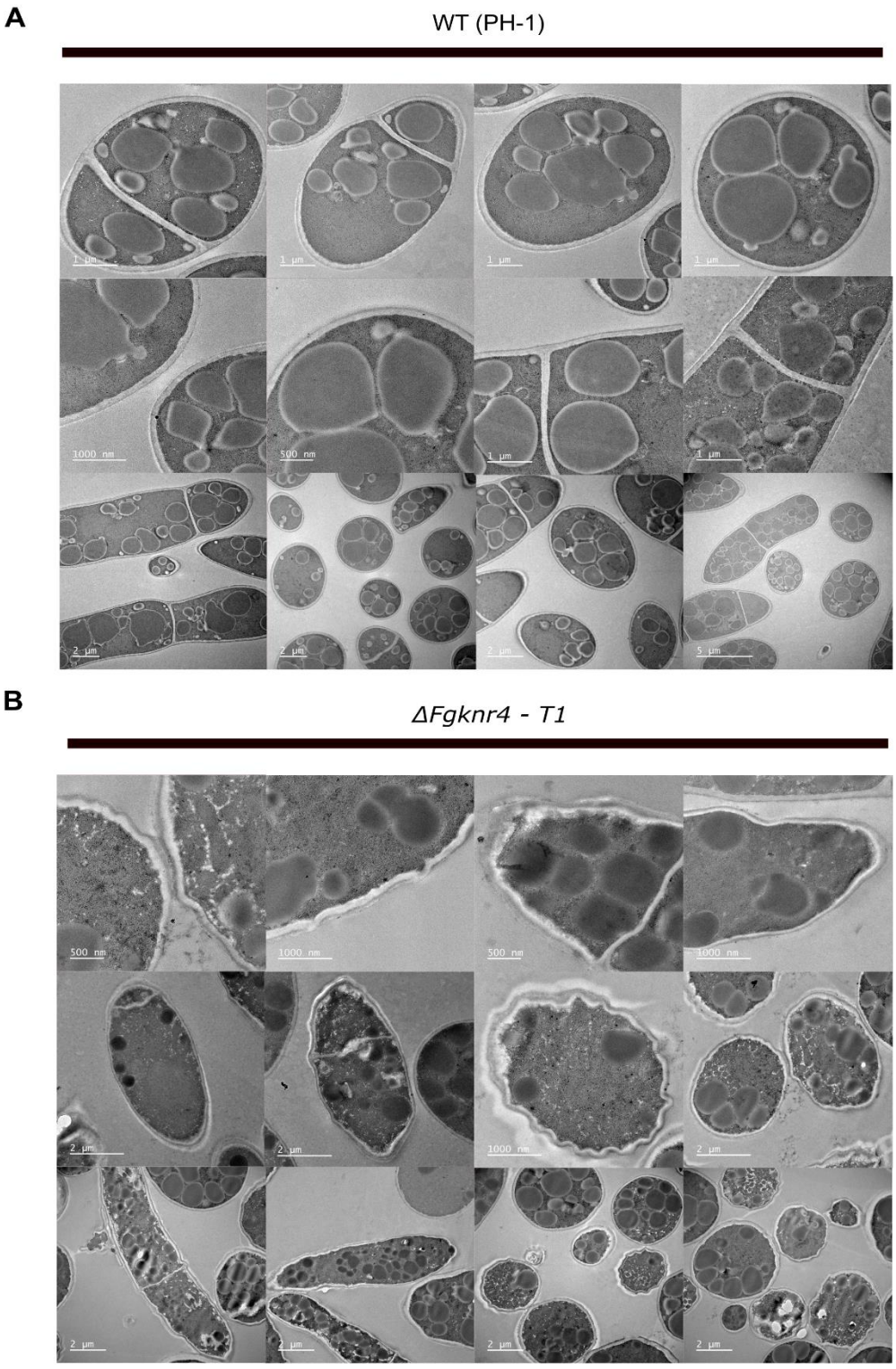

Figure 6 – figure supplement 5. Additional TEM images of abnormal cell wall morphology in *ΔFgknr4* conidia. TEM imaging of wild-type (**A**) and *ΔFgknr4* (**B**) conidia, showing differences in cell wall structure and different magnifications.

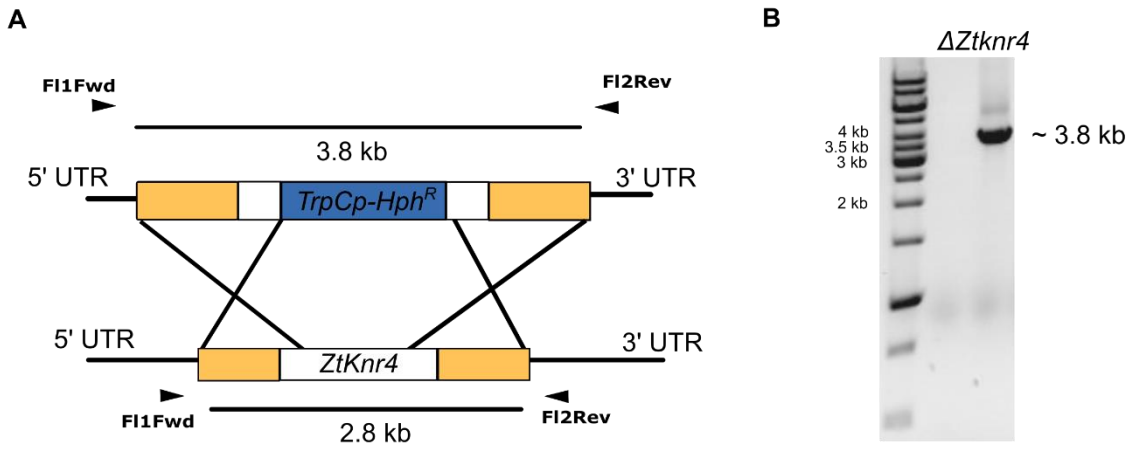

1293

1294 **Figure 8 – figure supplement 1.** *ΔZtknr4* diagnostic PCR and disruption deletion strategy.

1295 **A.** Hygromycin (*Hph*^{R}) replacement cassette inserts at *ZtKnr4* locus through homologues

1296 recombination via homologous flanks (yellow and white). **B.** Diagnostic PCR demonstrating

1297 presence of large insertion fragment in *ΔZtknr4* transformant using Fl1Fwd and Fl2Rev

1298 primers.

Supplementary File 1. Network module sizes and gene module assignments. Spreadsheet containing sizes of all modules in fungal and wheat networks. 'Fungal module assignments' and 'Wheat module assignments' tabs contain a column with all fungal IDs (RRES v.5 PH-1) or wheat IDs (Column A = IWGSC RefSeq v2.1; Column B = IWGSC RefSeq v1.1) with an adjacent column denoting which module they are clustered in.

Supplementary File 2. *F. graminearum* genes with known phenotypes with the PHI-base database (www.PHI-base.org) in each fungal module. Table provides RRES v5 gene ID, PHI identifier ID from PHI-base, Uniprot protein ID, gene function, mutant phenotype, author reference, and year published.

Supplementary File 3. Primer list. Primers used to generate mutant and complemented strains.

Table S1. Candidate gene selection in fungal module F16. Table provides details on the 15 candidates within module F16 with the highest module membership (MM) and reason for exclusion from further functional characterisation analysis. This table includes the MM score and associated *p*-values (p.MM), as well as correlation strength to corresponding wheat modules (Cor) and *p*-values (p.Cor).

ID	COR.W05	P.COR.W05	GS.W01	P.COR.W01	MM.F16	P.MM.F16	INTERPRO DESCRIPTION	REASON FOR EXCLUSION
FGRAMPH1_01T20453	0.79	0.00	0.93	0.00	0.95	0.00	N/A	Unknown domain
FGRAMPH1_01T06173	0.88	0.00	0.77	0.00	0.94	0.00	domain of unknown function DUF2405;	Unknown domain
FGRAMPH1_01T22959	0.69	0.00	0.94	0.00	0.93	0.00	RNA recognition motif domain;U1 small nuclear ribonucleoprotein of 70kDa N-terminal;snRNP70, RNA recognition motif;RNA-binding domain superfamily;U1 small nuclear ribonucleoprotein 70kDa	75 genes with this domain in *F. graminearum* proteome

FGRAMPH1_01T10513	0.73	0.00	0.76	0.00	0.91	0.00	Helicase, C-terminal;DEAD/DEAH box helicase domain;Helicase superfamily 1/2, ATP-binding domain;P-loop containing nucleoside triphosphate hydrolase	26 ancient paralogues on Ensembl (2022)
FGRAMPH1_01T00861	0.86	0.00	0.76	0.00	0.91	0.00	BRCT domain;AAA+ ATPase domain;ATPase, AAA-type, core;DNA polymerase III, clamp loader complex, gamma/delta/delta subunit, C-terminal;Replication factor C subunit 1;DNA replication factor RFC1, C-terminal;P-loop containing nucleoside triphosphate hydrolase;BRCT domain superfamily	2 ancient paralogues on Ensembl (2022)
FGRAMPH1_01T00671	0.69	0.00	0.80	0.00	0.91	0.00	PAP/25A-associated;Nucleotidyltransferase superfamily	1 ancient paralogue on Ensembl (2022)

FGRAMPH1_01T00977	0.83	0.00	0.85	0.00	0.90	0.00	Endoplasmic reticulum vesicle transporter, C-terminal;Endoplasmic reticulum vesicle transporter, N-terminal	1 ancient paralogue on Ensembl (2022)
FGRAMPH1_01T18141	0.72	0.00	0.83	0.00	0.90	0.00	CDC48, N-terminal subdomain;AAA+ ATPase domain;ATPase, AAA-type, core;ATPase, AAA-type, conserved site;CDC48, domain 2;Aspartate decarboxylase-like domain superfamily;Vps4 oligomerisation, C-terminal;P-loop containing nucleoside triphosphate hydrolase;CDC48 domain 2-like superfamily;AAA ATPase, AAA+ lid domain	15 ancient paralogues on Ensembl(2022)

FGRAMPH1_01T22333	0.83	0.00	0.75	0.00	0.90	0.00	AMP-dependent synthetase/ligase;Phosphopantetheine binding ACP domain;Trimeric LpxA-like superfamily;Polyketide synthase, phosphopantetheine-binding domain;ACP-like superfamily	BLAST hit in *F. graminearum* PH-1 genome (E = 4.5e-063)
FGRAMPH1_01T27545	0.71	0.00	0.88	0.00	0.90	0.00	Sterol-sensing domain;Protein patched/dispatched;Niemann-Pick C1, N-terminal	Previously studied. Reduced virulence phenotype (Breakspear et al. 2011)
FGRAMPH1_01T23707	0.82	0.00	0.74	0.00	0.90	0.00	Knr4/Smi1 family;Knr4/Smi1-like domain	
FGRAMPH1_01T27219	0.66	0.00	0.93	0.00	0.89	0.00	N/A	Unknown domain

FGRAMPH1_01T02111	0.81	0.00	0.85	0.00	0.89	0.00	DNA-directed RNA polymerase, subunit 2, hybrid-binding domain;RNA polymerase, beta subunit, conserved site;RNA polymerase Rpb2, domain 7;RNA polymerase Rpb2, domain 2;RNA polymerase, beta subunit, protrusion;RNA polymerase Rpb2, domain 3;RNA polymerase Rpb2, domain 4;RNA polymerase Rpb2, domain 5;DNA-directed RNA polymerase, subunit 2	2 ancient paralogues on Ensembl (2022)
FGRAMPH1_01T04893	0.75	0.00	0.69	0.00	0.88	0.00	SNF2-related, N-terminal domain;Helicase, C-terminal;Helicase superfamily 1/2, ATP-binding domain;DBINO domain;P-loop containing nucleoside triphosphate hydrolase	26 ancient paralogues on Ensembl (2022)
FGRAMPH1_01T07953	0.84	0.00	0.75	0.00	0.88	0.00	Folylpolyglutamate synthetase;Mur-like, catalytic domain	2 paralogues on Ensembl (2022)

		superfamily;Mur ligase, C-terminal domain superfamily

1315

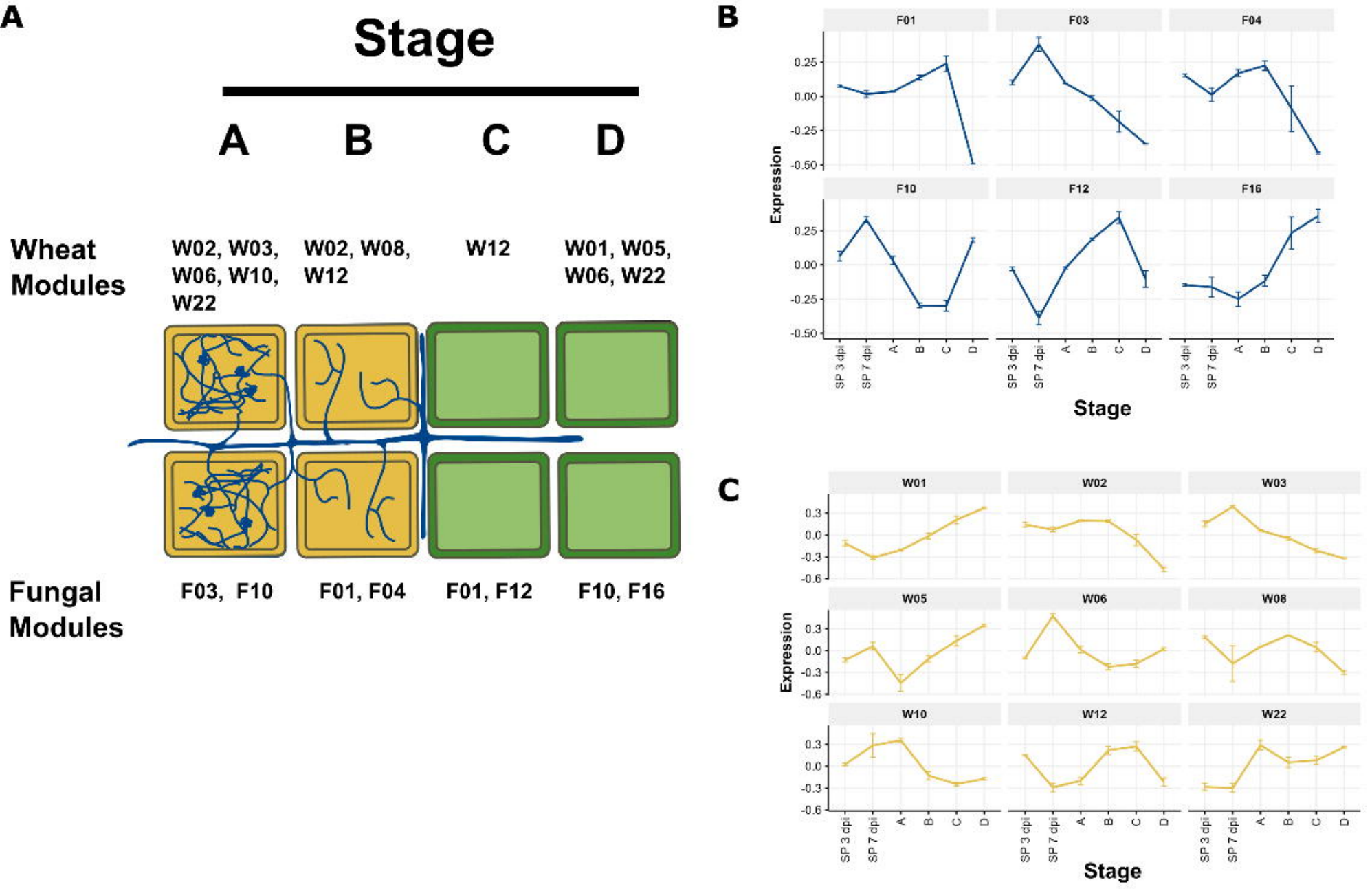
A
Stage
A
B
C
D
Wheat Modules
W02, W03, W06, W10, W22
W02, W08, W12
W12
W01, W05, W06, W22
Fungal Modules
F03, F10
F01, F04
F01, F12
F10, F16
B
F01
F03
F04
F10
F12
F16
Expression
0.25
0.00
-0.25
-0.50
SP 3 dpi
SP 7 dpi
A
B
C
D
Stage
C
W01
W02
W03
W05
W06
W08
W10
W12
W22
0.3
0.0
-0.3
-0.6

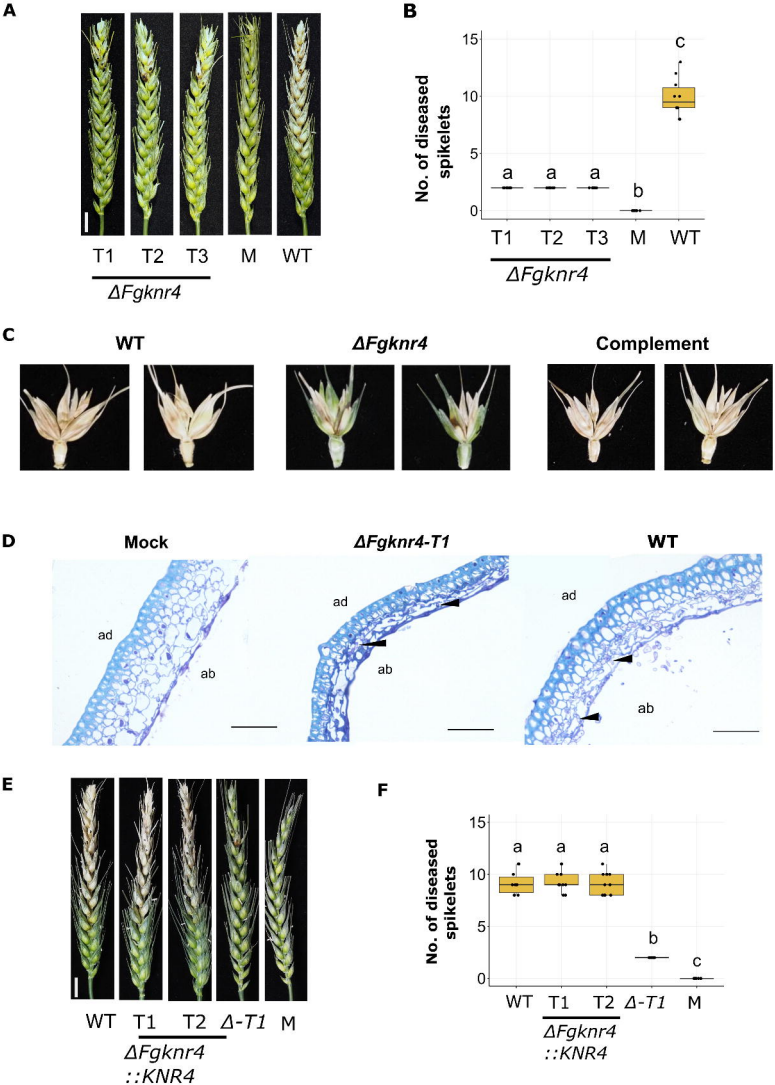
A
T1
T2
T3
M
WT
ΔFgknr4
B
No. of diseased spikelets
15
10
5
0
a
a
a
b
c
T1
T2
T3
M
WT
ΔFgknr4
C
WT
ΔFgknr4
Complement
D
Mock
ΔFgknr4-T1
WT
ad
ab
E
WT
T1
T2
Δ-T1
M
ΔFgknr4
::KNR4
F
No. of diseased spikelets
15
10
5
0
a
a
a
b
c
WT
T1
T2
Δ-T1
M
ΔFgknr4
::KNR4

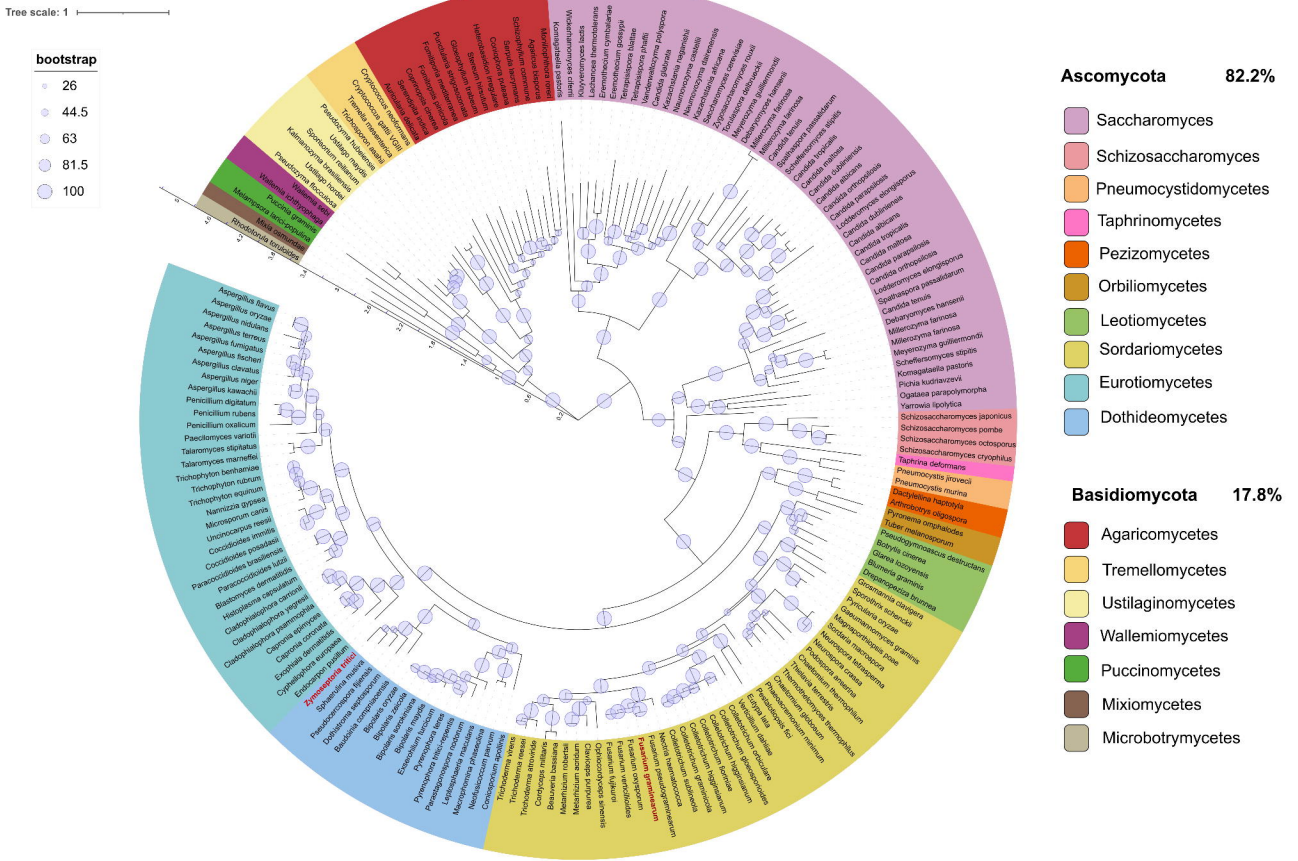
Tree scale: 1
bootstrap
26
44.5
63
81.5
100
Ascomycota 82.2%
Saccharomyces
Schizosaccharomycetes
Pneumocystidomycetes
Taphrinomycetes
Pezizomycetes
Orbiliomycetes
Leotiomycetes
Sordariomycetes
Eurotiomycetes
Dothideomycetes
Basidiomycota 17.8%
Agaricomycetes
Tremellomycetes
Ustilaginomycetes
Wallemiomycetes
Puccinomycetes
Mixiomycetes
Microbotrymycetes
Zymoseptoria tritici
Fusarium graminearum
Taphrina deformans

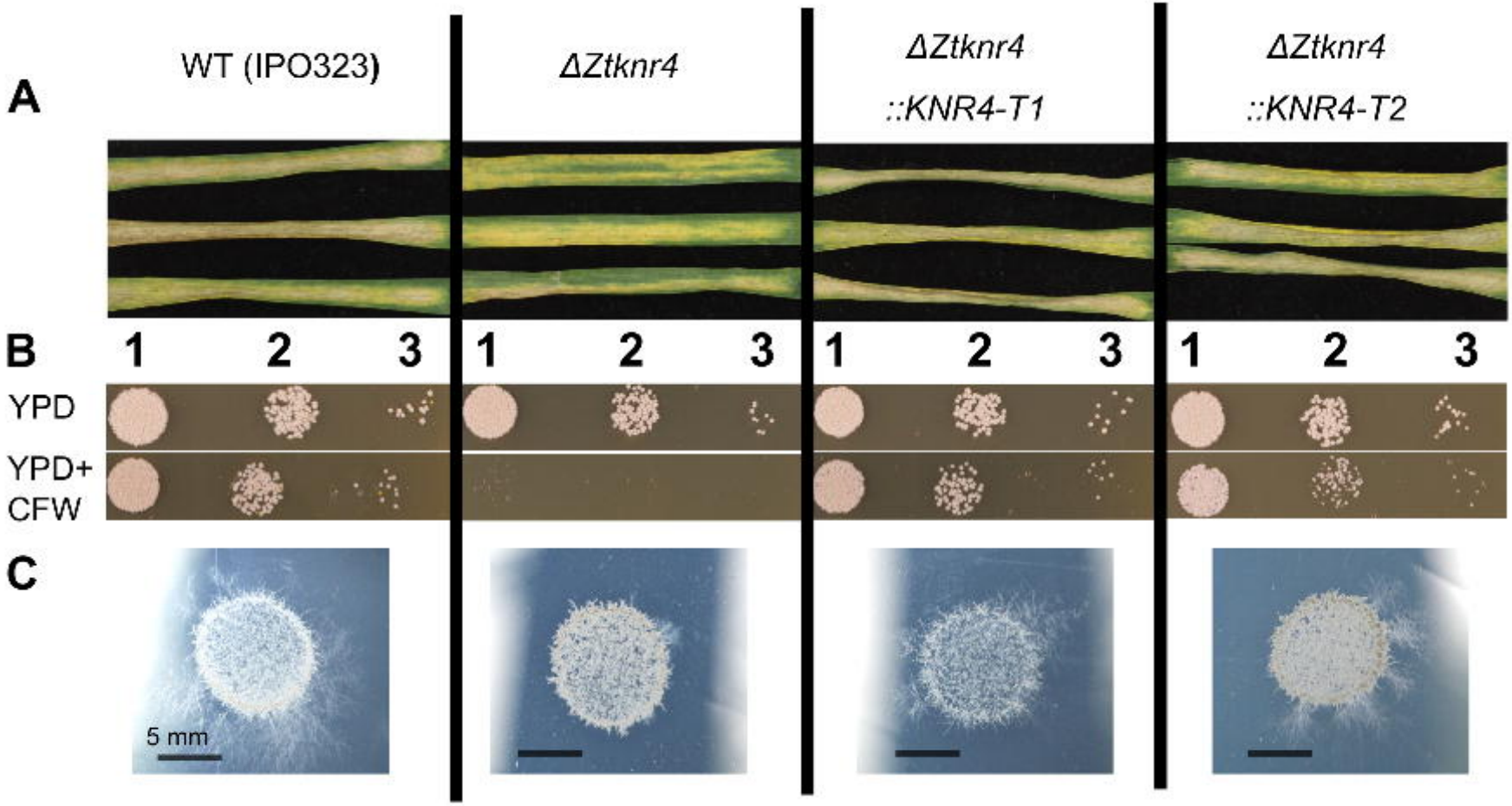
A
WT (IPO323)
ΔZtknr4
ΔZtknr4
::KNR4-T1
ΔZtknr4
::KNR4-T2
B
1
2
3
1
2
3
1
2
3
1
2
3
YPD
YPD+
CFW
C
5 mm

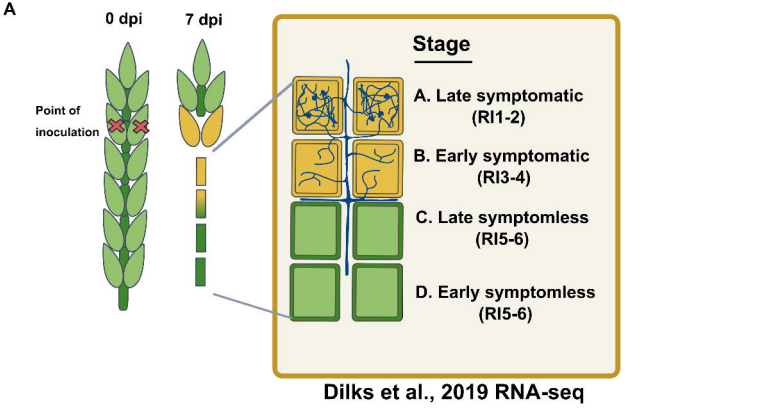
A
0 dpi
7 dpi
Point of inoculation
Stage
A. Late symptomatic (RI1-2)
B. Early symptomatic (RI3-4)
C. Late symptomless (RI5-6)
D. Early symptomless (RI5-6)
Dilks et al., 2019 RNA-seq

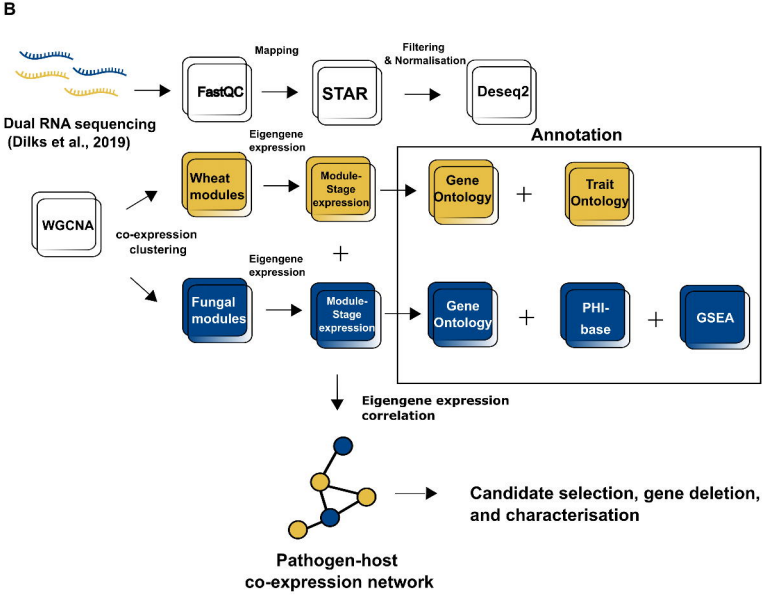
B
Dual RNA sequencing (Dilks et al., 2019)
FastQC
Mapping
STAR
Filtering & Normalisation
Deseq2
Annotation
WGCNA
co-expression clustering
Wheat modules
Fungal modules
Eigengene expression
Module-Stage expression
Gene Ontology
Trait Ontology
PHI-base
GSEA
Eigengene expression correlation
Candidate selection, gene deletion, and characterisation
Pathogen-host co-expression network

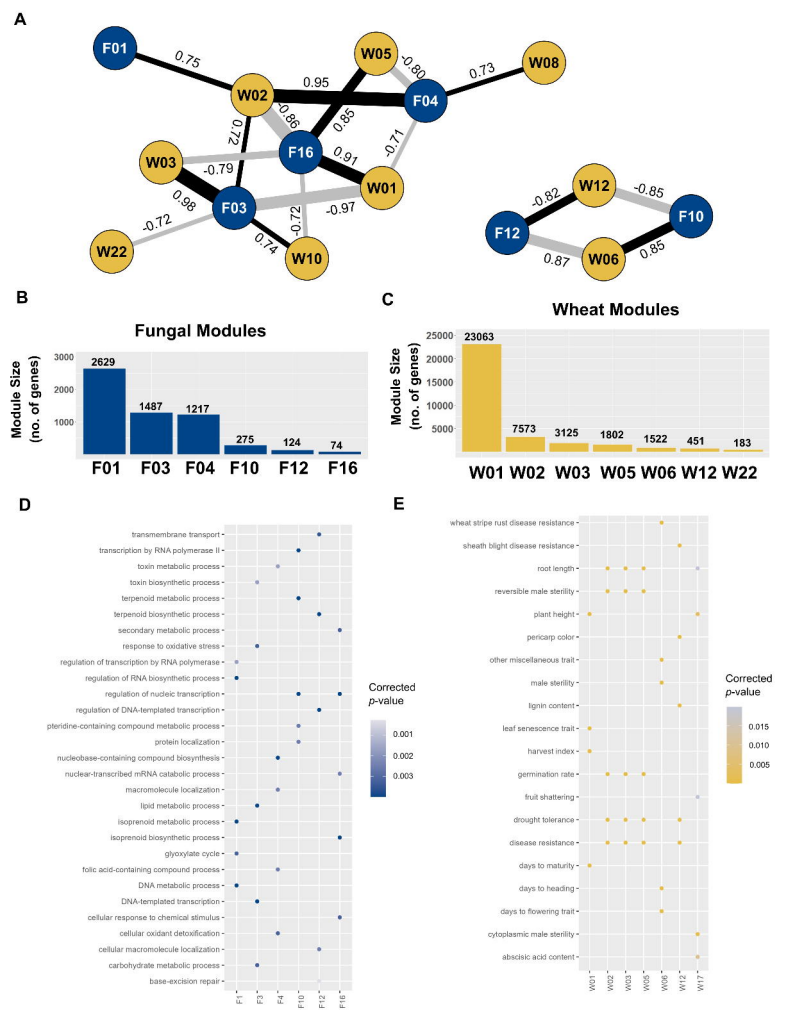
A
F01
W05
W08
W02
F04
W03
F16
W01
F03
W22
W10
W12
F10
F12
W06
0.75
0.95
-0.80
0.73
-0.86
0.85
0.72
-0.71
-0.79
0.91
0.98
-0.72
-0.97
-0.72
0.74
-0.82
-0.85
0.87
0.85
B
Fungal Modules
Module Size (no. of genes)
3000
2000
1000
2629
1487
1217
275
124
74
F01
F03
F04
F10
F12
F16
C
Wheat Modules
Module Size (no. of genes)
25000
20000
15000
10000
5000
23063
7573
3125
1802
1522
451
183
W01
W02
W03
W05
W06
W12
W22
D
transmembrane transport
transcription by RNA polymerase II
toxin metabolic process
toxin biosynthetic process
terpenoid metabolic process
terpenoid biosynthetic process
secondary metabolic process
response to oxidative stress
regulation of transcription by RNA polymerase
regulation of RNA biosynthetic process
regulation of nucleic transcription
regulation of DNA-templated transcription
pteridine-containing compound metabolic process
protein localization
nucleobase-containing compound biosynthesis
nuclear-transcribed mRNA catabolic process
macromolecule localization
lipid metabolic process
isoprenoid metabolic process
isoprenoid biosynthetic process
glyoxylate cycle
folic acid-containing compound process
DNA metabolic process
DNA-templated transcription
cellular response to chemical stimulus
cellular oxidant detoxification
cellular macromolecule localization
carbohydrate metabolic process
base-excision repair
F01
F03
F04
F10
F12
F16
Corrected p-value
0.001
0.002
0.003
E
wheat stripe rust disease resistance
sheath blight disease resistance
root length
reversible male sterility
plant height
pericarp color
other miscellaneous trait
male sterility
lignin content
leaf senescence trait
harvest index
germination rate
fruit shattering
drought tolerance
disease resistance
days to maturity
days to heading
days to flowering trait
cytoplasmic male sterility
abscisic acid content
W01
W02
W03
W05
W06
W12
W17
Corrected p-value
0.015
0.010
0.005

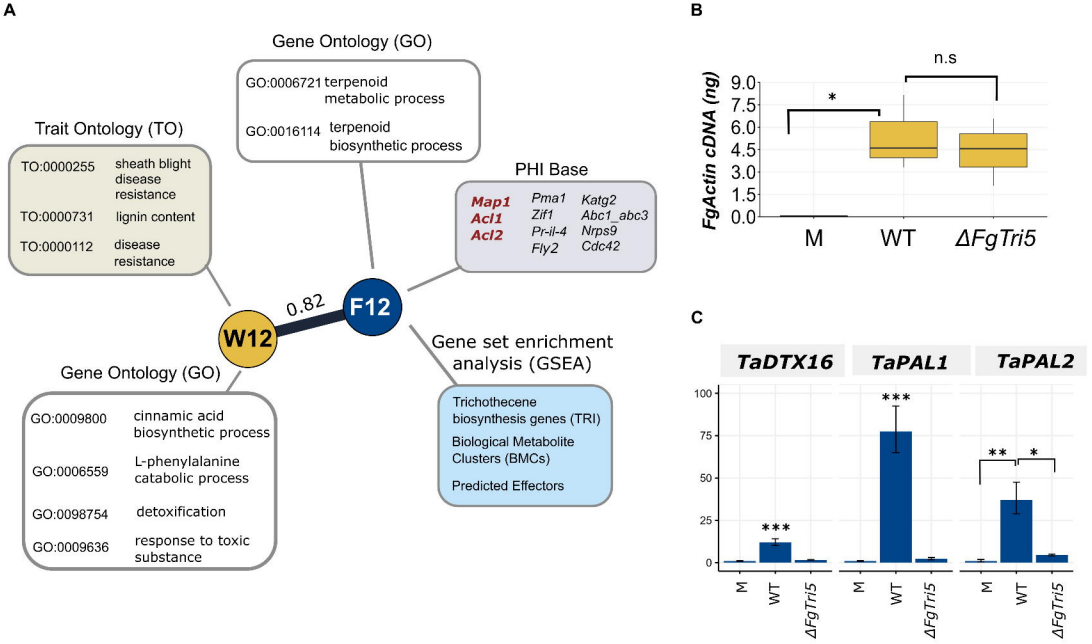
A
Gene Ontology (GO)
GO:0006721 terpenoid metabolic process
GO:0016114 terpenoid biosynthetic process
Trait Ontology (TO)
TO:0000255 sheath blight disease resistance
TO:0000731 lignin content
TO:0000112 disease resistance
PHI Base
Map1 Acl1 Acl2
Pma1 Zif1 Pr-il-4 Fly2
Katg2 Abc1_abc3 Nrps9 Cdc42
0.82
W12
F12
Gene set enrichment analysis (GSEA)
Trichothecene biosynthesis genes (TRI)
Biological Metabolite Clusters (BMCs)
Predicted Effectors
Gene Ontology (GO)
GO:0009800 cinnamic acid biosynthetic process
GO:0006559 L-phenylalanine catabolic process
GO:0098754 detoxification
GO:0009636 response to toxic substance
B
n.s
*
FgActin cDNA (ng)
9.0
7.5
6.0
4.5
3.0
1.5
0.0
M
WT
ΔFgTri5
C
TaDTX16
TaPAL1
TaPAL2
100
75
50
25
0
***
***
**
*
M
WT
ΔFgTri5

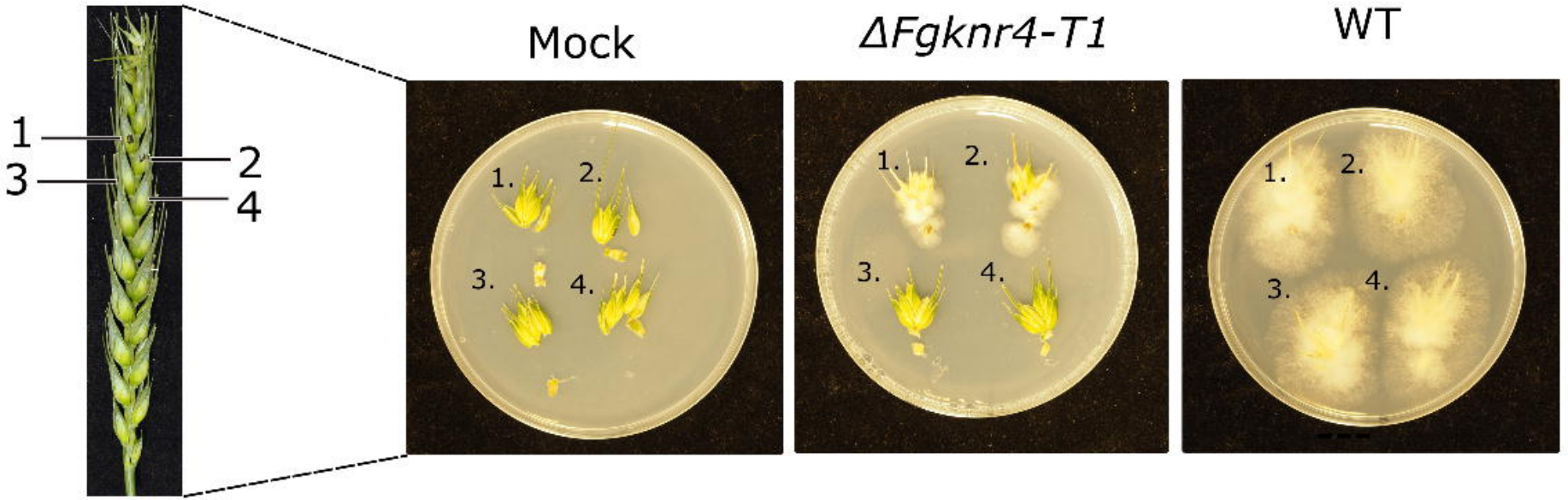
1
2
3
4
Mock
ΔFgknr4-T1
WT
1.
2.
3.
4.
1.
2.
3.
4.
1.
2.
3.
4.

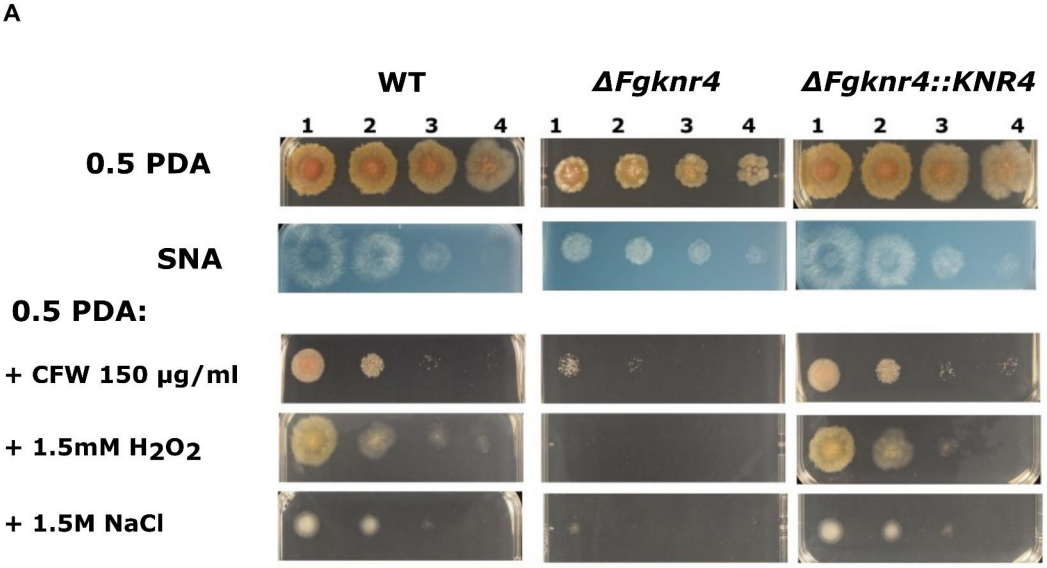
A
WT
ΔFgknr4
ΔFgknr4::KNR4
1 2 3 4
0.5 PDA
SNA
0.5 PDA:
+ CFW 150 µg/ml
+ 1.5mM H2O2
+ 1.5M NaCl

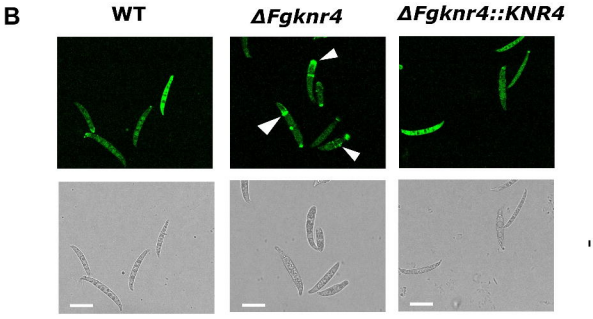
B
WT
ΔFgknr4
ΔFgknr4::KNR4

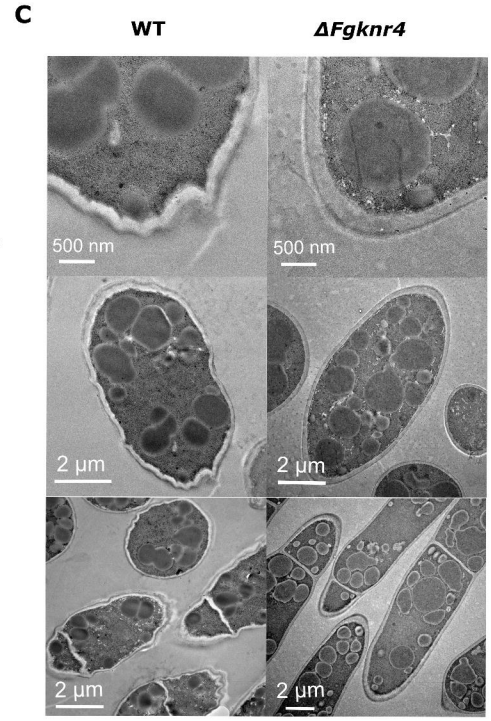
C
WT
ΔFgknr4
500 nm
2 µm

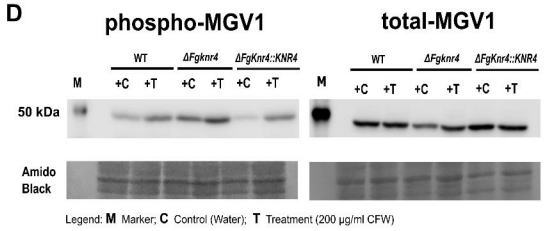
D
phospho-MGV1
total-MGV1
WT
ΔFgknr4
ΔFgKnr4::KNR4
M
+C +T
50 kDa
Amido Black
Legend: M Marker; C Control (Water); T Treatment (200 µg/ml CFW)

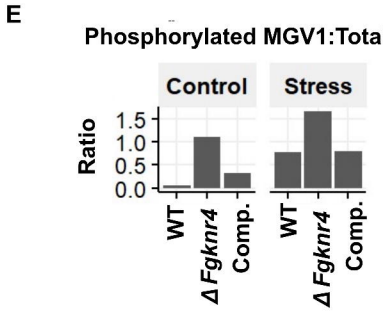
E
Phosphorylated MGV1:Total MGV1
Control
Stress
Ratio
1.5
1.0
0.5
0.0
WT
Δ Fgknr4
Comp.

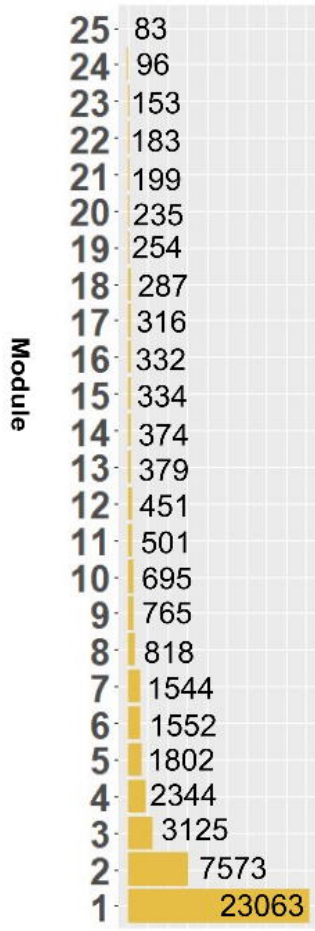

GO MF/BP Summary	GO CC Summary	Trait Ontology (TO)
DNA integration	Cell periphery	ethylene sensitivity
Isopentenyl diphosphate biosynthesis	-	callus induction
Protein modification	-	other miscellaneous trait
-	-	other miscellaneous trait
-	-	total root number
DNA packaging	Nucleosome	cytoplasmic male sterility
Lipid biosynthesis and proteasome activity	Lipid droplet	cytoplasmic male sterility
Ubiquitination and protein catabolism	Proteosome complex	auxin sensitivity
Diterpenoid biosythesis	Extracellular region	cytoplasmic male sterility
Protein phosphorylation and kinase activity	Integral component of membrane	disease resistance
Fatty acid metabolism and synthesis	-	plant height
Translation	Cytosilic ribosome	stem elongation
Structural constituent of ribosome	Cytosilic ribosome	leaf senescence trait
Detoxification and response to toxic substance	-	sheath blight disease resistance
Glycolysis	-	self-incompatibility
Protein localisation and autophagy	Protein-containing complex	male sterility
Protein phosphorylation and kinase activity	Integral component of membrane	germination rate
Protein phosphorylation and defense response	Integral component of membrane	disease resistance
Response to water and water channel activity	Chloroplast	cold tolerance
Protein catabolism and autophagy	Proteasome complex	days to flowering trait
Vesicle transport and hydrolase activity	Vesicle	disease resistance
Gene expression	Ribonucleoprotein complex	disease resistance
Proteolysis and autophagy	Peroxisome	disease resistance
Gluthathione metabolism and response to biotic stimuli	Extracellular region	disease resistance
RNA modification and defense response	Chloroplast	harvest index

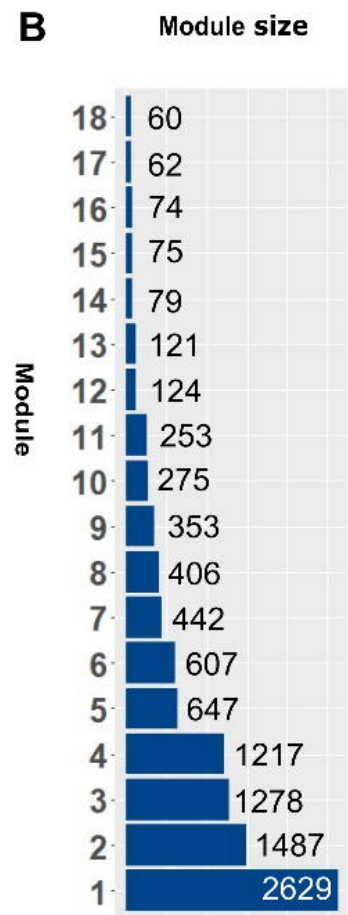

Phenotype				GO MF/BP Summary	GO CC Summary	Gene set enrichment
LOP	RV	L	U			
0	0	0	3	-	-	
0	0	0	3	-	-	
0	4	0	2	-	-	
0	0	0	2	-	-	
0	2	1	3	-	-	
0	2	0	6	-	-	
3	11	0	6	Terpenoid metabolic process	Extracellular region	
0	6	1	15	-	-	
0	11	0	14	-	-	
1	13	5	25	-	-	
0	10	1	9	-	-	
0	0	0	1	Translation	Cytoplasm	
0	9	3	35	-	-	
2	43	13	26	Metabolic processes	Cytoplasm	
1	9	6	88	Transcription factor activity	Ribosome	
0	6	1	77	Oxidoreductase activity	Membrane	
4	66	12	88	Cellular Organisation	Membrane	
4	65	16	184	Transcription factor activity	Nucleus	

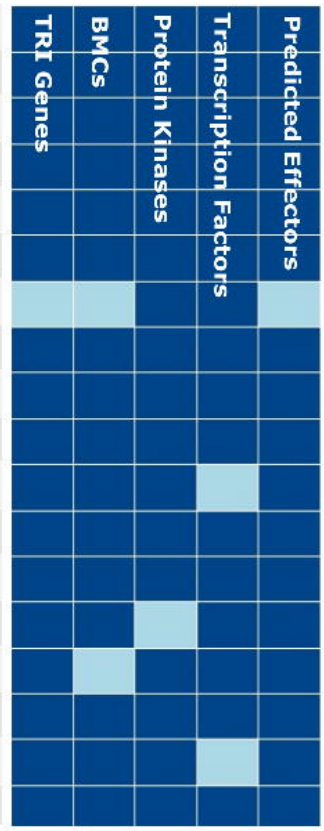

Fungal

Wheat

A. Scale Free Model Fit

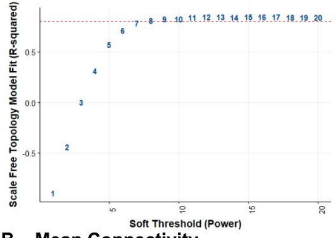

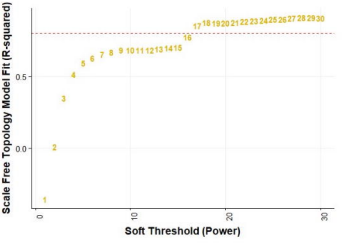

B. Mean Connectivity

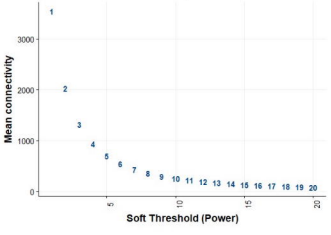

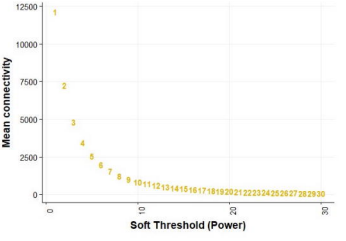

C. Module Quality

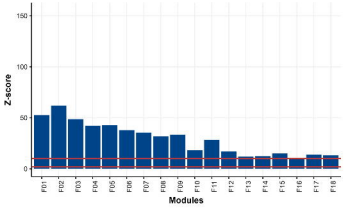

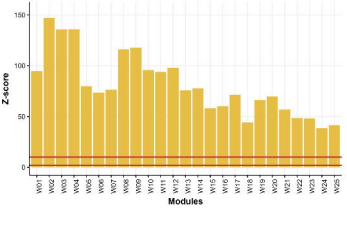

D. Module Preservation

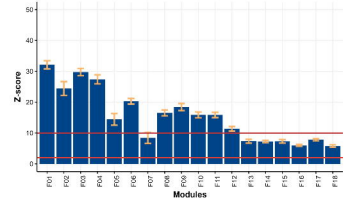

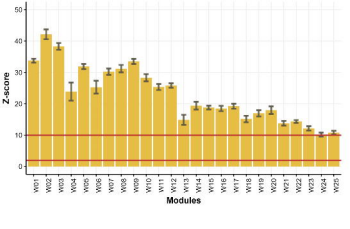

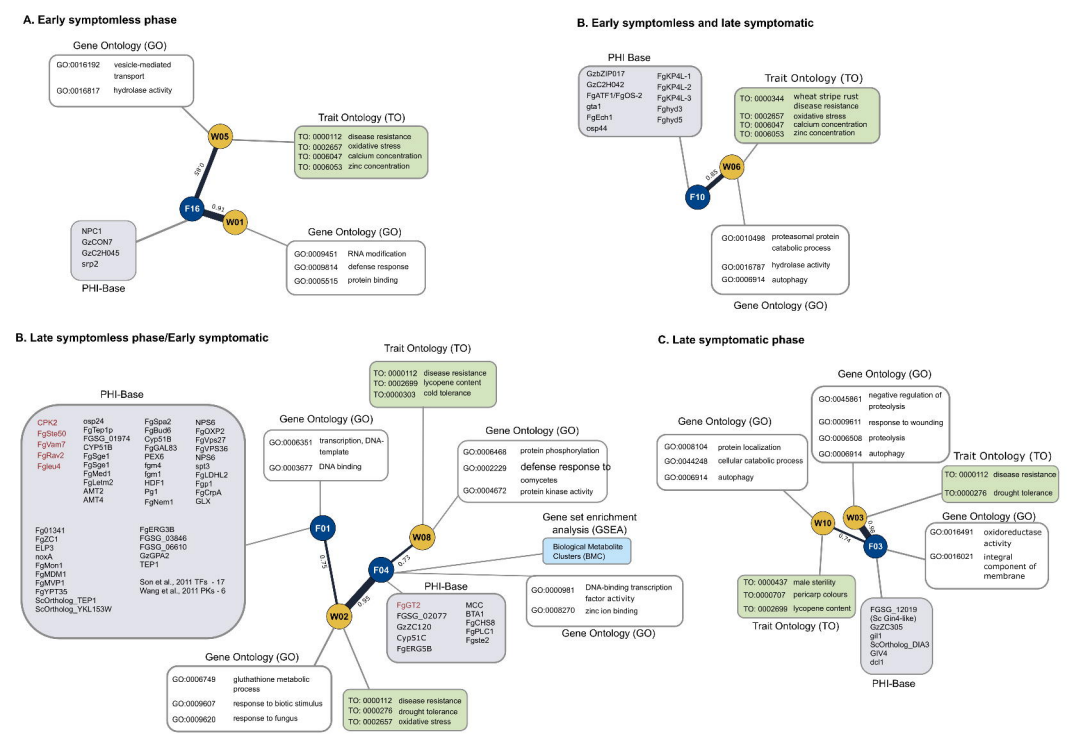
A. Early symptomless phase
Gene Ontology (GO)
GO:0016192 vesicle-mediated transport
GO:0016817 hydrolase activity
W05
0.0
Trait Ontology (TO)
TO: 0000112 disease resistance
TO: 0002657 oxidative stress
TO: 0006047 calcium concentration
TO: 0006053 zinc concentration
F16
0.91
W01
NPC1
GzCON7
GzC2H045
srp2
PHI-Base
Gene Ontology (GO)
GO:0009451 RNA modification
GO:0009814 defense response
GO:0005515 protein binding
B. Early symptomless and late symptomatic
PHI Base
GzbZIP017
GzC2H042
FgATF1/FgOS-2
gta1
FgEch1
osp44
FgKP4L-1
FgKP4L-2
FgKP4L-3
Fghyd3
Fghyd5
Trait Ontology (TO)
TO: 0000344 wheat stripe rust disease resistance
TO: 0002657 oxidative stress
TO: 0006047 calcium concentration
TO: 0006053 zinc concentration
W06
0.92
F10
GO:0010498 proteasomal protein catabolic process
GO:0016787 hydrolase activity
GO:0006914 autophagy
Gene Ontology (GO)
B. Late symptomless phase/Early symptomatic
PHI-Base
CPK2
FgSte50
FgVam7
FgRav2
Fgleu4
osp24
FgTep1p
FGSG_01974
CYP51B
FgSge1
FgSge1
FgMed1
FgLetm2
AMT2
AMT4
FgSpa2
FgBub6
Cyp51B
FgGAL83
PEX6
fgm4
fgm1
HDF1
Pg1
FgNem1
NPS6
FgVps27
FgVPS36
NPS6
spl3
FgLDHL2
Fgp1
FgCrpA
GLX
Fg01341
FgZC1
ELP3
noxA
FgMon1
FgMDM1
FgMVP1
FgYPT35
ScOrtholog_TEP1
ScOrtholog_YKL153W
FgERG3B
FGSG_03846
FGSG_06610
Gz3FA2
TEP1
Son et al., 2011 TFs - 17
Wang et al., 2011 PKs - 6
Trait Ontology (TO)
TO: 0000112 disease resistance
TO: 0002699 lycopene content
TO:0000303 cold tolerance
Gene Ontology (GO)
GO:0006351 transcription, DNA-template
GO:0003677 DNA binding
Gene Ontology (GO)
GO:0006468 protein phosphorylation
GO:0002229 defense response to oomycetes
GO:0004672 protein kinase activity
Gene set enrichment analysis (GSEA)
Biological Metabolite Clusters (BMC)
F01
0.0
W08
0.73
F04
0.93
W02
PHI-Base
FgGT2
FGSG_02077
GzZC120
Cyp51C
FgERG5B
MCC
BTA1
FgCHS8
FgPLC1
Fgste2
GO:0000981 DNA-binding transcription factor activity
GO:0008270 zinc ion binding
Gene Ontology (GO)
Gene Ontology (GO)
GO:0006749 gluthathione metabolic process
GO:0009607 response to biotic stimulus
GO:0009620 response to fungus
TO: 0000112 disease resistance
TO: 0000276 drought tolerance
TO: 0002657 oxidative stress
C. Late symptomatic phase
Gene Ontology (GO)
GO:0045861 negative regulation of proteolysis
GO:0009611 response to wounding
GO:0006508 proteolysis
GO:0006914 autophagy
Gene Ontology (GO)
GO:0008104 protein localization
GO:0044248 cellular catabolic process
GO:0006914 autophagy
Trait Ontology (TO)
TO: 0000112 disease resistance
TO:0000276 drought tolerance
W03
0.0
W10
0.74
F03
Gene Ontology (GO)
GO:0016491 oxidoreductase activity
GO:0016021 integral component of membrane
TO: 0000437 male sterility
TO:0000707 pericarp colours
TO: 0002699 lycopene content
Trait Ontology (TO)
FGSG_12019 (Sc Gin4-like)
GzZC305
gil1
ScOrtholog_DIA3
GlV4
dcl1
PHI-Base

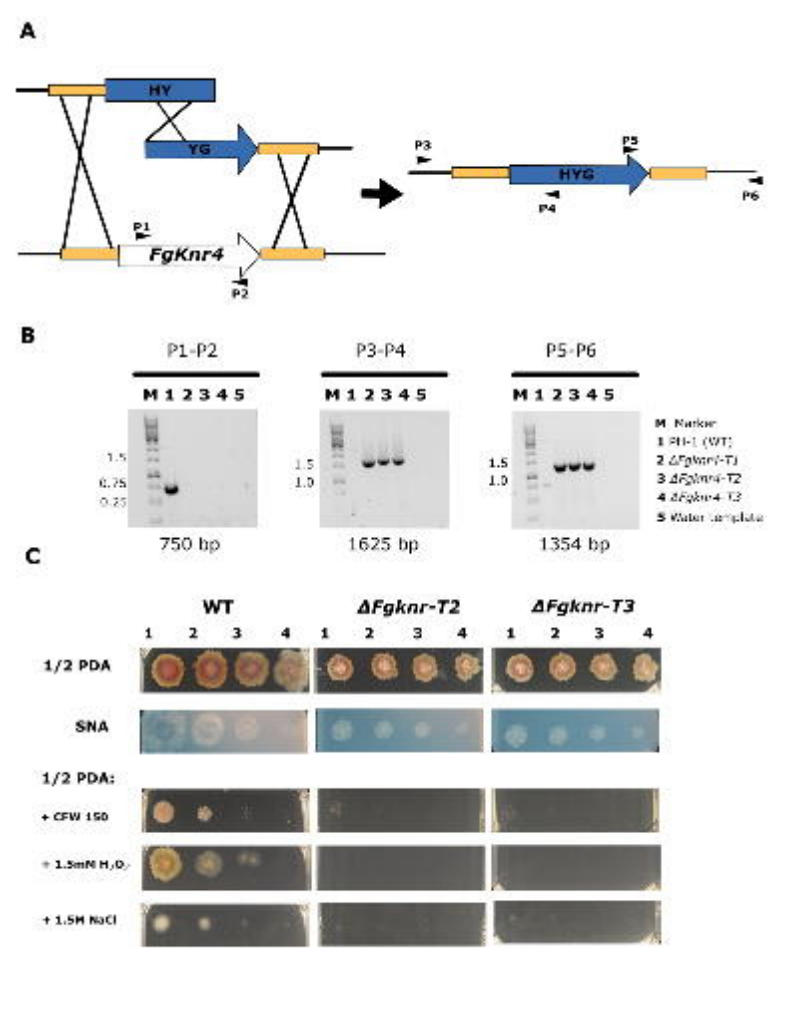
A
HY
YG
FgKnr4
P1
P2
P3
P4
P5
P6
HYG
B
P1-P2
P3-P4
P5-P6
M 1 2 3 4 5
1.5
0.75
0.25
1.5
1.0
M Marker
1 PH-1 (WT)
2 ΔFgknr1-T1
3 ΔFgknr1-T2
4 ΔFgknr1-T3
5 Water template
750 bp
1625 bp
1354 bp
C
WT
ΔFgknr-T2
ΔFgknr-T3
1 2 3 4
1/2 PDA
SNA
1/2 PDA:
+ CFW 150
+ 1.5mM H2O2
+ 1.5M NaCl

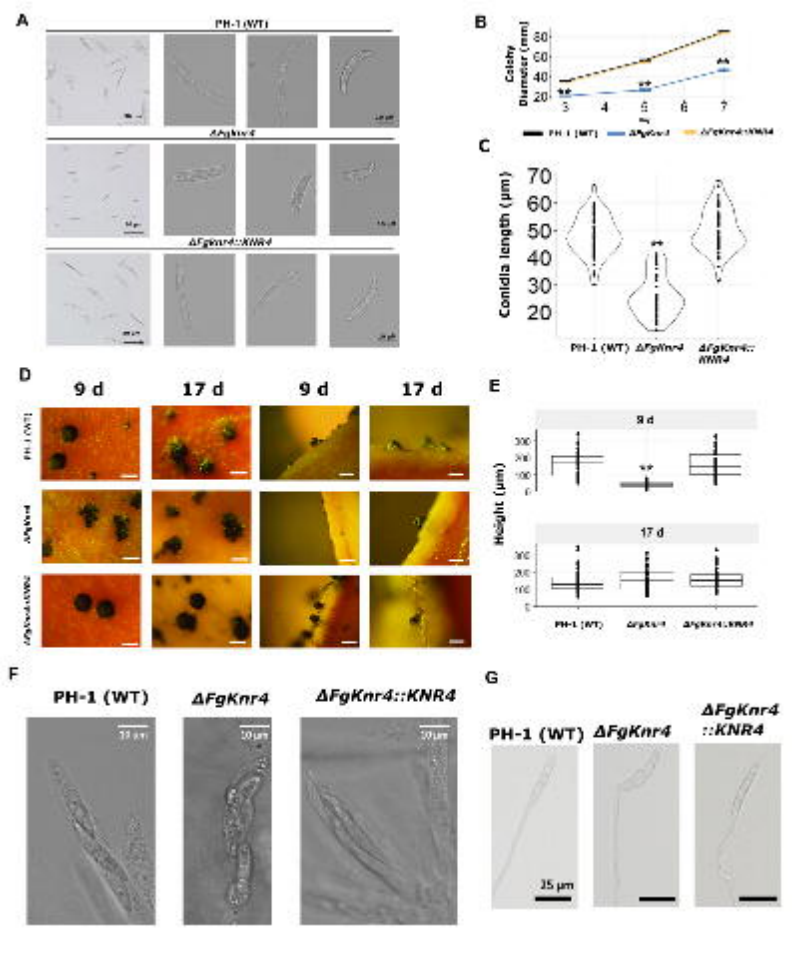
A
PH-1 (WT)
ΔFgKnr4
ΔFgKnr4::KNR4
B
Colony Diameter (mm)
80
60
40
20
3
4
5
6
7
Day
**
**
PH-1 (WT)
ΔFgKnr4
ΔFgKnr4::KNR4
C
Conidia length (μm)
70
60
50
40
30
20
**
PH-1 (WT)
ΔFgKnr4
ΔFgKnr4::KNR4
D
9 d
17 d
9 d
17 d
PH-1 (WT)
ΔFgKnr4
ΔFgKnr4::KNR4
E
9 d
17 d
Height (μm)
300
200
100
0
**
a
b
b
PH-1 (WT)
ΔFgKnr4
ΔFgKnr4::KNR4
F
PH-1 (WT)
ΔFgKnr4
ΔFgKnr4::KNR4
10 μm
10 μm
10 μm
G
PH-1 (WT)
ΔFgKnr4
ΔFgKnr4 ::KNR4
35 μm

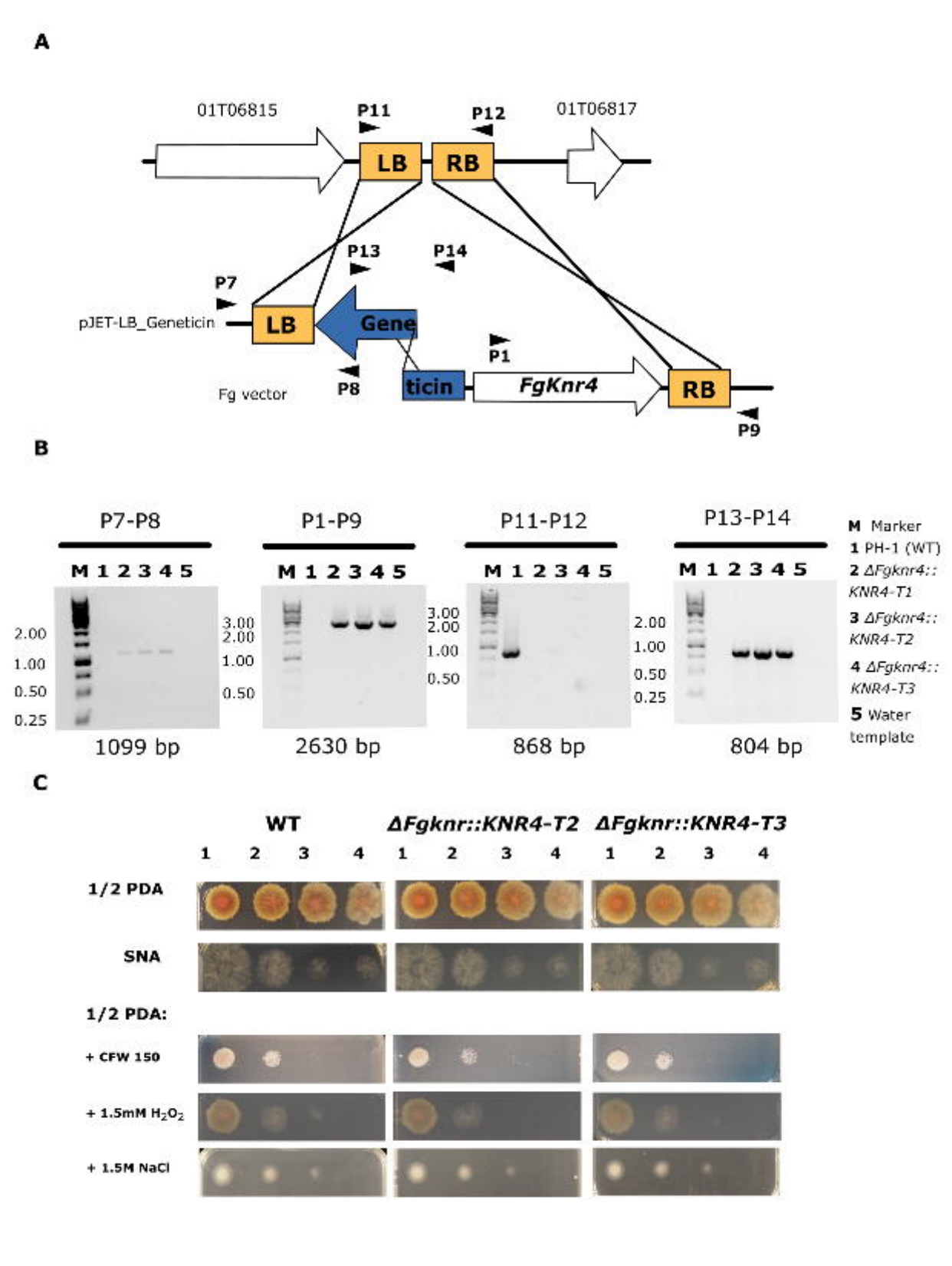
A
01T06815
P11
P12
01T06817
LB
RB
P13
P14
P7
pJET-LB_Geneticin
LB
Gene
P1
Fg vector
P8
ticin
FgKnr4
RB
P9
B
P7-P8
P1-P9
P11-P12
P13-P14
M 1 2 3 4 5
2.00
1.00
0.50
0.25
3.00
2.00
1.00
0.50
1099 bp
2630 bp
868 bp
804 bp
M Marker
1 PH-1 (WT)
2 ΔFgknr4::KNR4-T1
3 ΔFgknr4::KNR4-T2
4 ΔFgknr4::KNR4-T3
5 Water template
C
WT
ΔFgknr::KNR4-T2
ΔFgknr::KNR4-T3
1 2 3 4 1 2 3 4 1 2 3 4
1/2 PDA
SNA
1/2 PDA:
+ CFW 150
+ 1.5mM H2O2
+ 1.5M NaCl

A

WT (PH-1)

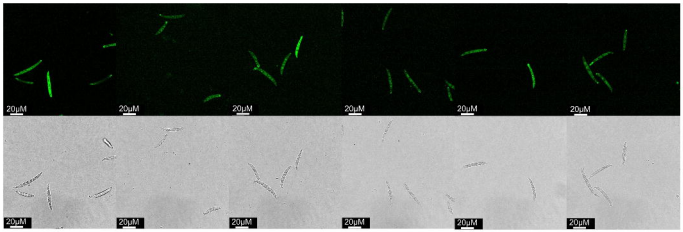

B

ΔFgknr4 - T1

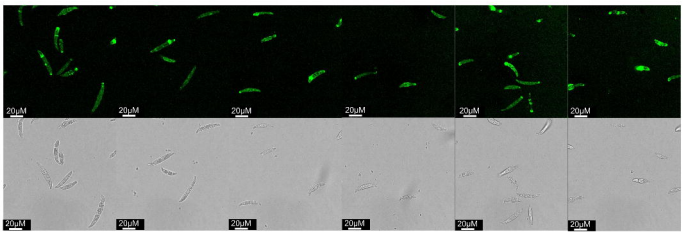

C

ΔFgknr4::KNR4-T1

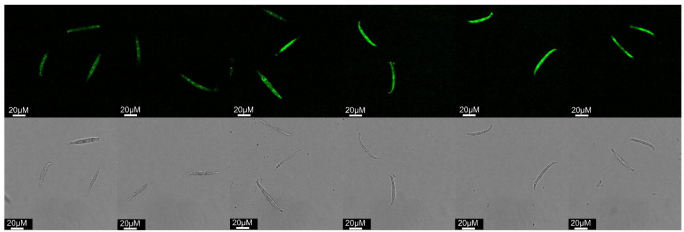

A

WT (PH1)

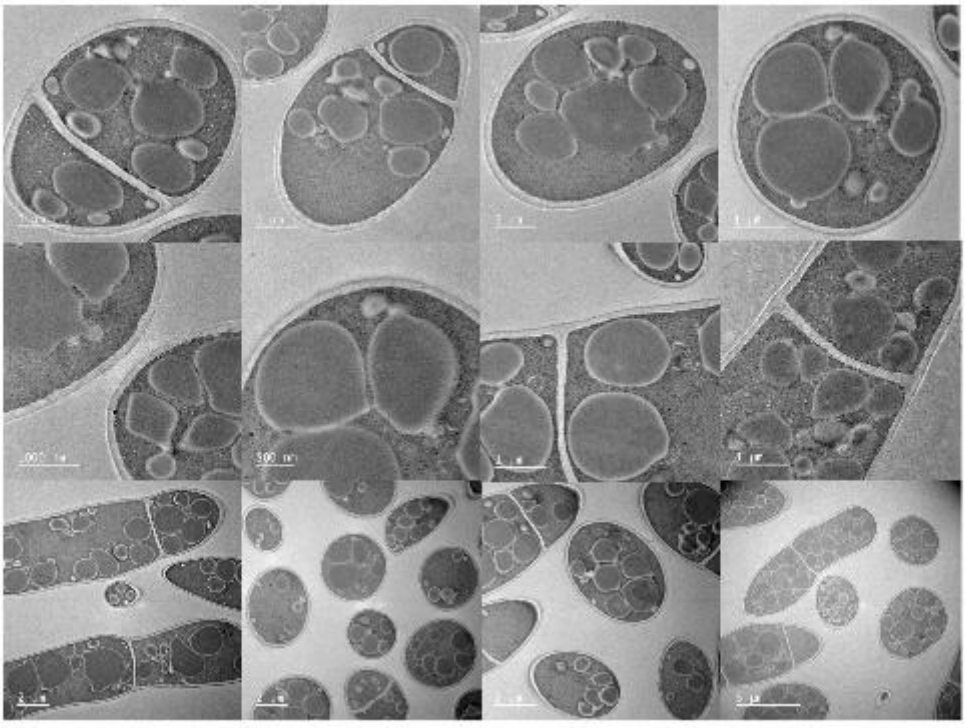

B

ΔFgknr4 - T1

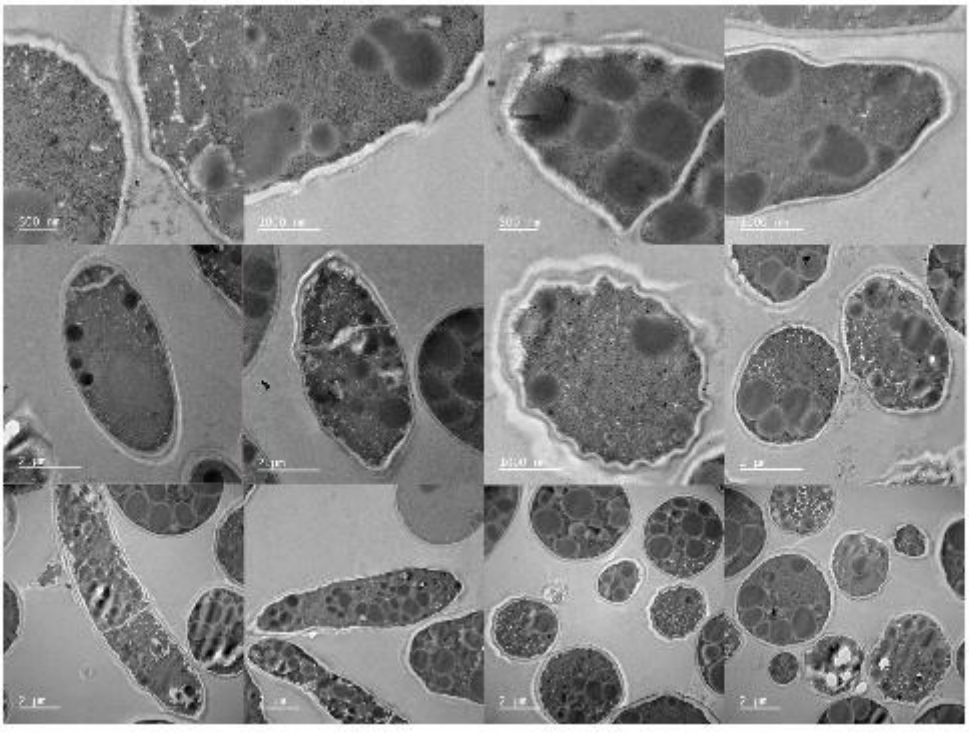

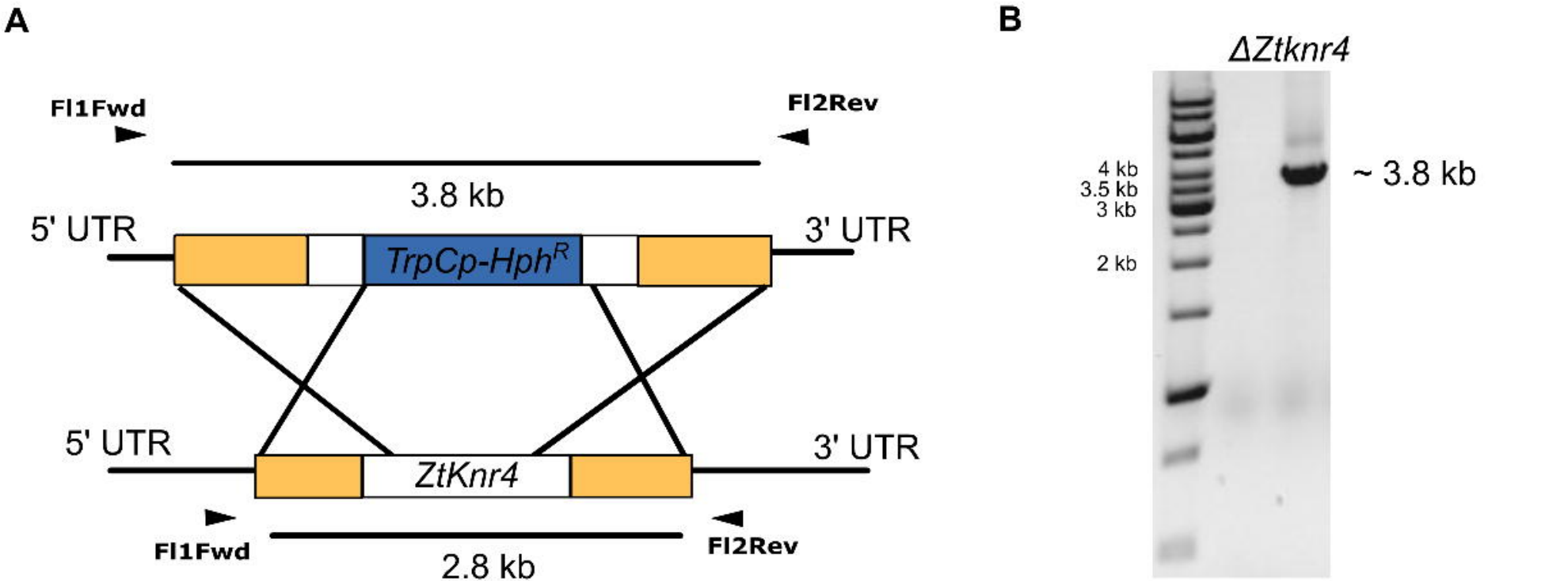
A
Fl1Fwd
Fl2Rev
3.8 kb
5' UTR
TrpCp-Hph^R
3' UTR
5' UTR
ZtKnr4
3' UTR
Fl1Fwd
Fl2Rev
2.8 kb
B
ΔZtknr4
4 kb
3.5 kb
3 kb
2 kb
~ 3.8 kb